

On the Role of Delays in Biological Systems: Analysis and Design

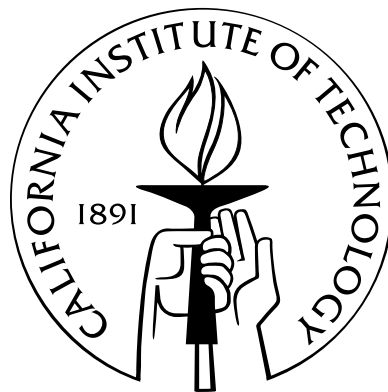
Thesis by

Marcella Mary Gomez

In Partial Fulfillment of the Requirements

for the Degree of

Doctor of Philosophy



California Institute of Technology

Pasadena, California

2015

(Submitted August 28, 2014)

© 2014

Marcella Mary Gomez

All Rights Reserved

To My Dad

Acknowledgements

I would like to thank my advisor Richard M. Murray for his continual guidance and support. In particular, I am thankful and grateful for the freedom he has given me in pursuing my own research interests. I would also like to thank Gabor Orosz for his guidance through our collaboration. I would like to thank Gabor's students Wubing Qin and Mehdi Sadeghpour, who I have worked with through my collaboration with Gabor. Their hard work is very much appreciated. I thank Mark J. Balas for his great feedback in my work and for his personal interest in my success. I also thank Matthew R. Bennett for his mentorship and guidance through our collaboration. I also thank my colleague Enoch Yeung, who has always provided me with stimulating conversations on research. Thanks for always having great questions at group meeting and following up with me. I also thank my colleague Ophelia Venturelli. The initial motivation behind my ideas was partly inspired through conversations with her about the galactose regulatory network in yeast.

I have to thank Anissa Scott and all of Richard's students, who have provided a wonderfully supportive working environment. Especially, Anu Thubagere and Victoria Hsiao, who have stuck by me. I also thank the Diversity Center and my friends from Grad Chat who have allowed me time and space to be my other self. I thank Mike Anaya and Nadia Herrera for helping me out with Club Latino.

I thank my family for all their love and support, especially my parents, who sacrificed a lot for my success. They unconditionally supported me even when they didn't understand my decisions. I thank my husband, who has always kept me grounded and focused. He has been my biggest supporter and my rock.

Last, I thank God for all these people He placed in my path. I thank God for the privileges and opportunities that have been given to me without reason. I thank God for helping me to overcome my struggles and push forward with great strength.

Abstract

This work quantifies the nature of delays in genetic regulatory networks and their effect on system dynamics. It is known that a time lag can emerge from a sequence of biochemical reactions. Applying this modeling framework to the protein production processes, delay distributions are derived in a stochastic (probability density function) and deterministic setting (impulse function), whilst being shown to be equivalent under different assumptions. The dependence of the distribution properties on rate constants, gene length, and time-varying temperatures is investigated. Overall, the distribution of the delay in the context of protein production processes is shown to be highly dependent on the size of the genes and mRNA strands as well as the reaction rates. Results suggest longer genes have delay distributions with a smaller relative variance, and hence, less uncertainty in the completion times, however, they lead to larger delays. On the other hand large uncertainties may actually play a positive role, as broader distributions can lead to larger stability regions when this formalization of the protein production delays is incorporated into a feedback system.

Furthermore, evidence suggests that delays may play a role as an explicit design into existing controlling mechanisms. Accordingly, the recurring dual-feedback motif is also investigated with delays incorporated into the feedback channels. The dual-delayed feedback is shown to have stabilizing effects through a control theoretic approach. Lastly, a distributed delay based controller design method is proposed as a potential design tool. In a preliminary study, the dual-delayed feedback system re-emerges as an effective controller design.

Contents

Acknowledgements	iv
Abstract	v
1 Introduction	1
2 Characterization of Delays	7
2.1 Delays as a sequence of chemical reactions	7
2.1.1 Stochastic delays	7
2.1.2 Distributed delays	13
2.2 Time-varying delays	19
2.2.1 Time-varying delay distribution	19
2.2.2 Time-varying discrete delay	23
3 Stochastic Delay-Based Model	28
3.1 Discrete-time model	30
3.2 Notions of Stability for Stochastic Systems	32
3.3 Stability Conditions	33
3.4 Examples	41
3.5 Application to an Autoregulatory network with stochastic delays	47
4 Deterministic Delay-Based Model	49
4.1 Review of DDEs	50
4.2 Distributed-delay feedback system	51
4.2.1 Stability	51
4.2.2 Frequency Response	57
4.2.3 Gain margin	59

4.2.4	Limit cycles	61
4.3	Temperature dependent oscillators	66
4.3.1	Goodwin oscillator	68
4.3.2	Temperature compensating circuit	73
5	Delay-Based Controllers	77
5.1	Dual-delayed feedback system	78
5.2	Delay-based controller design	84
5.2.1	Problem Formulation	85
5.2.2	A Cone Complementarity Linearization Algorithm	88
5.3	Application to a genetic auto-regulatory network	90
5.3.1	Model	90
5.3.2	Design Results	92
5.3.3	Implementation	94
5.3.4	Discussion	95
6	Conclusions and Future Work	99
6.1	Conclusions	99
6.2	Future Work	100
	Bibliography	104

Chapter 1

Introduction

Delay plays a significant role in the self-regulation of genetic regulatory networks. Even though delay imparts unpredictable behavior and is a notorious force of destabilization in man-made control systems, research suggests that delay can play a positive role in the smooth functioning of genetic regulatory networks. This work explores this concept further, which requires an understanding of the nature of the delays. Heretofore scientists have overlooked quantifying delay distributions in protein production, where delay distributions refers to the existing time delays in the process and the quantified uncertainties in those delays. Additionally, reduced state space models can be achieved with delays. In modeling, there is a need to find a balance between accuracy (complexity) and capturing essential qualitative behavior, which involves identifying important system properties. Significant delays can arise in regulatory networks from large sequences of chemical reactions [50] such as those involved in transcription [75] and protein folding [55]. There has been more recent interest in capturing delays in models, for example in Danino *et al.* [11] and Hussain *et al.* [32]. Delays have played a detrimental role in control efforts of man-made systems; however, performance of genetic regulatory networks seems to not only be unhindered by delays but also appears to incorporate delays as part of their controller design. Thus, delays are important to consider in reduced models; even if translation rates and protein folding times seem negligible, intermediate chemical reactions omitted can impart effective delays on the system as well.

This work focuses on biological systems at the cellular level, namely protein regulatory networks. On the cellular level, uncertainty complicates robustness, so extensive efforts have been made to quantify uncertainties such as stochasticity in protein production and cell-to-cell variability [16,35,69,76]. This work quantifies the uncertainties in transcriptional and translational delays. The delays to be characterized are those that arise from the various reactions involved in protein production, namely transcription and translation [2]. Activation of protein production is initiated

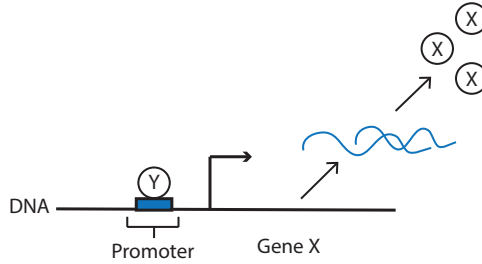


Figure 1.1: Protein production process.

when a transcription factor protein binds to the promoter site of the target gene. This allows RNA polymerase to begin transcription of the target gene, the process of copying the sequence through production of a complementary mRNA strand. If the transcription factor protein is an inhibitor, then binding to the promoter site inhibits the RNA polymerase from transcribing the target gene, thereby inhibiting protein production. The second step in the protein production process is translation, which is similar from a modeling perspective to the transcription process. Each triplet of nucleotides in the mRNA sequence is translated into an amino acid. A string of amino acids is generated as the ribosome traverses the mRNA. This string of amino acids then undergoes folding into a steady state structure, which is the resulting final product, that is, the protein.

Chapter 2 focuses on characterizing transcriptional and translational delays with constant and time-varying rate coefficients. Chapters 3 and 4 focus on understanding the influence of the delays on dynamics of autoregulatory networks in a stochastic and deterministic modeling framework, respectively. Chapter 5 investigates control mechanisms of feedback systems with large delays. This is expanded on below.

Chapter 2 investigates the nature of delays in genetic regulatory networks and the different modeling frameworks. Incorporating delays in models of biological systems has allowed scientists to simplify models, while maintaining qualitative similarities to experimental data [11,67]. This has allowed researchers to identify key functional components of larger networks. To date this has been done in a very *ad hoc* fashion. There is a need for a more systematic method of deriving predictable delay-based models of systems. To do this the nature of the delays needs to be understood and correctly modeled. Focusing on transcriptional delays, the delay distribution is shown to be an *Erlang* distribution through a stochastic and deterministic approach. The Erlang distribution is a

special case of the Gamma probability density function and given by

$$p(\tau; N, a) = \frac{a^N \tau^{N-1}}{(N-1)!} e^{-a\tau} \quad \forall \tau \geq 0 \quad \text{and} \quad N \in \mathbb{N}^+. \quad (1.1)$$

The *Erlang* distribution can be interpreted as the probability distribution on the waiting times in queue for N occurrences of an event, where the waiting times between occurrences are exponentially distributed with common rate a and mutually independent. The mean time through the queue is then given by N/a , which is the first moment of the *Erlang* distribution. In the stochastic approach, this becomes a good description of transcriptional elongation. In the deterministic approach, the impulse function from the input to the output of the system is found to have the exact form of the *Erlang* distribution. Furthermore, expressing the output state as an explicit function of the input and the impulse function leads to a distributed-delay differential equation, also sometimes known as an integro-differentiable equation. From here on out the impulse function and the probability density function characterizing the delays are both referred to as delay distributions. In this case they are thought to be synonymous in the sense that the deterministic dynamics are thought of as the average of the stochastic dynamics, hence, the convolution of the delayed state over the probability density function of the delays. In the thermodynamic limit, it is shown that the stochastic system does indeed approach a deterministic system, whose impulse function is the probability density function of the delay. Last, the distribution is evaluated for time-varying rate coefficients. The resulting time-varying distribution reduces to the Erlang distribution for a constant rate coefficient. This new result provides a method of analyzing delay-based models under time-varying conditions. For example, the result is applied when time-varying temperatures are considered in Chapter 4.

Chapter 3 investigates the effect of stochastic delays on stability of a feedback system. Delays often lead to instabilities in dynamic systems which can make control design a challenging task. In addition, in systems where delays vary stochastically, the difficulty of ensuring stability increases significantly. Much investigation has been done on linear systems with a stochastic state matrix [68] but little has been done on analysis of systems with stochastically varying delays and even less analyzing the effects of stochastic delay variations. Most methods have applied Lyapunov-type analysis to derive sufficient conditions for stability of equilibria. For linear systems, this leads to matrix inequalities [19,59,80], which typically provide conservative results. Similarly, taking the worst case scenario (e.g., largest delay) can lead to unnecessary conservativeness or may simply give erroneous results. Finally, calculating stability for each delay and taking the intersection of the stable regimes in parameter space do not necessarily give the stability of the stochastic system [20].

However, in a recent paper [34], it was shown that stochastic delay variations can have a positive impact on stability in genetic regulatory networks. Consequently, there is demand for a method that allows the derivation of exact stability bounds for these types of problems. Additionally, there are different notions of stability for stochastic systems, which must be addressed when discussing stability. This chapter presents a derivation of conditions for pointwise asymptotic convergence of a state for a discrete-time linear system with a stochastically time-varying delay in feedback. The results hinge on the selected delays at each time step being mutually exclusive and selected from the same distribution with finite support. We argue these are reasonable assumptions in the context of genetic regulatory networks. The method is applied to a scalar system with delays selected from simplified probability density functions. This illustrates the nonintuitive effect of stochastic delays on stability. Lastly, the method is applied to an autoregulatory network where the effect of the Erlang distribution parameters on system stability is investigated. For the case studies included, a larger relative variance (more uncertainty) leads to a larger stability region.

Chapter 4 investigates the effect of the Erlang distribution parameters on dynamics in a deterministic modeling framework via applications of existing control theoretic tools. First, the chapter looks at stability bounds for varying values of the mean and relative variance. Similar to what was found in Chapter 3, a larger relative variance leads to a larger stability region. This is less surprising in a deterministic model. Similar results have been found for different distribution functions [4,5,6,73]. Heretofore, only stability has been considered and robustness properties have been overlooked. Here, robustness properties of the distributed-delay feedback system is investigated through computation of the gain margin. The gain margin is found to increase with the relative variance. This means a system with a larger delay distribution can permit larger fluctuations or uncertainties in protein concentrations before being rendered unstable. This is crucial since exact protein concentrations cannot be achieved in genetic regulatory networks due to environmental variabilities and uncertainties. Next, the case of instability is considered. It is shown that feedback systems of the type used up until now (e.g., the autoregulatory network) exhibit stable limit cycles when the equilibrium point goes unstable. These autoregulatory networks fall into the category of the broadly used term Goodwin oscillator [25]. The original model was developed as the first description of a genetic oscillator and its variants have been used for other models of oscillatory networks such as circadian clocks [63] and physiological control systems [52]. Hence, the study of the influence of delays on such limit cycles is broadly useful. We look at the relationship between the distributed delay parameters and the period of the induced limit cycle in an unstable autoregulatory network

through an application of harmonic balancing. Last, we look at the effects of time-varying temperatures on the oscillators. The limit cycle of the oscillator for a constant delay distribution with a small relative variance is found to be dependent on the mean of the distribution. In the case of periodically time-varying temperature, the fluctuations become negligible when the period is close to the value of the delay in the feedback.

Chapter 5 investigates control mechanisms for feedback systems with large delays. The ability of the networks to perform well in the presence of large delays is remarkable and the control mechanisms less understood. A dual-delayed feedback system is studied and a method of delay-based controller design is proposed, in which the distribution is treated as the design variable.

Delay-based feedback designs are considered as control architectures since they can be more easily implemented than an arbitrary controller. It has been shown that in some biological systems, feedback loops exhibit a time delay through the involved chemical reactions that take time to synthesize the proteins that regulate or activate gene expression. Furthermore, additional delays can be artificially implemented in transcription and translation through placement of the gene with respect to the promotor region and secondary structure design, respectively. For example, one way the delays can be implemented is by adding “junk” DNA (non-coding DNA sequence) in-between the promotor site and the gene to delay the initiation of transcription. The RNA polymerase would be forced to transcribe this sequence before beginning transcription of the target gene.

Adding delays to a system is, in some cases, known to have stabilizing effects [1,56]. However, the method of adding delays has not been well formulated as a general control mechanism. Some preliminary work can be found in Kharitonov *et al.* [37] and Michiels *et al.* [54]. In the first section the stabilizing effects of an added delayed pathway is investigated, motivated by the robust properties of dual-feedback systems. Authors Longo *et al.* [47] investigate the role of a secondary feedback channel in the production of NF- κ B, a protein complex that plays a role in regulating the immune response to infection. The secondary feedback path is shown numerically to improve the stability region. Bhartiya *et al.* [7] demonstrate robust behavior of genetic regulatory networks with multiple delayed feedbacks, where they show increased response time and robustness to variations in system parameters. In Venturelli *et al.* [74], the authors show that dual positive feedback loops work to increase the range of parameters that induce a bimodal response. Here, we derive an expression relating the phase margin of a single-input single-output system with dual-delayed feedback to the difference between the two delays. This allows us to demonstrate not just the potential stabilizing effect of an added delay to an already delayed system but the robustness of the system with respect

to perturbations in any of the two delays.

In the second section (collaborative work with Seungil You) we explore the possibility of implementing simple proportional feedback where the time delayed output signal is the only component used in the controller design. In Javad *et al.* [43], a controller is designed using traditional control theory tools and then approximated with delays. Alternatively and preferably, one can directly design a controller with delays. This is motivated by biological systems, where arbitrary controllers cannot be easily synthesized as in a digital system. In biological systems, the tools for controller design are limited [60]. If we choose delays as our building blocks for controllers, controllers may be easier to implement in a wet lab through added transcriptional pathways. We start with a continuous-time distributed-delay feedback system which is discretized in time. The delay distribution then reduces to a sum of weighted delayed states. The optimal weights for the added feedback channels are found using optimization techniques. In particular, we reduce the H_∞ norm of the closed loop transfer function with multiple delayed feedback using techniques from static output feedback design and imposed constraints on the feedback gain. The method is then applied to a scalar genetic autoregulatory network where additional constraints are imposed on the gain for a feasible implementation of the feedback controller in an experimental setting. Surprisingly, we get back a dual-feedback type controller. In addition to improved performance, we find added delayed feedback channels can increase the stability regime of a delayed system.

Finally, Chapter 6 summarizes the results and discusses future research directions. Future work includes extending current results to more general cases and incorporating experimental work.

Chapter 2

Characterization of Delays

For a high order system and comparably high reaction rates, one can approximate a large sequence of reactions in a model with a delay, which can be interpreted as the time needed to go through the “queue”. Such types of delays can arise in protein production, for example. This modeling framework is used and the case is considered where the number of chain chemical reactions approach infinity as the reaction rates also approach infinity. In essence, this provides a model for a system with a large number of consecutive chemical reactions happening almost instantaneously. For example, one may consider this a good model for the process of transcription. In the limit of infinite instantaneous reactions it is shown that a discrete delay emerges. Additionally, time varying rate coefficients are considered as well as their effects on the found delay distributions. In the same limits, it is shown that a time-varying rate constant leads to a time-varying discrete delay.

2.1 Delays as a sequence of chemical reactions

2.1.1 Stochastic delays

Here, delays are characterized based on an abstract understanding of transcriptional elongation. Consider the steps following the moment transcription is initiated. Upon transcription initiation the RNA polymerase binds to the gene and begins to build an mRNA strand through a collection of nucleotides complementary to the template strand on the unraveled double stranded DNA.

Consider the case of a single transcription on a single gene. The elongation dynamics are de-

where $P(\lambda, \mu)d\lambda$ is the probability that given the state of the system at time t , the next reaction will occur in an infinitesimal time interval $(t + \lambda, t + \lambda + d\lambda)$ and that the reaction that fires will be the μ -th reaction channel. Therefore, λ is the time of the next reaction and μ is the reaction channel that fires. The state dependent variable a_μ is the propensity function for the reaction channel μ . In this example, the propensity function is defined as

$$a_\mu \doteq a[X_\mu]$$

and

$$a_0 \doteq \sum_{\nu=1}^N a_\nu.$$

The brackets around X_μ denote the total concentration of species X_μ . A main assumption made in the derivation of the algorithm is that the system is well-mixed (the temperature is constant and diffusion is fast) in a fixed volume.

First, consider a model of an isolated system consisting only of transcription with no feedback or additional dynamics. Also, assume that a subsequent transcription cannot initiate until completion of the current one. When an RNA polymerase binds to the DNA, transcription begins. In this case, in a Gillespie simulation, after initiation the probability density function reduces to

$$P(\lambda, \mu) = a_\mu e^{-a_\mu \lambda},$$

where

$$a_\mu = \begin{cases} a & \text{for } X_\mu \neq 0 \\ 0 & \text{otherwise.} \end{cases}$$

Recall that under the given assumptions only one state can have a nonzero value and that value will be one. With these assumptions, the process reduces to a Poisson process which describes the time at which the RNA polymerase moves forward at each nucleotide. Note that the inter-arrival time between complements to each subsequent nucleotide on the gene is identically, independently, and exponentially distributed. The transcriptional delay τ is then the sum of the inter-arrival times of the nucleotides. Given this model, the distribution on the transcriptional delay is then given by the *Erlang* distribution

$$h(\tau) = \frac{a^N \tau^{N-1}}{(N-1)!} e^{-a\tau}, \quad (2.3)$$

which can be shown by an induction proof. Consider the probability density function for the elon-

gation time S_2 of an mRNA strand that is two nucleotides in length with $S_2 = \tau_1 + \tau_2$:

$$\begin{aligned} p(S_2) &= \int_0^\tau p(\tau_2|\tau_1) p(\tau_1) d\tau_1 \\ &= \int_0^\tau p(\tau_2) p(\tau_1) d\tau_1, \end{aligned} \quad (2.4)$$

where τ_1 and τ_2 are the inter-arrival times of the two independent nucleotides respectively. The constraint $\tau_1 \leq S_2$ is in the integral range. Substituting the exponential distribution $p(\tau_i) = a e^{-a\tau_i}$ and $\tau_2 = S_2 - \tau_1$ into equation (2.4) gives

$$\begin{aligned} p(S_2) &= \int_0^{S_2} a e^{-a\tau_1} a e^{-a(S_2-\tau_1)} d\tau_1 \\ &= \int_0^{S_2} a^2 e^{-aS_2} d\tau_1 \\ &= a^2 e^{-aS_2} S_2. \end{aligned} \quad (2.5)$$

Consider the probability density function for the elongation time S_3 of an mRNA strand that is three nucleotides in length and $\tau_3 = S_3 - S_2$:

$$\begin{aligned} p(S_3) &= \int_0^{S_3} p(\tau_3|S_2) p(S_2) dS_2 \\ &= \int_0^{S_3} p(\tau_3) p(S_2) dS_2 \\ &= \int_0^{S_3} (a e^{-a(S_3-S_2)}) (a^2 e^{-aS_2} S_2) dS_2 \\ &= \int_0^{S_3} a^3 e^{-aS_3} S_2 dS_2 \\ &= a^3 e^{-aS_3} \frac{S_3^2}{2}. \end{aligned} \quad (2.6)$$

Following the same iterative procedure, it can be shown that the probability density function for the elongation time S_N of an mRNA strand N nucleotides in length is given by the following equation:

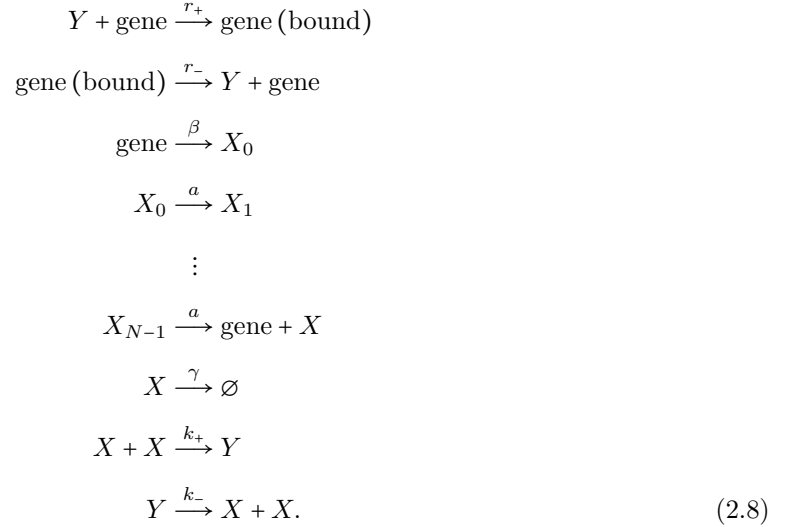
$$p(S_N) = a^N \frac{S_N^{N-1}}{(N-1)!} e^{-aS_N}. \quad (2.7)$$

Replacing S_N with τ in (2.7) gives back equation (2.3).

This derivation of the delay distribution requires many strong assumptions for the reason that all the propensity functions are accounted for in the exponential of the probability density function. Any additional dynamics or simultaneously occurring transcriptions will result in a large coefficient in the exponential, meaning the time between events will decrease. However, given that no two

reactions are allowed to occur in a single time step, one can imagine that the distribution may continue to hold as an approximation. In the next section, the same distribution is found to emerge from a deterministic system through the impulse function with very different assumptions held. For now, it is suggested through simulation that the distribution can remain a good approximation.

The following auto-regulatory network is simulated:



The third reaction represents the initiation of transcription through binding of an RNAP to a gene without a repressor bound. It is assumed that RNAP cannot skip over each other. This is a single gene system and only a maximum of 10 transcriptions can occur simultaneously on a single gene. This averages roughly to a maximum of 20 transcripts/min which is within reasonable range [45]. The binding of the RNAP to the gene is not explicitly modeled since RNAP does not appear to be a limiting factor [38]. Instead, a constant rate of initiation is assumed for unbound genes. Figure 2.2 shows a histogram of the measured delays in the simulation. The predicted *Erlang* distribution is shown in black for comparison. The approximation breaks down a bit for this particular system with the indicated parameters but it is still not a bad fit. In the next section, it will be shown that the *Erlang* distribution can remain a good fit for system (2.8) under some very different assumptions. In fact, the same exact distribution will re-emerge.

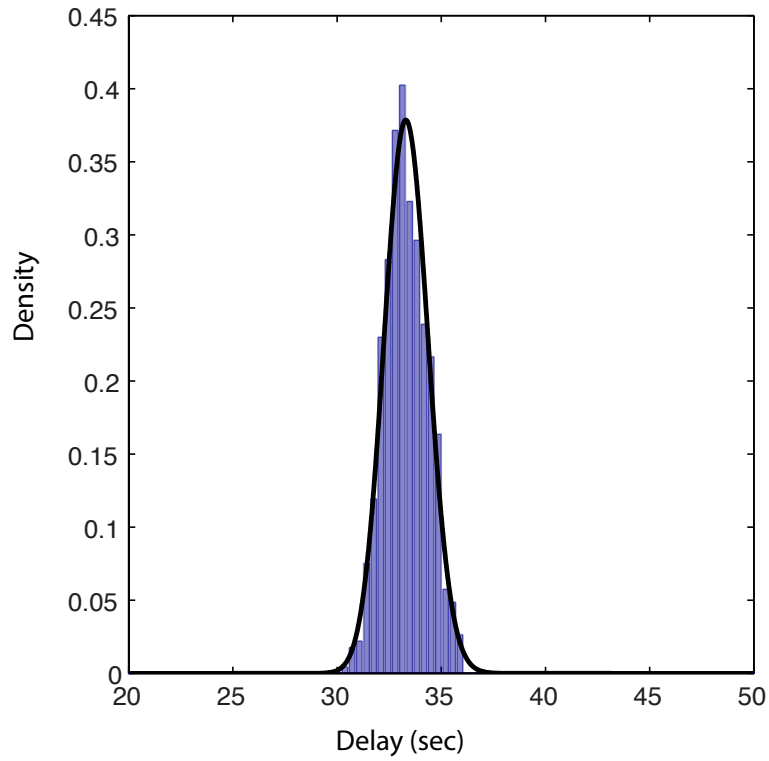
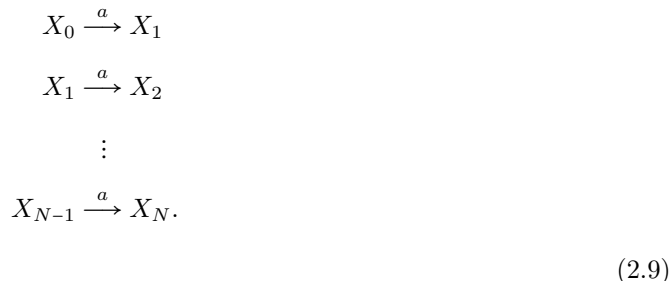


Figure 2.2: Normalized histogram of transcriptional delay for the system described in equation (2.8) with $N = 1000$, $a = 30$ bp/sec, $k_+ = 0.018 \text{ min}^{-1}$, $k_- = 0.00018 \text{ min}^{-1}$, $r_+ = 0.18 \text{ min}^{-1}$, $k_- = 1.8 \text{ min}^{-1}$, $\beta = 10 \text{ min}^{-1}$, and $\gamma = 0.5 \text{ min}^{-1}$. The black curve is an Erlang distribution with mean $E = N/a$ and relative variance $R = 1/N$.

2.1.2 Distributed delays

The delay distribution can also be found by looking at the generalized mass action (GMA) equations, a set of ordinary differential equations (ODEs) derived from the same set of reaction equations;



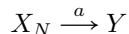
In the generalized mass action approach it is assumed that the number of molecules of each species can be represented by a continuous, single-valued function and the reactions are treated as continuous rate processes. In essence, the differential equations represent the average dynamics. From this, one would expect the dynamics to include an averaging over the delay distribution found in the previous section. First, a more rigorous derivation of the generalized mass action equations is considered.

Consider the descriptive chemical Langevin equation, an approximation to the chemical master equation [22]. The chemical master equation is an exact description of the time evolution of the probability function, which characterizes the stochastic state of the system. Typically, the equation cannot easily be solved. The following conditions must hold in order for the Langevin method to hold as a good approximation:

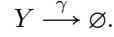
Condition (i) : The time step in the evolution of the state must be small enough that the propensity functions remain fairly constant.

Condition (ii) : The time step in the evolution of the state must be large enough that the expected number of times each reaction channel fires is much larger than one.

The two conditions seem to counter each other, however, an easy way to satisfy the conditions for the Langevin equations to hold is to have large molecular populations of the reactant species. This of course includes a large number of promoter and repressor sites on genes, which are also considered reactants. In [29], the authors derive the chemical Langevin equation for a system of chemical reactions with delays. The method is applied to the open loop system (2.9) with an added reaction



and degradation term



However, the intermediate steps in the sequence of chemical reactions are ignored and only the total delay is considered. The reduced order system becomes



where the dashed line indicates a stochastic process delay with probability density function $h(\tau)$. Note that after the initiation of the reaction, the involved molecule X_0 is no longer available. The corresponding Langevin equation is

$$dy = \left(\int_0^\infty a x_0(t-\tau)h(\tau)d\tau - \gamma y \right) dt + \frac{1}{\sqrt{\Omega}} \sqrt{\left(\int_0^\infty a x_0(t-\tau)h(\tau)d\tau + \gamma y \right)} dW, \tag{2.11}$$

Ω is the volume size of the system and W represents Gaussian white noise. Additionally, the states $y = [Y]/\Omega$ and $x_0 = [X_0]/\Omega$ are concentrations. The system above can be rewritten as

$$\begin{aligned} dy &= (a x_N - \gamma y) dt + \frac{1}{\sqrt{\Omega}} \sqrt{(a x_N + \gamma y)} dW \\ x_N(t) &= \int_0^\infty x_0(t-\tau)h(\tau)d\tau, \end{aligned} \tag{2.12}$$

where the second expression is actually the mean of concentration $x_N(t)$ with respect to the uncertain time delay τ . For now, the distribution is taken to be the Erlang distribution

$$h(\tau) = \frac{a^N \tau^{N-1}}{(N-1)!} e^{-a\tau}$$

found in the previous section. However, it will be shown that this same distribution emerges through a direct application of the generalized mass action approach through the impulse function.

Next, consider the system in the thermodynamic limit as the volume goes to infinity while the density remains constant. The assumptions imply an infinite number of all species, including gene copy numbers if the density is to remain constant. In the thermodynamic limit ($N \rightarrow \infty$), the second term goes to zero and the system approaches the generalized mass action equations, as will

be shown next. The stochastic component of the system becomes negligible in the thermodynamic limit. Additionally, in [22], the fluctuations in the species populations are shown to scale as one over the square root of the reactant populations.

The assumptions held in the generalized mass action approach have now been clearly laid out. Applying the more direct method to the original system (2.9) with the added reaction and degradation term, the generalized mass action equations are given by

$$\begin{aligned}\dot{x}_j &= -a(x_j - x_{j-1}) \quad \text{for } j = 1, \dots, N, \\ \dot{y} &= -\gamma y + a x_N\end{aligned}\tag{2.13}$$

with $x_j = [X_j]$, where the bracket indicates the concentration of species X_j . The frequency response of the first N linear differential equations with input x_0 and output x_N [61] is

$$H_{x_0 \rightarrow x_N} = \frac{a^N}{(s + a)^N}.\tag{2.14}$$

In general, system (2.13) can be represented as a differential distributed-delayed system [50]

$$\begin{aligned}\dot{y} &= -\gamma y + a x_N^* \\ x_N^* &= \int_0^\infty h(\tau) x_0(t - \tau) d\tau,\end{aligned}\tag{2.15}$$

where

$$h(\tau) = \frac{a^N \tau^{N-1}}{(N-1)!} e^{-a\tau}\tag{2.16}$$

and $\int_0^\infty h(\tau) d\tau = 1$. The distribution was found by taking the Laplace inverse of equation (2.14). The same distribution from the stochastic approach emerges, however, in the deterministic model, where the state is convolved with the distribution function as expected. In the stochastic case, it was shown that the Erlang distribution was an accurate description of the delay distribution under some unrealistic assumptions, namely, in an isolated environment. Based on a Gillespie simulation, it was hypothesized that the distribution may hold under some more general assumptions. In this section it is shown that, the distribution indeed holds under assumptions on the opposite extreme in the thermodynamic limit as the molecular populations get really large.

The distribution can be characterized using descriptive statistics. The relative variance of the

distribution function is defined as

$$R = \frac{V}{E^2},$$

where E is the expected value defined by the first moment of the distribution function $f(\tau)$,

$$E = \int_0^{\infty} \tau f(\tau) d\tau$$

and V is the variance defined by the second moment of the distribution function around E ,

$$V = \int_0^{\infty} (\tau - E)^2 f(\tau) d\tau.$$

The resulting relative variance and expectation are

$$R = \frac{1}{N}$$

and

$$E = \frac{N}{a}.$$

The mean of the distribution $E = N/a$ is referred to as the effective delay. Figure 2.3 shows the distribution in equation (2.16) for different values of N with a constant mean.

Note that the relative variance of transcriptional delays is a linear function of the size of the gene, where N represents the number of nucleotides in a gene. One can imagine two genes of different lengths but with the same transcription rate. The longer gene will take longer to transcribe but the relative variance of the distribution will be smaller. It is well known that as the complexity of an organism increases in eukaryotes, the fraction of introns in the genome also increases [3]. In Table 2.1, transcriptional delays are estimated for different organisms. Note significant differences in delays. The average transcription rate for *E. coli* was taken from Bremer *et al.* [10], the transcription rate for the fruit fly was found in Swinburne *et al.* [70], and the average transcription rate for humans was found in Singh *et al.* [66]. The genome size for *E. coli* can be found in Rogozin *et al.* [62]. Furthermore, the number of genes in each of the genomes is found in Lynch *et al.* [49]. It is clear that the presence of introns introduces significant delays to transcription but significantly decreases the relative variance. The existence of significant delays in humans is not surprising given the slow response of the endocrine system.

Often delay-based models of systems incorporate discrete delays, but one may wonder under

	$E = N/a$ (mean)	$R = Var/E^2$ (relative variance)
<i>Escherichia coli</i>	19.3 sec	9.43×10^{-4}
<i>Drosophila melanogaster</i>	4.3 min	1.68×10^{-4}
<i>Homo Sapiens</i>	12.4 min	2.14×10^{-5}

Table 2.1: The mean and relative variance of transcriptional delays for various organisms. Values are based on average gene size and introns are assumed to be evenly distributed among all genes.

what assumptions will a discrete delay hold as a good approximation. Consider the limit as $N \rightarrow \infty$ such that $\frac{N}{a}$ remains constant, in which case equation (2.14) gives

$$\lim_{N \rightarrow \infty} H_{x_0 \rightarrow x_N} = \lim_{N \rightarrow \infty} \frac{a^N}{(s+a)^N} = \lim_{N \rightarrow \infty} \frac{1}{\left(\frac{sE}{N} + 1\right)^N} = \frac{1}{e^{sE}} = e^{-sE}, \quad (2.17)$$

where the substitution $E = N/a$ was applied. The term in the last equality is exactly the frequency response for a delta function $\delta(t - E)$ in the time domain. Therefore, the distribution function will approach a delta function centered at E as $N \rightarrow \infty$. In the limit as $N \rightarrow \infty$, system (2.13) becomes

$$x_N = x_0(t - E), \quad (2.18)$$

where E is the mean of the distribution function (2.16). Figure 2.4 shows simulations for a unit step input into the open loop system (2.13) for different effective delays. It is worth noting that this specific limit only exists in this framework where all the reaction rates are the same but this simplification helps us to gain insight. In addition, in the limit as $N \rightarrow \infty$ the rates must also approach infinity for the distribution to approach a delta function.

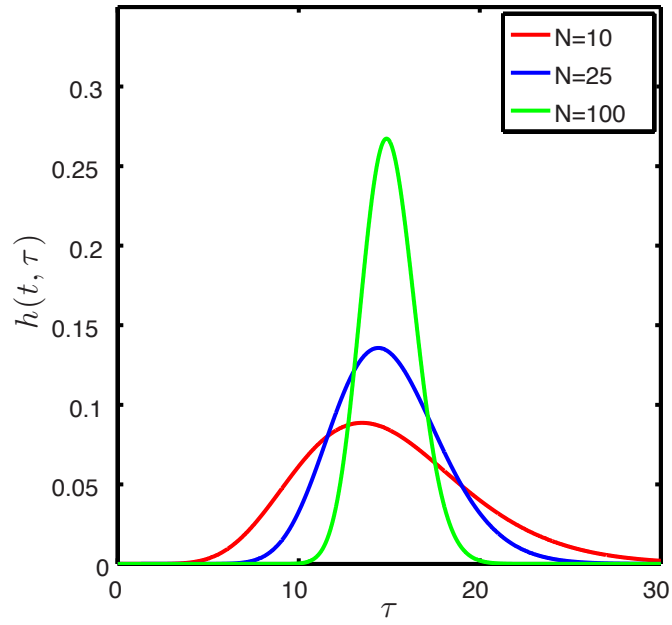


Figure 2.3: Delay distribution for different values of N with $E = 15$.

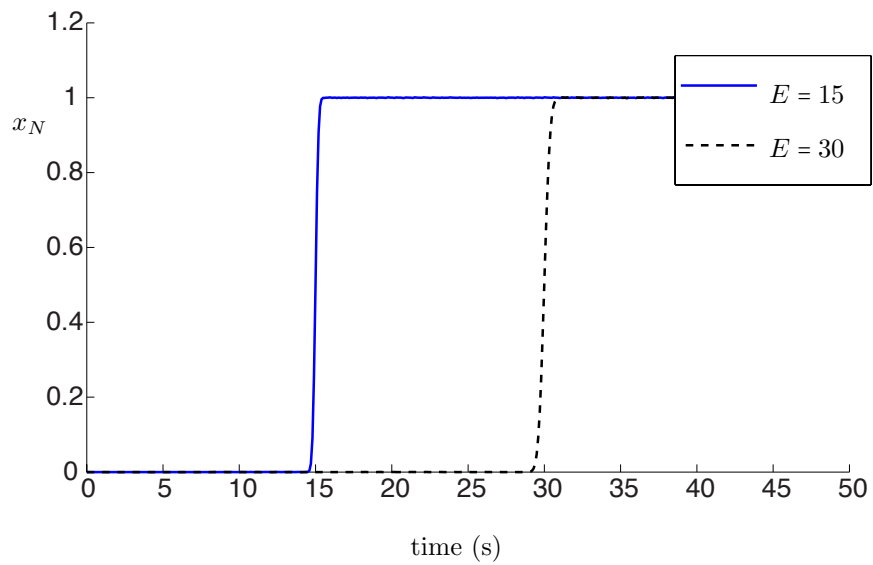


Figure 2.4: Open loop simulation with step input for different E and $N = 10,000$.

2.2 Time-varying delays

We investigate the effects of time-varying rate coefficients on delay distributions. Time-varying rate constants may, for example, arise from temperature fluctuations. We begin by considering the open loop system

$$\begin{aligned}\dot{x}_0 &= -a(t)x_0 + a(t)u(t), \\ \dot{x}_j(t) &= -a(t)(x_j(t) - x_{j-1}(t)) \quad \text{for } j = 1, \dots, N,\end{aligned}\tag{2.19}$$

with input $u(t)$ and the time-varying rate coefficient $a(t)$.

2.2.1 Time-varying delay distribution

Now we proceed to find the distribution function in continuous time. We can put system (2.19) into state space form

$$\dot{X}(t) = A(t)X(t) + B(t)u(t),\tag{2.20}$$

where

$$X(t) = \begin{bmatrix} x_N \\ x_{N-1} \\ \vdots \\ x_0 \end{bmatrix}\tag{2.21}$$

and with matrices

$$A(t) = a(t) \begin{bmatrix} -1 & 1 & 0 & \dots & 0 \\ 0 & -1 & 1 & & \\ \vdots & & \ddots & \ddots & \\ & & & -1 & 1 \\ 0 & \dots & 0 & -1 \end{bmatrix}, \quad B(t) = \begin{bmatrix} 0 \\ \vdots \\ 0 \\ a(t) \end{bmatrix}.\tag{2.22}$$

The general solution to system (2.20) is

$$X(t) = \phi(t, t_0)X(t_0) + \int_{t_0}^t \phi(t, \sigma) \mathbb{B}(\sigma) u(\sigma) d\sigma,\tag{2.23}$$

where ϕ is the state-transition matrix [77]. For $A(t_1)A(t_2) = A(t_2)A(t_1)$ for any t_1 and t_2 , the state-transition matrix can be gives as

$$\phi(t, \zeta) = \exp\left(\int_{\zeta}^t A(s) ds\right). \quad (2.24)$$

Accordingly, we can write the solution as

$$X(t) = \exp\left(\int_{t_0}^t A(s) ds\right) X(t_0) + \int_{t_0}^t \exp\left(\int_{\sigma}^t A(s) ds\right) B(\sigma) u(\sigma) d\sigma. \quad (2.25)$$

Without loss of generality we set $t_0 = 0$ and substituting $\sigma = t - \tau$, we rewrite this expression into the distributed delay format

$$X(t) = \exp\left(\int_0^t A(s) ds\right) X(0) + \int_0^t \exp\left(\int_{t-\tau}^t A(s) ds\right) B(t - \tau) u(t - \tau) d\tau. \quad (2.26)$$

The structure of the system allows for further simplification. Note the Jordan block-like structure of the system. With this we find

$$\exp\left(\int_{t-\tau}^t A(s) ds\right) = \exp\left(\int_{t-\tau}^t a(s) ds J_{-1, N+1}\right), \quad (2.27)$$

where $J_{-1, N+1}$ is the $N + 1$ Jordan matrix with eigenvalues -1 . Defining

$$\alpha(t, \tau) \doteq \int_{t-\tau}^t a(s) ds, \quad (2.28)$$

the exponential can be computed and is given by

$$e^{\alpha(t, \tau) J_{-1, N+1}} = \begin{bmatrix} e^{-\alpha(t, \tau)} & \alpha(t, \tau) e^{-\alpha(t, \tau)} & \dots & \frac{\alpha(t, \tau)^{N-1}}{(N-1)!} e^{-\alpha(t, \tau)} & \vdots & \frac{\alpha(t, \tau)^N}{N!} e^{-\alpha(t, \tau)} \\ \hline & & & & \frac{\alpha(t, \tau)^{N-1}}{(N-1)!} e^{-\alpha(t, \tau)} & \\ & & & \star & \vdots & \\ & & & & \alpha(t, \tau) e^{-\alpha(t, \tau)} & \\ & & & & e^{-\alpha(t, \tau)} & \\ & & & & & \vdots \end{bmatrix}, \quad (2.29)$$

where \star denotes non-zero entries that are irrelevant due to the structure of $B(t)$ and our desired output. In order to extract the expression relating the input $u(t)$ to the measured output $x_N(t)$, we multiply equation (2.26) by $C = [1, 0, \dots, 0]$ on the left-hand side. Then for $X(t_0) = 0$, the output

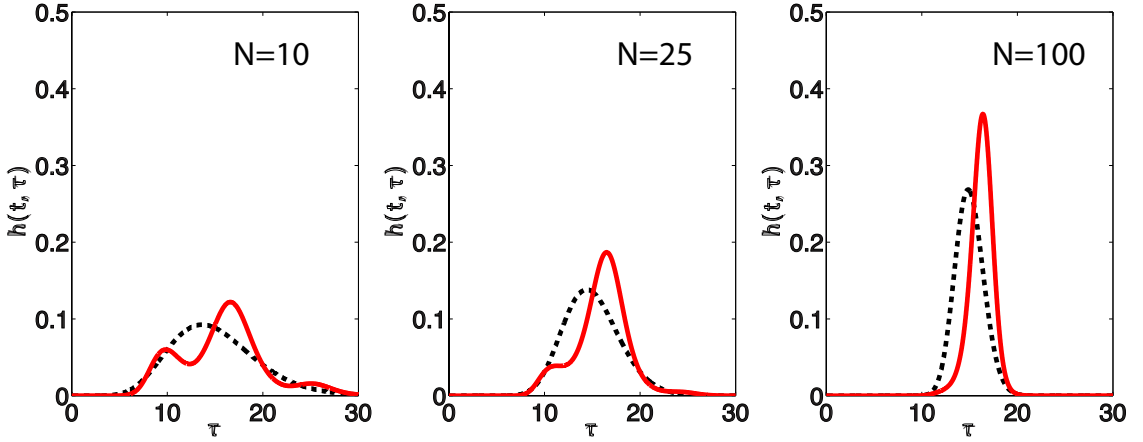


Figure 2.5: Distribution as a function of time with $a(t) = a_0 \delta_p \sin(\omega t) + a_0$, $(N + 1)/a_0 = 15$, $\delta_p = .5$, and $\omega = 2\pi/10$. The dashed line indicates the nominal time-invariant distribution with $a(t) = a_0$.

$x_N(t)$ is related to the input $u(t)$ by

$$x_N(t) = \int_0^t h(t, \tau) u(t - \tau) d\tau, \quad (2.30)$$

where

$$h(t, \tau) = C e^{\alpha(t, \tau) J^{-1, N+1}} B(t - \tau). \quad (2.31)$$

Only the top right element of the exponential matrix is needed. The function $h(t, \tau)$ is the impulse response function relating the output to the input of the system which, as in the case of the generalized mass action dynamics in Section 2.1 can be thought of as the delay distribution and is referred to here as such. This gives the delay distribution function

$$h(t, \tau) = a(t - \tau) \frac{\alpha(t, \tau)^N}{N!} e^{-\alpha(t, \tau)}. \quad (2.32)$$

This solution holds for a general $a(t)$. Note for $a(t) \equiv \text{const.}$ and $N \rightarrow N - 1$, equation (2.32) reduces to the familiar *Erlang* distribution in Section 2.1. Figures 2.5 and 2.6 show how this time-varying distribution changes with N and with time for a given $a(t)$.

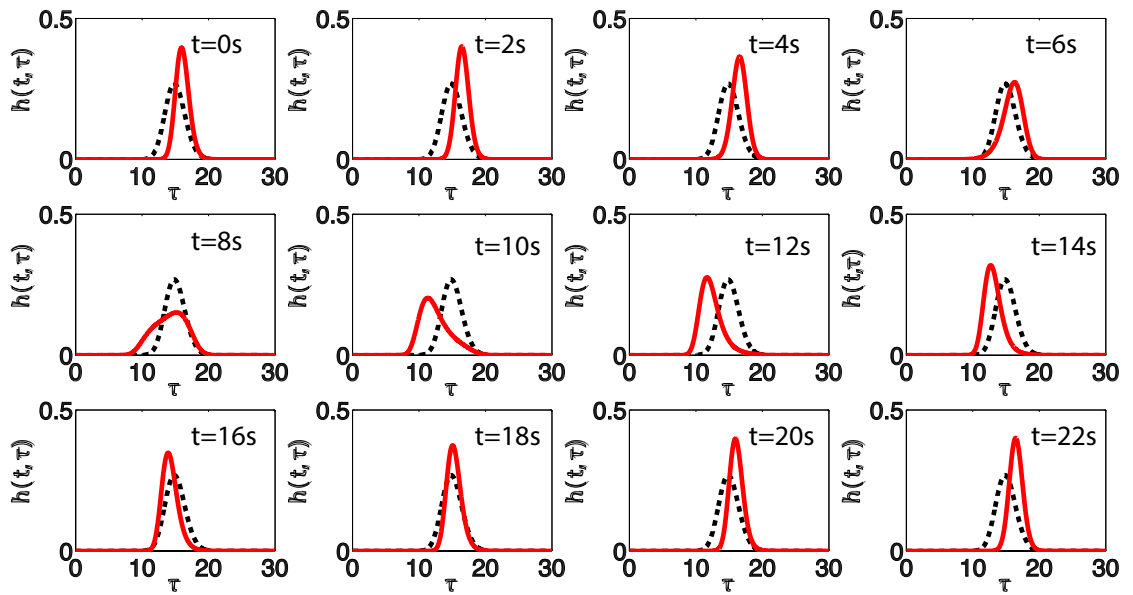


Figure 2.6: Distribution as a function of time with $a(t) = a_0 \delta_p \sin(\omega t) + a_0$, $N = 100$, $(N+1)/a_0 = 15$, $\delta_p = .5$, and $\omega = 2\pi/20$. The dashed line indicates the nominal time-invariant distribution with $a(t) = a_0$.

2.2.2 Time-varying discrete delay

Similarly, as was done for a constant rate coefficient a , the limit as the sequence of reactions tends to infinity is investigated. In the analysis to follow, t is treated as a constant variable. The distribution found in the limit as $N \rightarrow \infty$ is at a single point in time. This requires some necessary conditions on the function $a(t)$. It must hold that the integral over the distribution for all time t equals 1:

$$\int_0^\infty h(t, \tau) d\tau = 1. \quad (2.33)$$

This can be shown by expressing the integral as a path integral:

$$\begin{aligned} \int_0^\infty h(t, \tau) d\tau &= \int_0^\infty a(t - \tau) \frac{\alpha(t, \tau)^N}{(N)!} e^{-\alpha(t, \tau)} d\tau \\ &= \int_0^\infty \frac{\alpha(t, \tau)^N}{(N)!} e^{-\alpha(t, \tau)} \left| \frac{\partial}{\partial \tau} (\alpha(t, \tau)) \right| d\tau \\ &= \int_C \frac{s^N}{N!} e^{-s} ds, \end{aligned} \quad (2.34)$$

where the curve C is the domain of integration that is defined by $\alpha(t, \tau)$ for t held fixed. Note that the expression in the last line is an integral over the Erlang distribution, which is known to equal one, when integrated along the curve $C \equiv a\tau$. For the path integral in equation (2.34) to equal 1, $\alpha(t, \tau)$ must be an injective function in τ ($d\alpha(t, \tau)/d\tau = a(t - \tau) > 0$) with $\alpha(t, 0) = 0$ and $\alpha(t, \infty) = \infty$.

Additionally, some structure on the rate coefficient $a(t)$ is assumed. Previously the limit as $N \rightarrow \infty$ was taken such that $N/a = E$. It is assumed that the rate coefficient takes the form

$$a(t) = a_0 f(t) < M, \quad (2.35)$$

where $a_0, M \in \mathbb{R}$ are finite and the limit as $N \rightarrow \infty$ is taken such that

$$\lim_{N \rightarrow \infty} \frac{N}{a_0} \equiv \text{const.} \quad (2.36)$$

By definition of $\alpha(t, \tau)$ in equation (2.28), this implies

$$\lim_{N \rightarrow \infty} \frac{N}{\alpha(t, \tau)} < \infty. \quad (2.37)$$

The time-varying distribution is now investigated in the limit of an infinite sequence of instan-

taneous chemical reactions. Applying Stirling's formula for large N , namely

$$N! \approx \sqrt{2\pi N} \left(\frac{N}{e}\right)^N, \quad (2.38)$$

the distribution (2.32) is approximated by

$$h(t, \tau) = a(t - \tau) \frac{\alpha(t, \tau)^N}{N!} e^{-\alpha(t, \tau)} \quad (2.39)$$

$$\approx \frac{a(t - \tau)}{\sqrt{2\pi N}} \left(\frac{e\alpha(t, \tau)}{N}\right)^N e^{-\alpha(t, \tau)} \quad (2.40)$$

and asymptotically converges to equation (2.32) in the limit as $N \rightarrow \infty$. Rearranging terms in equation (2.40) and making use of the substitution (2.35) gives

$$\begin{aligned} h(t, \tau) &\approx \frac{a(t - \tau)}{\sqrt{2\pi N}} \left(\frac{\alpha(t, \tau)}{N} e^{1 - \alpha(t, \tau)/N}\right)^N \\ &= \frac{a_0 f(t - \tau)}{\sqrt{2\pi N}} \left(\frac{\alpha(t, \tau)}{N} e^{1 - \alpha(t, \tau)/N}\right)^N \\ &= \left(\frac{N}{E_0}\right) \frac{f(t - \tau)}{\sqrt{2\pi N}} \left(\frac{\alpha(t, \tau)}{N} e^{1 - \alpha(t, \tau)/N}\right)^N \\ &= \frac{f(t - \tau)}{E_0 \sqrt{2\pi}} \left(\frac{\alpha(t, \tau)}{N} e^{1 - \alpha(t, \tau)/N}\right)^N N^{\frac{1}{2}}. \end{aligned} \quad (2.41)$$

Note that if we set $a(t) = a_0$ in equation (2.32) the mean of the distribution is $E = (N + 1)/a_0$, but for ease of notation we define $E_0 = N/a_0$, which approaches a constant in the limit.

We define

$$K(\tau) \doteq \frac{\alpha(\tau)}{N} e^{1 - \alpha(\tau)/N} \quad (2.42)$$

and investigate the limit for different ranges of K . Applying l'Hôpital's rule for $K < 1$

$$\lim_{N \rightarrow \infty} \frac{N^{\frac{1}{2}}}{1/K^N} = \lim_{N \rightarrow \infty} \frac{\frac{1}{2}N^{-\frac{1}{2}}}{N/K^{N+1}} = \lim_{N \rightarrow \infty} \frac{K^{N+1}}{2N^{3/2}} = 0, \quad (2.43)$$

and for $K \geq 1$

$$\lim_{N \rightarrow \infty} \frac{N^{\frac{1}{2}}}{1/K^N} = \infty. \quad (2.44)$$

It remains to show that $K \leq 1$ for all τ . We would like to determine when K reaches its maximum

value. As a necessary condition for an extremum we must have

$$\frac{d}{d\tau}(K) = \frac{d}{d\tau} \left(\frac{\alpha(t, \tau)}{N} \right) e^{1 - \frac{\alpha(t, \tau)}{N}} \left(1 - \frac{\alpha(t, \tau)}{N} \right) = 0. \quad (2.45)$$

Since the first two terms are always strictly positive, we find that an extremum occurs at τ_{eff} , where

$$1 - \frac{\alpha(t, \tau_{\text{eff}})}{N} = 0. \quad (2.46)$$

Plugging equation (2.46) back into equation (2.42),

$$K(\tau) = 1 \cdot e^0 = 1 \quad (2.47)$$

we find $K = 1$ at the extremum. It can be easily shown that

$$\frac{d^2}{d^2\tau}(K) > 0, \quad (2.48)$$

therefore, the extremum is a maximum, hence, $K \leq 1$ for all τ . We see that in the limit as $N \rightarrow \infty$, $h(t, \tau)$ is zero everywhere for all τ except for at τ_{eff} , where $K(\tau) = 1$ and $h(t, \tau) = \infty$. Furthermore, since $\alpha(t, \tau)$ is an injective function in τ , equation (2.46) has a single solution, hence, τ_{eff} provides a global maximum at a given time t . In the limit as $N \rightarrow \infty$ such that $N/a_0 = E_0$ the distribution

$$\lim_{N \rightarrow \infty} h(t, \tau) = \delta(t - \tau_{\text{eff}}(t)) \quad (2.49)$$

approaches a delta function centered at τ_{eff} , which is necessarily a function of $a(t)$, and therefore time-varying. As an example we choose $a(t) = a_0 \delta_p \sin(\omega t + \phi) + a_0$ and plot $\tau_{\text{eff}}(t)$ in Fig. 2.7. In order to characterize the time-dependent delay as a function of the parameters of $a(t)$, the average value and peak-to-peak amplitude of τ_{eff} is plotted against parameters δ_p , E , and $w(\text{Hz})$ in Fig. 2.8.

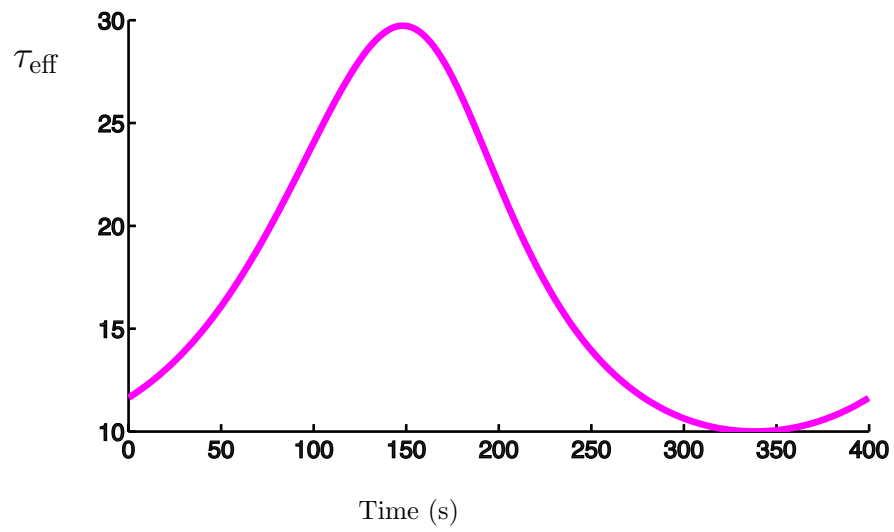


Figure 2.7: Delay τ_{eff} as a function of time for $a(t) = a_0 \delta_p \sin(\omega t) + a_0$ with $a_0 = 15$, $\delta_p = .5$ and $\omega = 2\pi/400$.

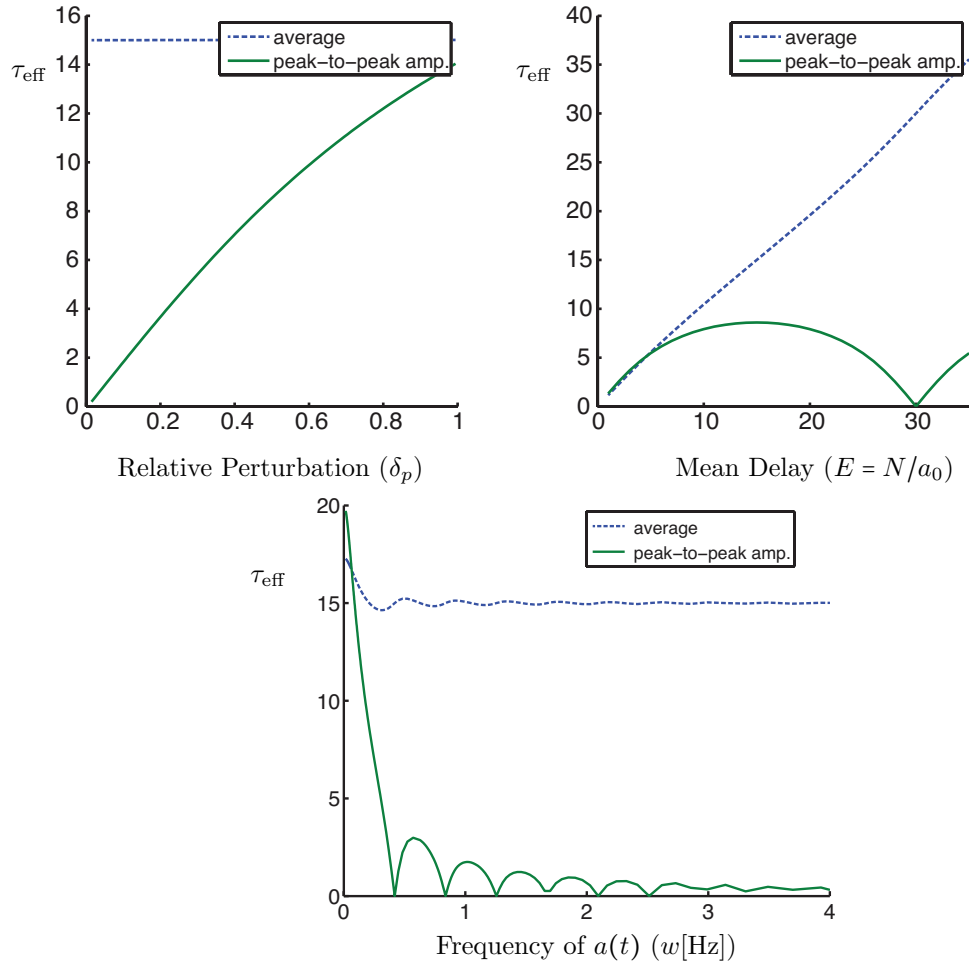


Figure 2.8: Mean and peak-to-peak amplitude of τ_{eff} as a function of δ_p , E , and w . Top Left: $w = \pi/E$, $\phi = 0$, and $E = 15$. Top Right: $w = \pi/15$, $\phi = 0$, and $\delta_p = .5$. Bottom: $\phi = 0$, $E = 15$, and $\delta_p = .5$

Chapter 3

Stochastic Delay-Based Model

In this chapter the effects of delays on system dynamics are investigated through a stochastic modeling framework. On the cellular level, uncertainty complicates robustness, so extensive efforts have been made to quantify uncertainties such as stochasticity in protein production and cell-to-cell variability [16,35,69,76]. Less work has focused on the effects of stochasticity in protein production delays and few delay-based models consider these variable delays. A hybrid model may prove advantageous in predicting system behavior. In a system with large molecular populations but a bounded number of genes, it may be reasonable to assume fluctuations are negligible in processes such as degradation, association, and dissociation. However, assuming fluctuations in delay are negligible may lead to erroneous results. A discrete-time system with stochastically varying delays can provide a potential modeling framework for single cell dynamics in genetic regulatory networks. We consider a heuristic argument to support this modeling framework.

Consider the following description for the dynamics of protein production:

$$X(t + \Delta t) = X(t) - \gamma \Delta t X(t) + \Delta t f(Y(t - \tau(t))), \quad (3.1)$$

where Y is a transcription factor protein that activates the production of protein X , $\gamma > 0$ is the degradation rate, and $f()$ is the nonlinear production rate often described by a Hill function. The concentration of X at time $t + \Delta t$ is the concentration of X at time t , minus the degraded proteins and plus the newly produced proteins in the time interval Δt for time $t < T < t + \Delta t$. For a small enough Δt , one can assume that the production rate at an incremental time step Δt depends on the concentration of Y some $\tau(t)$ time ago, since any protein assuming its final state in that incremental time step would have been initiated at time $t - \tau(t)$ where $\tau(t)$ is a random variable. We are interested in stability analysis, so we would like to examine the dynamics of the system near the

equilibrium point.

Nonlinear analysis in controls is typically performed through system linearization, because linearization often supplies sufficient conditions for nonlinear system stability. Performance analysis of linearized systems often provides useful information about the full nonlinear system, even though the time varying delays are difficult to deal with: on the one hand, delays in continuous time lead to infinite dimensional systems [39]; on the other hand, delays in discrete-time are generally easier to work with and may provide a good approximation [33].

We consider the linear approximation

$$X(t + \Delta t) = X(t) - \gamma \Delta t X(t) + \Delta t \kappa Y(t - \tau(t)), \quad (3.2)$$

where κ is the linearization of the protein production rate evaluated at the equilibrium point

$$\kappa = \left. \frac{\partial f}{\partial Y} \right|_{Y=Y^*}.$$

A discrete-time map can be given by

$$X((k+1)\Delta t) = X(k\Delta t) - \gamma \Delta t X(k\Delta t) + \Delta t \kappa Y(k\Delta t - \tau(k\Delta t)), \quad (3.3)$$

where $\tau(k\Delta t)$ is assumed to be i.i.d. and selected from a discrete-distribution. The discrete-distribution can be found by allocating a continuous distribution into a finite number of bins.

There are various notions of stability for stochastic systems which must be considered. For example $X(k) \xrightarrow{r} X$ denotes that the sequence $X(k)$ converges to a constant X in r^{th} order, for $r \geq 1$, which holds if $\mathbb{E}[|X(k)|^r] < \infty$ for all k and

$$\mathbb{E}[|X(k) - X|^r] \rightarrow 0 \quad \text{as } k \rightarrow \infty.$$

Convergence of the second moment $\mathbb{E}[X(k)^2]$ is then equivalent to convergence in 2^{nd} order since $X(k)^2$ is positive definite. Additionally, $X(k) \xrightarrow{P} X$ and $X(k) \xrightarrow{D} X$ denote convergence in probability and distribution [27]. Notice that convergence in r^{th} order guarantees convergence in probability and distribution. Finally, $X(k) \xrightarrow{w.p.1} X$ denotes convergence with probability one (w.p.1), that is, for every $\epsilon > 0$, $|X(k) - X| \geq \epsilon$ occurs only finitely often. Consequently, for each path ω , there is a number $k(\omega)$ so that $|X(k) - X| \geq \epsilon$, for all $k > k(\omega)$ (see [40]). Each sequence of possible values of $(X(0), X(1), \dots)$ is equivalent to a point ω in a sample space. We may say that, with the exception

of a finite set of sequences, all sequences $\{X(k)\}$ converge pointwise towards X . The latter notion of the stability is the one most analogous to point wise asymptotic stability in a deterministic system. Based on this problem formulation necessary and sufficient conditions are derived for point-wise asymptotic stability of a discrete-time system with i.i.d. stochastically varying delays in feedback for an auto-regulatory network.

3.1 Discrete-time model

Consider the system

$$X(k+1) = \mathbf{A}X(k) + \mathbf{B}X(k - \tau(k)), \quad (3.4)$$

where $X(k) \in \mathbb{R}^n$ is a vector-valued stochastic variable and $\tau(k)$ is a family of mutually independent integer-valued random variables. At each k , the present delay $\tau(k)$ is selected from an identical distribution and can take positive integer values $\tau(k) \in [1, \dots, N]$ where N denotes the maximum delay. The density function $p_{\tau(k)}$ for the delay is

$$p_{\tau(k)}(\sigma) = \sum_{i=1}^N w_i \delta(\sigma - i) \quad (3.5)$$

and is subject to the condition

$$\sum_{i=1}^N w_i = 1, \quad (3.6)$$

where δ is the Dirac delta (i.e. $\tau(k) = i$ with probability w_i). The initial condition includes the state values in the past N time steps and it may contain uncertainty when $X(0), X(-1), \dots, X(-N)$ are selected from known distributions.

Define the augmented vector as

$$\hat{X}(k) = \begin{bmatrix} X(k) \\ X(k-1) \\ X(k-2) \\ \vdots \\ X(k-N) \end{bmatrix}. \quad (3.7)$$

Then, the discrete-time Markov process

$$\hat{X}(k+1) = \hat{\mathbf{A}}(k)\hat{X}(k) \quad (3.8)$$

is equivalent to system (3.4), where $\hat{\mathbf{A}}(k)$ takes the values

$$\hat{\mathbf{A}}_i = \begin{bmatrix} \mathbf{A} & \mathbf{I}_1(i)\mathbf{B} & \mathbf{I}_2(i)\mathbf{B} & \cdots & \mathbf{I}_N(i)\mathbf{B} \\ \mathbf{I} & \mathbf{0} & \mathbf{0} & \cdots & \mathbf{0} \\ \mathbf{0} & \mathbf{I} & \mathbf{0} & \cdots & \mathbf{0} \\ \vdots & \ddots & \ddots & \ddots & \vdots \\ \mathbf{0} & \cdots & \mathbf{0} & \mathbf{I} & \mathbf{0} \end{bmatrix} \quad (3.9)$$

with probabilities w_i (cf. equation (3.5)) for $i = 1, \dots, N$. Here, $\mathbf{I}_j(i)$ is the indicator function such that

$$\mathbf{I}_j(i) = \begin{cases} 1 & \text{if } i = j, \\ 0 & \text{if } i \neq j, \end{cases} \quad (3.10)$$

and $\mathbf{I} \in \mathbb{R}^{n \times n}$ and $\mathbf{0} \in \mathbb{R}^{n \times n}$ denote the n -dimensional identity and zero matrices, respectively. The matrix $\hat{\mathbf{A}}(k) \in \mathbb{R}^{n(N+1) \times n(N+1)}$ is a stochastic variable whose probability distribution is independent of $\hat{X}(k)$. So we have

$$\begin{aligned} p_{\hat{X}(k), \hat{\mathbf{A}}(k)}(\hat{X}, \hat{\mathbf{A}}) &= p_{\hat{\mathbf{A}}(k) | \hat{X}(k)}(\hat{\mathbf{A}} | \hat{X}) p_{\hat{X}(k)}(\hat{X}) \\ &= p_{\hat{\mathbf{A}}(k)}(\hat{\mathbf{A}}) p_{\hat{X}(k)}(\hat{X}). \end{aligned} \quad (3.11)$$

Notice that the sequence $\{\hat{X}(k)\}$ is a Markov chain and the sequence $\{\hat{\mathbf{A}}(k)\}$ is mutually independent. The matrix $\hat{\mathbf{A}}(k)$ can only take on a finite set of values, each of which corresponds to one of the possible delays, henceforth, its probability distribution becomes

$$p_{\hat{\mathbf{A}}(k)}(\hat{\mathbf{A}}) = \sum_{i=1}^N w_i \delta(\hat{\mathbf{A}} - \hat{\mathbf{A}}_i), \quad (3.12)$$

cf. equation (3.5).

We will apply probability principles to derive expressions for the evolution of the mean and second moment dynamics of system (3.8)-(3.9), which is equivalent to equation (3.4). The mean provides necessary conditions for stability of the trivial solution, while the second moment provides necessary and sufficient conditions.

3.2 Notions of Stability for Stochastic Systems

We will derive deterministic discrete time equations whose stability determine the stability of the mean and second moment for the non-deterministic system (3.8,3.9). However, the first and second moments converging to zero does not guarantee that the state converges to zero with probability one (w.p.1) in all circumstances. We restate a theorem that can be found in [27]:

Theorem 3.2.1 *The following implications hold*

$$\begin{array}{ccc}
 (X(k) \xrightarrow{w.p.1} X) & & \\
 \Downarrow & & \\
 (X(k) \xrightarrow{P} X) & \Rightarrow & (X(k) \xrightarrow{D} X) \\
 \Uparrow & & \\
 (X(k) \xrightarrow{r} X) & &
 \end{array}$$

for any $r \geq 1$. Also, if $r > s \geq 1$ then

$$(X(k) \xrightarrow{r} X) \Rightarrow (X(k) \xrightarrow{s} X).$$

No other implications hold in general.

Given some conditions on a system, one can derive another useful implication. Given the general vector case $\vec{X}(k+1) = \mathbf{A}(k)\vec{X}(k)$, where $\{\mathbf{A}(k)\}$ are mutually independent random matrices, [40] provides the following theorem, using a Lyapunov function of the form $\vec{X}^T \mathbf{Q} \vec{X}$, where \mathbf{Q} is positive definite (denoted as $\mathbf{Q} > 0$).

Theorem 3.2.1 *Let $\mathbf{Q} > 0$, $\mathbf{C} \geq 0$ and*

$$\mathbb{E}[\mathbf{A}(k)^T \mathbf{Q} \mathbf{A}(k)] - \mathbf{Q} = -\mathbf{C}. \quad (3.13)$$

Then $\mathbb{E}[\vec{X}(k)^T \mathbf{C} \vec{X}(k)] \rightarrow 0$ and $\vec{X}(k)^T \mathbf{C} \vec{X}(k) \rightarrow 0$ w.p.1. Let the $\mathbf{A}(k)$ be identically distributed. If $\{\vec{X}(k)\}$ is mean square stable (that is, $\mathbb{E}[\vec{X}(k)^T \vec{X}(k)] \rightarrow 0$), then for any $\mathbf{C} > 0$, there is a $\mathbf{Q} > 0$ satisfying (3.13).

Given this theorem, if $\{\mathbf{A}(k)\}$ are identically distributed and mutually independent in (3.4), there exists a solution \mathbf{Q} for (3.13) if we choose $\mathbf{C} = \mathbf{I}$. According to the theorem, the existence of the solution implies $\vec{X}(k)^T \vec{X}(k) \rightarrow 0$ w.p.1. This is a sufficient condition for w.p.1 stability when

$\{\mathbf{A}(k)\}$ are chosen independently of each other and from the same distribution at each k in equations (3.8)-(3.9).

3.3 Stability Conditions

First, we find the expression for the evolution of the mean dynamics by taking the expected value of system (3.8):

$$\begin{aligned}
\mathbb{E}[\hat{X}(k+1)] &= \mathbb{E}[\hat{\mathbf{A}}(k)\hat{X}(k)] \\
&= \int_{\mathbb{R}^{n(N+1)} \times n(N+1)} \int_{\mathbb{R}^{n(N+1)}} \hat{\mathbf{A}}\hat{X} p_{\hat{X}(k), \hat{\mathbf{A}}(k)}(\hat{X}, \hat{\mathbf{A}}) d\hat{X} d\hat{\mathbf{A}} \\
&= \sum_{i=1}^N w_i \int_{\mathbb{R}^{n(N+1)}} \hat{\mathbf{A}}_i \hat{X} p_{\hat{X}(k)}(\hat{X}) d\hat{X} \\
&= \sum_{i=1}^N w_i \hat{\mathbf{A}}_i \mathbb{E}[\hat{X}(k)],
\end{aligned} \tag{3.14}$$

where we exploited the property in equation (3.11). Define the deterministic variable $\hat{Y} = \mathbb{E}[\hat{X}]$. Then, the mean dynamics are given by

$$\hat{Y}(k+1) = \hat{\mathbf{A}} \hat{Y}(k), \tag{3.15}$$

where

$$\begin{aligned}
\hat{\mathbf{A}} &= \sum_{i=1}^N w_i \hat{\mathbf{A}}_i \\
&= \begin{bmatrix} \mathbf{A} & w_1 \mathbf{B} & w_2 \mathbf{B} & \dots & w_N \mathbf{B} \\ \mathbf{I} & \mathbf{0} & & \dots & \mathbf{0} \\ \mathbf{0} & \mathbf{I} & \mathbf{0} & \dots & \mathbf{0} \\ \vdots & \ddots & \ddots & \ddots & \vdots \\ \mathbf{0} & \dots & \mathbf{0} & \mathbf{I} & \mathbf{0} \end{bmatrix}.
\end{aligned} \tag{3.16}$$

By exploiting the structure of matrix (3.16), one may show that the characteristic equation can be simplified as

$$0 = \det(s\hat{\mathbf{I}} - \hat{\mathbf{A}}) = \det\left(s^{N+1}\mathbf{I} - s^N\mathbf{A} - \sum_{i=1}^N s^{N-i}w_i\mathbf{B}\right). \tag{3.17}$$

If all the $n(N+1)$ roots s of this equation lie inside the unit circle in the complex plane, the mean dynamics (5.12, 3.16) are asymptotically stable. We later show conditions under which the mean

dynamics provide a good deterministic approximation for the stochastic system.

Now, we determine the stability of the second moment, which implies point-wise asymptotic stability of the system (3.8)-(3.9). We remark that such an implication does not hold in general [27], but holds for system (3.8)-(3.9), for the case when $\hat{\mathbf{A}}$ is identically independently distributed [40]. The governing equations for the second moment of $\hat{X}(k)$ can be obtained from system (3.8) by calculating

$$\hat{X}(k+1)\hat{X}^T(k+1) = \hat{\mathbf{A}}(k)\hat{X}(k)\hat{X}^T(k)\hat{\mathbf{A}}^T(k), \quad (3.18)$$

and then taking the expected value on both sides

$$\mathbb{E}[\hat{X}(k+1)\hat{X}^T(k+1)] = \mathbb{E}[\hat{\mathbf{A}}(k)\hat{X}(k)\hat{X}^T(k)\hat{\mathbf{A}}^T(k)], \quad (3.19)$$

where the expectation operator is taken element-wise and the right hand side can be evaluated as

$$\begin{aligned} \mathbb{E}[\hat{\mathbf{A}}(k)\hat{X}(k)\hat{X}^T(k)\hat{\mathbf{A}}^T(k)] &= \int_{\mathbb{R}^{n(N+1)} \times \mathbb{R}^{n(N+1)}} \int_{\mathbb{R}^{n(N+1)}} \hat{\mathbf{A}}\hat{X}\hat{X}^T\hat{\mathbf{A}}^T p_{\hat{X}(k), \hat{\mathbf{A}}(k)}(\hat{X}, \hat{\mathbf{A}}) d\hat{X} d\hat{\mathbf{A}} \\ &= \sum_{i=1}^N w_i \int_{\mathbb{R}^{n(N+1)}} \hat{\mathbf{A}}_i \hat{X} \hat{X}^T \hat{\mathbf{A}}_i^T p_{\hat{X}(k)}(\hat{X}) d\hat{X} \\ &= \sum_{i=1}^N w_i \hat{\mathbf{A}}_i \int_{\mathbb{R}^{n(N+1)}} \hat{X} \hat{X}^T p_{\hat{X}(k)}(\hat{X}) d\hat{X} \hat{\mathbf{A}}_i^T \\ &= \sum_{i=1}^N w_i \hat{\mathbf{A}}_i \mathbb{E}[\hat{X}(k)\hat{X}^T(k)] \hat{\mathbf{A}}_i^T, \end{aligned} \quad (3.20)$$

where, again, we used property (3.11). Defining the deterministic matrix-valued variable

$$\hat{\mathbf{G}}(k) = \mathbb{E}[\hat{X}(k)\hat{X}^T(k)], \quad (3.21)$$

and substituting this into equations (3.19) and (5.15) we obtain the deterministic system

$$\hat{\mathbf{G}}(k+1) = \sum_{i=1}^N w_i \hat{\mathbf{A}}_i \hat{\mathbf{G}}(k) \hat{\mathbf{A}}_i^T. \quad (3.22)$$

Note that $\hat{\mathbf{G}}$ is symmetric. The equation for the second moment is linear, but it is not trivial to determine stability as both sides are matrix valued. To resolve this problem we transform system (3.22) into state space form where the state vector is composed of only the first n columns of $\hat{\mathbf{G}}$ stacked on top of each other and their delayed versions. We show that no other elements of $\hat{\mathbf{G}}$ need be considered. Then, by exploiting the structure of $\hat{\mathbf{A}}_i$, we obtain a state matrix whose eigenvalues can be calculated to determine stability. The following notation is used throughout the rest of the

paper:

$[\hat{\mathbf{G}}(k)]_{i,j} \in \mathbb{R}$ the element of the $\hat{\mathbf{G}}(k)$ matrix in the i -throw and j -th column

$[\hat{\mathbf{G}}(k)]_{:,j} \in \mathbb{R}^{n(N+1)}$ the j -th column of the matrix $\hat{\mathbf{G}}(k)$

$[\hat{\mathbf{G}}(k)]_{l:m,p:q} \in \mathbb{R}^{(m-l+1) \times (q-p+1)}$ the submatrix contained in rows l through m and columns p through q

We also define

$$G_m^i(k) = [\hat{\mathbf{G}}(k)]_{in+1:(i+1)n,m} \in \mathbb{R}^n. \quad (3.23)$$

With this we define

$$\hat{G}_j(k) = \begin{bmatrix} G_j^0(k) \\ G_j^1(k) \\ G_j^2(k) \\ \vdots \\ G_j^N(k) \end{bmatrix}, \quad \tilde{G}(k) = \begin{bmatrix} \hat{G}_1(k) \\ \hat{G}_2(k) \\ \vdots \\ \hat{G}_n(k) \end{bmatrix}, \quad (3.24)$$

where $\hat{G}_j(k) \in \mathbb{R}^{n(N+1)}$ is the j -th column vector of the second moment matrix $\hat{\mathbf{G}}(k)$ and the vector $\tilde{G}(k) \in \mathbb{R}^{n^2(N+1)}$ stacks the first n columns of $\hat{G}_j(k)$ under each other.

Using index notation for system (3.22), we find an expression for each element of the second moment matrix in the form

$$\begin{aligned} [\hat{\mathbf{G}}(k+1)]_{p,j} &= \sum_{i=1}^N w_i [\hat{\mathbf{\Lambda}}_i \hat{\mathbf{G}}(k) \hat{\mathbf{\Lambda}}_i^T]_{p,j} \\ &= \sum_{i=1}^N w_i \sum_{m=1}^{n(N+1)} [\hat{\mathbf{\Lambda}}_i]_{p,m} \sum_{k=1}^{n(N+1)} [\hat{\mathbf{\Lambda}}_i]_{j,k} [\hat{\mathbf{G}}(k)]_{k,m}. \end{aligned} \quad (3.25)$$

The expression of each element can be simplified by looking at special cases for index values, given that we know the structure of $\hat{\mathbf{\Lambda}}_i$; cf. matrix (3.9).

For example, notice that for $l > n$ the elements of $\{\hat{\mathbf{\Lambda}}_i\}$ are such that

$$[\hat{\mathbf{\Lambda}}_i]_{l,m} = \delta(l - (m + n)),$$

where δ is the Dirac delta. Applying this property for $j, p > n$, equation (3.25) implies that

$$\begin{aligned}
[\hat{\mathbf{G}}(k+1)]_{p,j} &= \sum_{i=1}^N w_i \sum_{m=1}^{n(N+1)} \delta(p-(m+n)) \sum_{k=1}^{n(N+1)} \delta(j-(k+n)) [\hat{\mathbf{G}}(k)]_{k,m} \\
&= \sum_{i=1}^N w_i [\hat{\mathbf{G}}(k)]_{j-n,p-n} = [\hat{\mathbf{G}}(k)]_{j-n,p-n} \\
&= [\hat{\mathbf{G}}(k)]_{p-n,j-n},
\end{aligned} \tag{3.26}$$

which yields

$$G_j^i(k+1) = G_{j-n}^{i-1}(k) \quad \text{for } i \geq 1, j > n. \tag{3.27}$$

Similarly, considering $p \leq n$ and $j > n$ we obtain

$$\begin{aligned}
[\hat{\mathbf{G}}(k+1)]_{p,j} &= \sum_{i=1}^N w_i \sum_{m=1}^{n(N+1)} [\hat{\mathbf{A}}_i]_{p,m} \sum_{k=1}^{n(N+1)} \delta(j-(k+n)) [\hat{\mathbf{G}}(k)]_{k,m} \\
&= \sum_{i=1}^N w_i \sum_{m=1}^{n(N+1)} [\hat{\mathbf{A}}_i]_{p,m} [\hat{\mathbf{G}}(k)]_{j-n,m},
\end{aligned} \tag{3.28}$$

which gives

$$G_j^0(k+1) = \mathbf{A} G_{j-n}^0(k) + \sum_{i=1}^N w_i \mathbf{B} G_{j-n}^i(k). \tag{3.29}$$

We combine equations (3.27) and (3.29) to describe the column vector update

$$\hat{G}_j(k+1) = \hat{\mathbf{A}} \hat{G}_{j-n}(k), \tag{3.30}$$

where $\hat{\mathbf{A}}$ is given by matrix (3.16) and $\hat{G}_j(k)$ is defined by the first of vectors (3.24).

For $p, j \leq n$, equation (3.25) yields

$$\begin{aligned}
[\hat{\mathbf{G}}(k+1)]_{p,j} &= \sum_{i=1}^N w_i \sum_{m=1}^{n(N+1)} [\hat{\mathbf{A}}_i]_{p,m} (\hat{\mathbf{A}}_i \hat{G}_m(k))_j \\
&= \sum_{i=1}^N w_i \sum_{m=1}^{n(N+1)} [\hat{\mathbf{A}}_i]_{p,m} e_j^T \hat{\mathbf{A}}_i \hat{G}_m(k), \\
&= \sum_{m=1}^n [\mathbf{A}]_{p,m} e_j^T \hat{\mathbf{A}}_i \hat{G}_m(k) \\
&\quad + \sum_{i=1}^N w_i \sum_{m=in+1}^{n(i+1)} [\hat{\mathbf{A}}_i]_{p,m} e_j^T \hat{\mathbf{A}}_i \hat{G}_m(k), \\
&= \sum_{m=1}^n [\mathbf{A}]_{p,m} e_j^T \hat{\mathbf{A}}_i \hat{G}_m(k) \\
&\quad + \sum_{i=1}^N w_i \sum_{m=1}^n [\mathbf{B}]_{p,m} e_j^T \hat{\mathbf{A}}_i \hat{\mathbf{A}}^i \hat{G}_m(k-i),
\end{aligned} \tag{3.31}$$

where the last equality follows from the column vector update (3.30), $e_j \in \mathbb{R}^{n(N+1)}$, with all elements equal to 0 except the j -th element equal to 1 and $\hat{\Lambda}^i$ denotes taking the matrix $\hat{\Lambda}$ to the i -th power. Utilizing vectors (3.24), equation (3.31) implies

$$G_j^0(k+1) = (\mathbf{A} \otimes (e_j^T \hat{\Lambda})) \tilde{G}(k) + \sum_{i=1}^N w_i (\mathbf{B} \otimes (e_j^T \hat{\Lambda}_i \hat{\Lambda}^i)) \tilde{G}(k-i), \quad (3.32)$$

for $j \in [1, 2, \dots, n]$, where \otimes denotes the Kronecker product.

Last, we consider the case $p > n$ and $j \leq n$ in equation (3.25):

$$\begin{aligned} [\hat{\mathbf{G}}(k+1)]_{p,j} &= \sum_{i=1}^N w_i \sum_{k=1}^{n(N+1)} [\hat{\Lambda}_i]_{j,k} [\hat{\mathbf{G}}(k)]_{k,p-n} \\ &= \sum_{i=1}^N w_i e_j^T \hat{\Lambda}_i \hat{G}_{p-n}(k) = e_j^T \hat{\Lambda} \hat{G}_{p-n}(k), \end{aligned} \quad (3.33)$$

which implies

$$\begin{aligned} G_j^i(k+1) &= \begin{bmatrix} [\hat{\mathbf{G}}(k+1)]_{i n+1, j} \\ [\hat{\mathbf{G}}(k+1)]_{i n+2, j} \\ \vdots \\ [\hat{\mathbf{G}}(k+1)]_{(i+1)n, j} \end{bmatrix} \\ &= (\mathbf{I} \otimes (e_j^T \hat{\Lambda}^i)) \begin{bmatrix} \hat{G}_1(k-i+1) \\ \hat{G}_2(k-i+1) \\ \vdots \\ \hat{G}_n(k-i+1) \end{bmatrix}. \end{aligned} \quad (3.34)$$

Now we have an expression for every element of the vector $\hat{G}_j(k)$ in (3.24) for $j \in [1, \dots, n]$ given by equations (3.32)-(3.34) and we can, therefore, find an expression for the time evolution of the vector $\tilde{G}(k)$ in (3.24) as a function of itself and its delayed values. That is, we can write an expression for the evolution of the first n columns of the second moment matrix. Some algebraic manipulation leads to

$$\hat{\tilde{G}}(k+1) = \hat{\mathbf{A}} \hat{\tilde{G}}(k), \quad (3.35)$$

where

$$\hat{G}(k) = \begin{bmatrix} \tilde{G}(k) \\ \tilde{G}(k-1) \\ \vdots \\ \tilde{G}(k-N) \end{bmatrix}, \quad (3.36)$$

so that $\hat{G}(k) \in \mathbb{R}^{n^2(N+1)^2}$ (cf. equation (3.24)) and

$$\hat{\mathbf{A}} = \begin{bmatrix} \tilde{\mathbf{A}} & \tilde{\mathbf{B}}_1 & \tilde{\mathbf{B}}_2 & \cdots & \tilde{\mathbf{B}}_N \\ \tilde{\mathbf{I}} & \mathbf{0} & \mathbf{0} & \cdots & \mathbf{0} \\ \mathbf{0} & \tilde{\mathbf{I}} & \mathbf{0} & \cdots & \mathbf{0} \\ \vdots & \ddots & \ddots & \ddots & \vdots \\ \mathbf{0} & \cdots & \mathbf{0} & \tilde{\mathbf{I}} & \mathbf{0} \end{bmatrix}. \quad (3.37)$$

Here we used the identity matrix $\tilde{\mathbf{I}} \in \mathbb{R}^{n^2(N+1) \times n^2(N+1)}$ and

$$\tilde{\mathbf{A}} = \begin{bmatrix} \mathbf{A} \otimes (e_1^T \hat{\mathbf{\Lambda}}) \\ \mathbf{I} \otimes (e_1^T \hat{\mathbf{\Lambda}}) \\ \mathbf{0} \\ \vdots \\ \mathbf{0} \\ \hline \mathbf{A} \otimes (e_2^T \hat{\mathbf{\Lambda}}) \\ \mathbf{I} \otimes (e_2^T \hat{\mathbf{\Lambda}}) \\ \mathbf{0} \\ \vdots \\ \mathbf{0} \\ \hline \vdots \\ \hline \mathbf{A} \otimes (e_n^T \hat{\mathbf{\Lambda}}) \\ \mathbf{I} \otimes (e_n^T \hat{\mathbf{\Lambda}}) \\ \mathbf{0} \\ \vdots \\ \mathbf{0} \end{bmatrix}, \quad \tilde{\mathbf{B}}_i = \begin{bmatrix} w_i (\mathbf{B} \otimes (e_1^T \hat{\mathbf{\Lambda}}_i \hat{\mathbf{\Lambda}}^i)) \\ \mathbf{0} \\ \vdots \\ \mathbf{0} \\ \mathbf{I} \otimes (e_1^T \hat{\mathbf{\Lambda}}^{i+1}) \\ \mathbf{0} \\ \vdots \\ \mathbf{0} \\ \hline w_i (\mathbf{B} \otimes (e_2^T \hat{\mathbf{\Lambda}}_i \hat{\mathbf{\Lambda}}^i)) \\ \mathbf{0} \\ \vdots \\ \mathbf{0} \\ \mathbf{I} \otimes (e_2^T \hat{\mathbf{\Lambda}}^{i+1}) \\ \mathbf{0} \\ \vdots \\ \mathbf{0} \\ \hline \vdots \\ \hline w_i (\mathbf{B} \otimes (e_n^T \hat{\mathbf{\Lambda}}_i \hat{\mathbf{\Lambda}}^i)) \\ \mathbf{0} \\ \vdots \\ \mathbf{0} \\ \mathbf{I} \otimes (e_n^T \hat{\mathbf{\Lambda}}^{i+1}) \\ \mathbf{0} \\ \vdots \\ \mathbf{0} \end{bmatrix}, \quad (3.38)$$

for $i = 1, \dots, N - 1$ and

$$\tilde{\mathbf{B}}_N = \begin{bmatrix} w_N (\mathbf{B} \otimes (e_1^T \hat{\mathbf{\Lambda}}_N \hat{\mathbf{\Lambda}}^N)) \\ \mathbf{0} \\ \vdots \\ \mathbf{0} \\ \hline w_N (\mathbf{B} \otimes (e_2^T \hat{\mathbf{\Lambda}}_N \hat{\mathbf{\Lambda}}^N)) \\ \mathbf{0} \\ \vdots \\ \mathbf{0} \\ \hline \vdots \\ \hline w_N (\mathbf{B} \otimes (e_n^T \hat{\mathbf{\Lambda}}_N \hat{\mathbf{\Lambda}}^N)) \\ \mathbf{0} \\ \vdots \\ \mathbf{0} \end{bmatrix}. \quad (3.39)$$

The matrix $\mathbf{I} \otimes (e_j^T \hat{\mathbf{\Lambda}}^i) \in \mathbb{R}^{n \times n^2(N+1)}$ contains $e_j^T \hat{\mathbf{\Lambda}}^i \in \mathbb{R}^{1 \times n(N+1)}$ along the ‘‘diagonal’’. Each block delimited by the dashed line is of dimension $n^2(N+1) \times n^2(N+1)$ and for $\tilde{\mathbf{B}}_i$ the matrix $\mathbf{I} \otimes (e_j^T \hat{\mathbf{\Lambda}}^{i+1})$ begins in the $((i+1)n+1)$ -th row of each block. Notice that the structure of the matrix (3.37) resembles the structure of matrix (3.16). Thus, similarly to equation (3.17), the characteristic equation can be written as

$$0 = \det(s\hat{\mathbf{I}} - \hat{\mathbf{A}}) = \det\left(s^{N+1}\tilde{\mathbf{I}} - s^N\tilde{\mathbf{A}} - \sum_{m=1}^N s^{N-m}\tilde{\mathbf{B}}_m\right). \quad (3.40)$$

We are now ready to state the following theorem.

Theorem 3.3.1 *The stochastically delayed system (3.4) is point wise asymptotically stable if all $n^2(N+1)^2$ roots of equation (3.40) lie within the unit circle in the complex plane.*

Proof 1 The eigenvalues being within the unit circle imply stability of system (3.35) [28,41], which in turn implies second moment stability of system (3.22). Finally, stability of the second moment implies point-wise asymptotic stability of the stochastic system (3.4).

3.4 Examples

Here we apply the stability conditions derived for mean and second moment to scalar examples with different delay distributions $p_{\tau(k)}(\sigma)$. System (3.4) reduces to

$$x(k+1) = ax(k) + bx(k - \tau(k)). \quad (3.41)$$

Figure 3.1 shows uniform delay distributions (left) and distributions with two equally probable delays (right), which we refer to as toggle distributions. E and V refer to the expected value and the variance of the delay distributions.

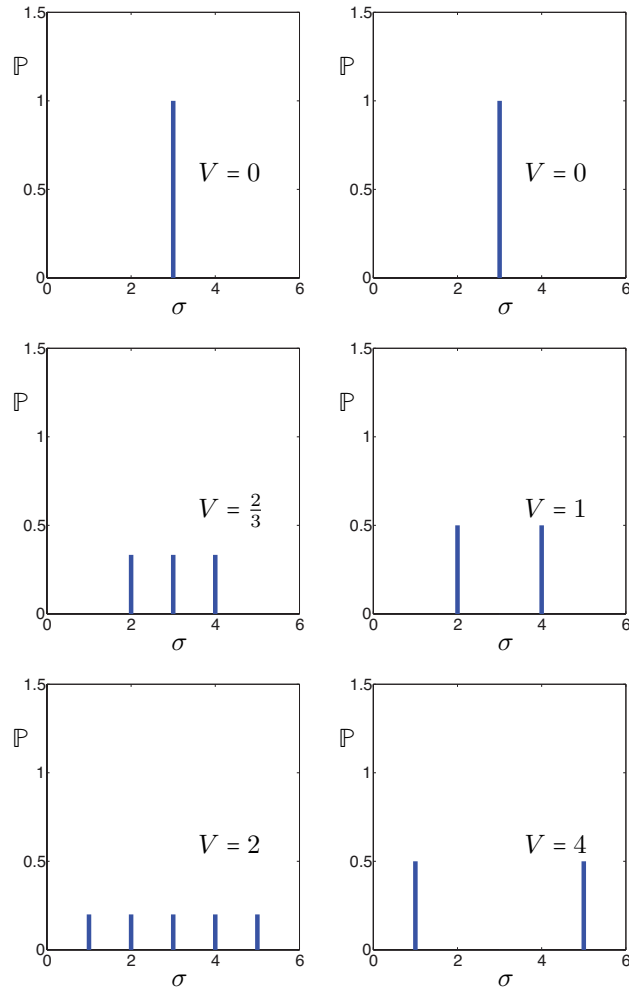


Figure 3.1: Left: Discrete uniform delay distribution with expected value $E = 3$. Right: Discrete toggle distribution with $E = 3$. The variance V is listed in each panel.

Although stability of the second moment implies stability of the mean, it is interesting to take

a look at the region of stability for the mean since it provides necessary conditions for stability. In [23] we showed that introducing additional delays to an already delayed continuous-time system may stabilize an unstable system. It is interesting to see that a similar result can be obtained for a discrete-time system.

Figure 3.2 shows the stability region for the mean dynamics

$$y(k+1) = a(k) + b \sum_{i=1}^N w_i y(k-i). \quad (3.42)$$

with uniform delay distribution (of expected value E and variance V). The black (dash-dot) and red (dotted) curves indicate an eigenvalue crossings of the unit circle on the complex plane at 1 and -1 . The green (solid) curves indicate a pair complex conjugate eigenvalues crossing the unit circle. One can see that as the variance is increased, the region of stability (shaded region) increases. It is important to point out the regions of stability for a single delay is not contained in the regions of stability for the distributed delays.

Next, we look at w.p.1 stability region. Recall that a system with identically independently distributed delays is stable w.p.1. if the second moment is stable. We first consider such systems with uniform delay distribution, then look at systems where the delay toggles between two values, each with equal probability.

The left panels in Fig. 3.3 show the stability boundaries of the non-deterministic system with uniform delay distribution. The curves indicate the stability losses of the mean as in Fig. 3.2, but here the shaded region indicates the region of w.p.1 stability (i.e., stability of the second moment). The shaded region was found by sweeping across the parameter space (a, b) and checking the eigenvalues of the corresponding Markovian representation in equation (3.35).

The right panels in Fig. 3.3 show stability charts for the toggle distribution. Again, we plot the mean stability curves and indicate the second moment stability regions, that imply w.p.1 stability, by shading. Here, the w.p.1 stability region is dominated by the region of stability for the mean of the system.

The introduction of stochasticity in the delay distorts the stability region when compared to the case of a single deterministic delay, as can be seen in Fig. 3.4. Since some of the w.p.1 stability regions extend outside the stability bounds for the deterministic system, we can stabilize the system by introducing uncertainty in the delay. We demonstrate this by numerical simulation in Fig. 3.4 where the parameters correspond to the mark “x” in the left panel.

We looked at two different types of delay distributions and found they had very different effects on

the region of stability. In the case of the uniformly distributed delays, a worst case scenario would certainly be conservative. However, for the cases with two equally probable delays, the stability region of the mean seemed to provide a good approximation of the w.p.1 stability region. We also demonstrated that introducing stochasticity in the delay may stabilize the system. This shows how the inclusion of stochastic delays can result in counterintuitive behavior.

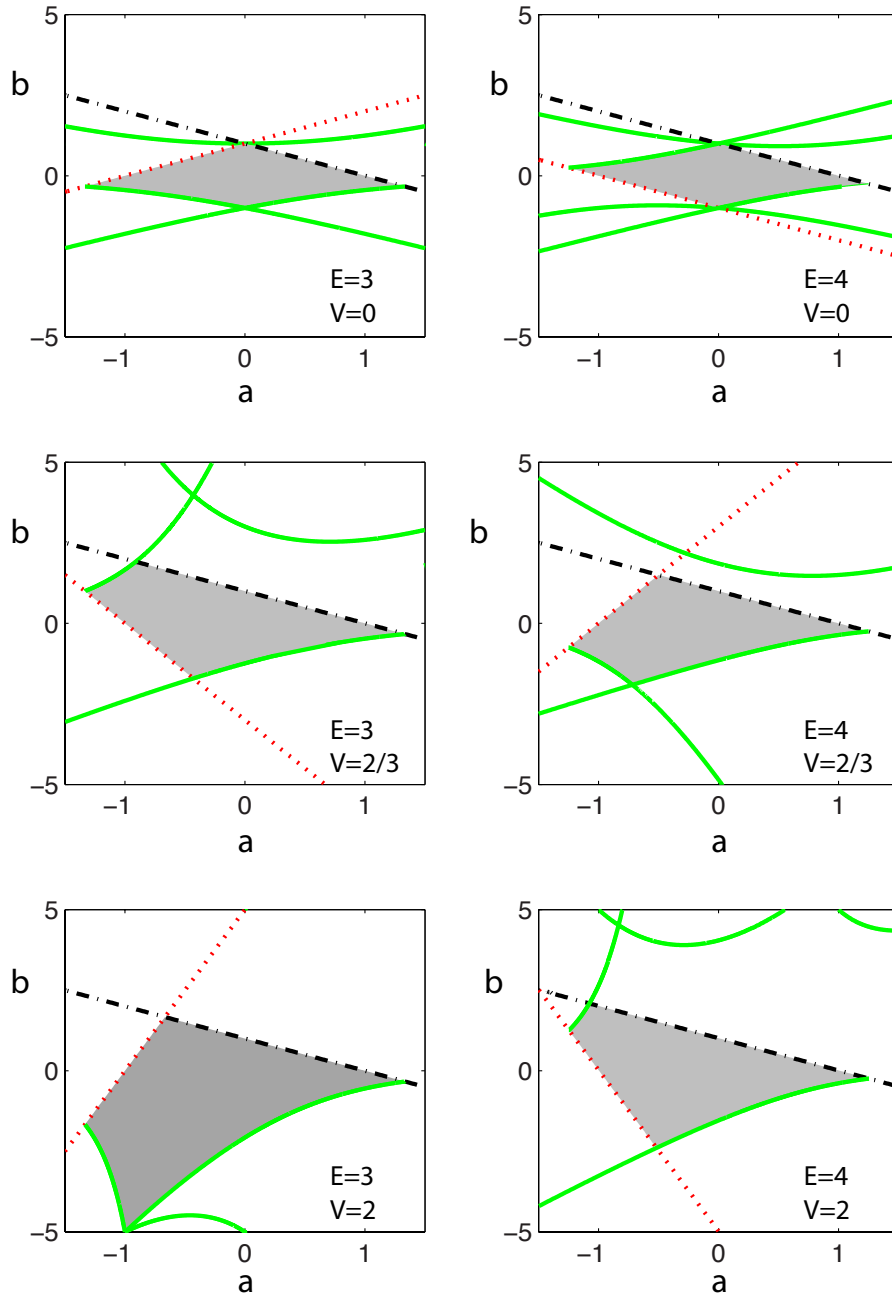


Figure 3.2: Stability charts for the mean for uniform delay distributions. Shading indicates stability. When crossing a black (dash-dot) curve (from stable to unstable) an eigenvalue crosses the unit circle at 1 (outward), while crossing a red (dotted) curve indicates that an eigenvalue crosses the unit circle at -1 . Crossing a green (solid) curve indicates that a pair of complex conjugate eigenvalues crosses the unit circle.

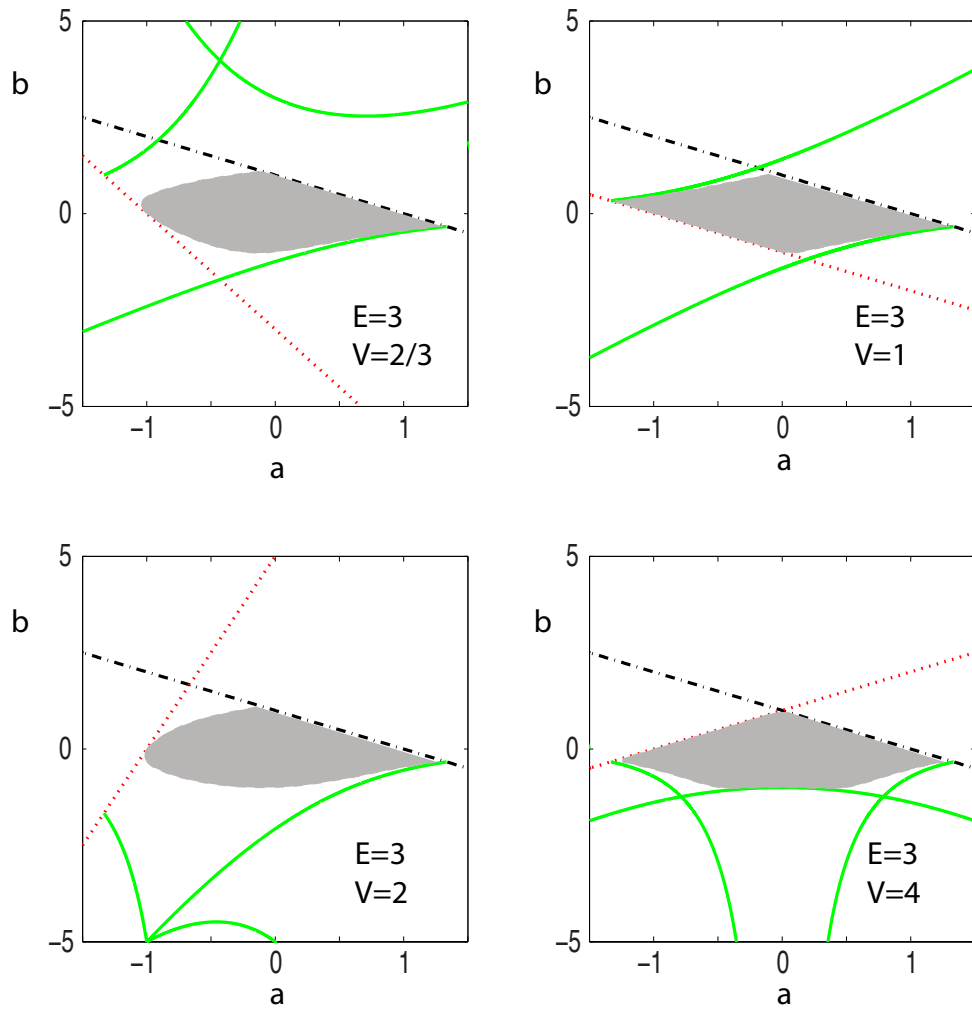


Figure 3.3: Left: Stability boundaries for a uniform delay distribution. Right: Stability boundaries for toggle distribution. In all panels, the curves represent the stability losses of the mean as in Fig. 3.2, while the shaded region indicates w.p.1 stability given by the second moment.

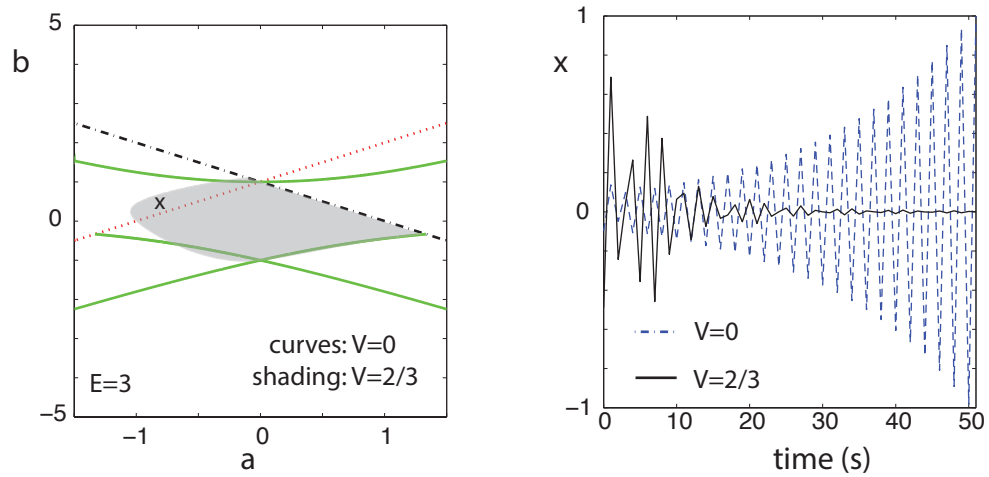


Figure 3.4: Left: Comparing stability for the case of a deterministic single delay of $\tau = 3$ (curves) with w.p.1 stability region (shaded) of a uniformly stochastically varying delay with mean $E = 3$. Right: Simulation comparing the cases deterministic and stochastic delay for $a = -0.79$ and $b = 0.3$ as indicated by “x”.

3.5 Application to an Autoregulatory network with stochastic delays

In this section the method derived in Chapter 3 is applied to an autoregulatory network with stochastically-varying delayed feedback. Consider the following model of an autoregulatory network

$$\dot{x}(t) = -\gamma x(t) + \alpha \frac{1}{1 + (x(t - \tau_t)/K_x)^2}, \quad (3.43)$$

where the delay τ_t varies stochastically and is selected from a distribution $g(\tau)$. Applying the zero order hold method with a sampling time of T , an equivalent discrete time system is given by,

$$x(k+1) = d_2 x(k) + d_1 \kappa x(k - \tau_k), \quad (3.44)$$

where $d_2 = e^{-T\gamma}$, $d_1 = \frac{1}{\gamma}(1 - e^{-T\gamma})$. The distribution from which the delay is selected is discretized using a rectangular approximation:

$$\begin{aligned} \mathbb{P}(n\Delta t < \tau_t < (n+1)\Delta t) &= \int_{n\Delta t}^{(n+1)\Delta t} g(\tau) d\tau \\ &\approx \int_{n\Delta t}^{(n+1)\Delta t} g((n+1/2)\Delta t) d\tau \\ &= g((n+1/2)\Delta t) \int_{n\Delta t}^{(n+1)\Delta t} d\tau \\ &= g((n+1/2)\Delta t) \Delta t. \end{aligned} \quad (3.45)$$

In order to apply the methods in Chapter 3, the distribution needs to have finite support. Therefore the distribution $g(\tau)$ is truncated such that $g(\tau) = 0$ for $\tau > E + 3 * \sigma$, where σ is the standard deviation. For the gamma distribution,

$$\sigma = \sqrt{E/a}.$$

The discrete delay τ_k will be selected from a discretized distribution such that

$$\mathbb{P}(\tau_k = n) = g((n+1/2)\Delta t) \Delta t. \quad (3.46)$$

Figure 3.5 shows stability plots for system (3.44) with different distribution parameters. The distribution is an Erlang distribution with mean $E = 3$. The mean is held constant and the relative variance is varied through N . Recall that $R = 1/N$. Furthermore, the stability curves of the stochas-

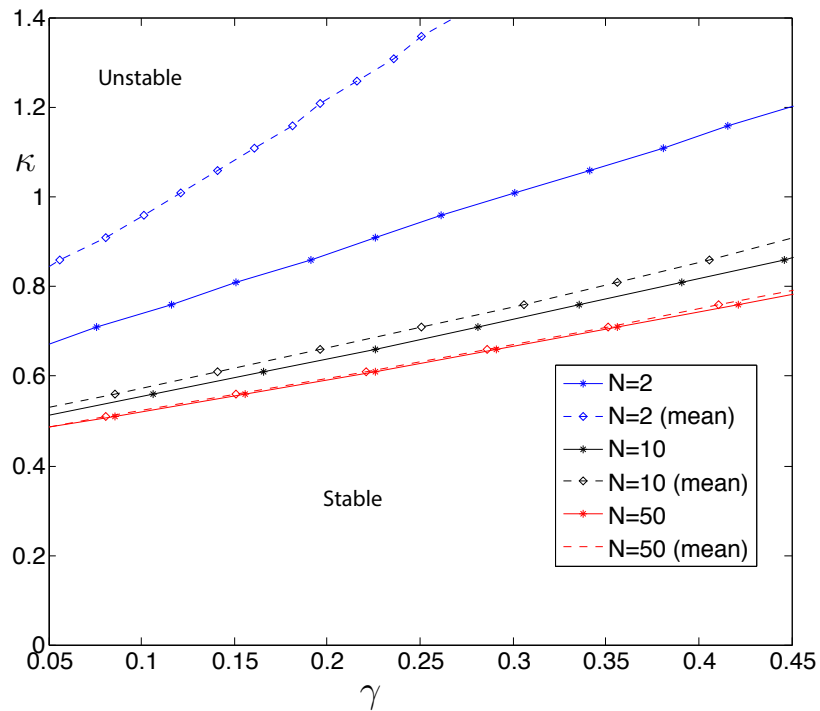


Figure 3.5: Stability plots for system (3.44) for the *Erlang* with $E = 3$ and various values of N . Stability curves for the stochastic system are compared to those of the mean dynamics.

tic system are compared to those of the mean dynamics. The stability region increases as the relative variance increases. This may be in line with intuition for the deterministic case, since the distribution approaches a discrete delay as $N \rightarrow 0$ and delays are known to destabilize systems. However, this is a bit more surprising in the stochastic case since the upper bound on the possible delays is being increased with an increased distribution. Also, note that the stability bounds for the stochastic system and the mean dynamics approach each other as the distribution gets tighter, just as one would expect.

Chapter 4

Deterministic Delay-Based Model

In this chapter the effects of delays on system dynamics are investigated through a deterministic delay-based modeling framework. Using the discretized, heuristically derived description in equation (3.3) we can rearrange terms and as $\Delta t \rightarrow 0$ we get the following differential equation:

$$\frac{dX}{dt} = -\gamma X(t) + f(Y(t - \tau(t))). \quad (4.1)$$

We note that the average dynamics in the limit as $\Delta t \rightarrow 0$ are given by the more familiar form

$$\frac{d\hat{X}}{dt} = -\gamma \hat{X}(t) + \int_0^\infty f(\hat{Y}(t - \tau))g(\tau)d\tau, \quad (4.2)$$

where $\hat{X} \doteq \mathbb{E}[X]$ and $\hat{Y} \doteq \mathbb{E}[Y]$. In the discretized system, the probability density function of the delay was also discretized such that $\tau(k\Delta t) = i$ with probability w_i . In the the continuous limit the distribution from which τ is selected converges to a continuous probability density function $g(\tau)$, which for transcription was shown to be the Erlang distribution. This is the form of the system that emerges in the thermodynamic limit of the Langevin equation for the stochastic system. Distributed-delay systems provide a model for the average dynamics which may hold as an appropriate model for systems with intercellular signaling or high plasmid copy numbers. Previous work has shown how stability regions of a system with delays greatly depend upon the shape of the distribution $g(\tau)$ of the delays [5,6,73]. Assuming the Erlang distribution derived previously captures well the distribution on protein production delays, system stability and robustness are investigated for systems with an Erlang distributed delay in feedback. Discrete delays are also considered, as the Erlang distribution was shown to approach a delta function in the appropriate limits.

First, a brief overview of delay differential equations is provided. Then, the dynamics of a system with an Erlang distributed-delay feedback is investigated. The stable parameter space and induced

limit cycles (in the case of instability) are analyzed as a functions of the mean and variance of the distribution function.

4.1 Review of DDEs

An brief overview of delay differential equations is given. More detailed information can be found in Hale *et al.* [30] and Lunel *et al.* [48]. Consider the simplest nonlinear delay differential equation with a single delay:

$$\frac{dx}{dt}(t) = F(x(t), x(t - \tau)). \quad (4.3)$$

For a unique solution one must specify an initial condition, which in this case is a continuous function $x(t) = \varphi(t)$ for $-r \leq t \leq 0$. Note that this is an infinite dimensional system. The solution $x(t)$ for $0 \leq t \leq \tau$ satisfies

$$\frac{dx}{dt}(t) = F(x(t), \varphi(t - \tau)) \quad \text{for } 0 \leq t \leq \tau, \quad x(0) = \varphi(0), \quad (4.4)$$

which can be shown to have a unique solution. Using the solution on the time interval $0 \leq t \leq \tau$, one can proceed to find the solution $x(t)$ for $\tau \leq t \leq 2\tau$ by repeating the same procedure. There exists methods to stability analysis for nonlinear delay differential equations through the method of Liapunov functionals. However, this is beyond the scope of the thesis. We reduce our attention to linear delay differential equations of the form

$$\frac{dx}{dt}(t) = \mathbf{A}x(t) + \mathbf{B}x(t - \tau). \quad (4.5)$$

This system has more familiar methods of stability analysis. Stability can be determined by the roots of the characteristic equation in much the same way as is done for differential equations without delays. The characteristic equation can be derived by substituting the exponential solution $x(t) = e^{\lambda t}$ into system 4.5:

$$\det p(z) = 0 \quad \text{with} \quad p(z) = \lambda \mathbf{I} - \mathbf{A} - \mathbf{B}e^{-\lambda \tau}. \quad (4.6)$$

Note that there are infinitely many roots. In the scalar case this reduces to solving

$$\lambda - a - b e^{-\lambda \tau} = 0, \quad (4.7)$$

from which one can derive bifurcation curves through the substitution $\lambda = j\omega$.

We have not discussed distributed delay differential equations, better known as integro-differential

equations. For the purpose of analysis, in this thesis, the differential equations with distributed delay take the following form:

$$\frac{dX}{dt} = -aX(t) + b \int_0^\infty X(t-\tau)g(\tau)d\tau. \quad (4.8)$$

These are generally difficult systems to deal with. In this work, we focus on the case where $g(\tau)$ is either the Erlang distribution, which we have shown to have a finite dimensional representation, or where $g(\tau) = \delta(c)$, where c is a constant, which reduces the system to a simple delay differential equation.

4.2 Distributed-delay feedback system

Using a different choice of state variable and closing the system by setting $Y = X$, system (4.2) can be represented as

$$\begin{aligned} \dot{x} &= -\gamma x + f(\tilde{x}) \\ \tilde{x} &= \int_0^\infty x(t-\tau)g(\tau) d\tau. \end{aligned} \quad (4.9)$$

Here, the state variable is the first state in the sequence of chemical reactions leading to a distributed delay, whereas in system (4.2) the state variable modeled was the last state in the sequence of chemical reactions or the concentration of the protein being measured. For stability analysis, the choice of the state variable is irrelevant, so we choose to work with the more tractable form in equation (4.9). We investigate a Goodwin-type negative feedback system where the nonlinearity $f(x)$ is a positive definite Hill-type function. Furthermore,

$$\dot{x}(t, x)|_{x=0} > 0$$

for any time t , initial condition or time history, so $x \geq 0$ for all t .

4.2.1 Stability

Here we investigate point wise asymptotic stability as a function of mean and variance of the delay distributions. We can do a bifurcation analysis on the nonlinear integro-differential equation [6].

The linearized system is

$$\frac{dx'}{dt} = -\gamma x' - \beta \tilde{x}', \quad (4.10)$$

where

$$x' = x - x_*$$

and

$$\tilde{x}' = \int_0^\infty x'(t - \tau)g(\tau)d\tau.$$

The subscript * refers to the equilibrium point of the system. Here $g(\tau)$ is the Erlang distribution function, and hence represents a finite sequence of chemical reactions which impart an effective delay.

Furthermore,

$$\beta = -\left.\frac{\partial f}{\partial \tilde{x}}\right|_{\tilde{x}=x_*} > 0, \quad (4.11)$$

since the Hill function $f(x)$ is monotonically decreasing for $x \geq 0$. Now we take the Laplace transform of the linearized system, which gives

$$sX'(s) = -\gamma X'(s) - \beta G(s)X'(s),$$

assuming $x'(0) = 0$. $G(s)$ is the Laplace transform of the impulse function $g(\tau)$, which was shown previously to be

$$G(s) = \frac{a^N}{(s+a)^N}.$$

The resulting characteristic equation is

$$s + \gamma + \beta G(s) = 0,$$

which can be rewritten as a function of the mean E and the relative variance R of the distribution

$$s + \gamma + \beta \left(\frac{1}{sRE + 1} \right)^{\frac{1}{R}} = 0, \quad \text{where } \frac{1}{R} \in \mathbb{Z}^+. \quad (4.12)$$

Stability is lost when an eigenvalue crosses to the left hand plane of the complex plane. The bifurcation boundary can be found by substituting $s = 0$ and $s = i\omega$ in equation (4.12). Substituting $s = 0$ gives

$$\gamma = -\beta$$

and substituting $s = i\omega$ gives the following system of equations:

$$\begin{aligned} & [i\operatorname{Im}(P(i\omega)) + \operatorname{Re}(P(i\omega))](i\omega + \gamma) + \beta = 0 \\ i[\gamma\operatorname{Im}(P(i\omega)) + \omega\operatorname{Re}(P(i\omega))] + [-\omega\operatorname{Im}(P(i\omega)) + \gamma\operatorname{Re}(P(i\omega)) + \beta] &= 0, \end{aligned} \quad (4.13)$$

which is equivalent to the following parametric equations:

$$\begin{aligned} \gamma &= -\frac{\omega\operatorname{Re}(P(i\omega))}{\operatorname{Im}(P(i\omega))} \\ \beta &= \omega\operatorname{Im}(P(i\omega)) - \gamma\operatorname{Re}(P(i\omega)) \\ &= \operatorname{Im}(P(i\omega))\left(\omega + \frac{\gamma^2}{\omega}\right), \end{aligned} \quad (4.14)$$

where $P(s) = (sRE + 1)^{\frac{1}{R}}$.

It was shown in Chapter 2 that as $R \rightarrow 0$ with E held constant the distribution approaches a delta function. For comparison purposes we find the bifurcation boundary for the discrete delayed system with characteristic equation

$$s + \gamma + \beta e^{-sE} = 0. \quad (4.15)$$

Substituting $s = 0$ gives the same delay-independent boundary $\gamma = -\beta$. Substituting $s = i\omega$ gives

$$\begin{aligned} i\omega + \gamma + \beta[\cos(\omega E) - i\sin(\omega E)] &= 0 \\ i[\omega - \beta\sin(\omega E)] + [\gamma + \beta\cos(\omega E)] &= 0, \end{aligned} \quad (4.16)$$

which gives

$$\begin{aligned} \beta &= \frac{\omega}{\sin(\omega E)} \\ \gamma &= -\beta\cos(\omega E). \end{aligned} \quad (4.17)$$

We expect the stability bounds in equation (4.14) to approach those in equation (4.17) in the same limit. Applying the trigonometric identity $\sin^2 + \cos^2 = 1$ to equation (4.17) gives the additional relation

$$\omega^2 + \gamma^2 = \beta^2. \quad (4.18)$$

In this case we only wish to consider $(\gamma, \beta) \geq 0$. Figure 4.1 shows selected bifurcation curves for

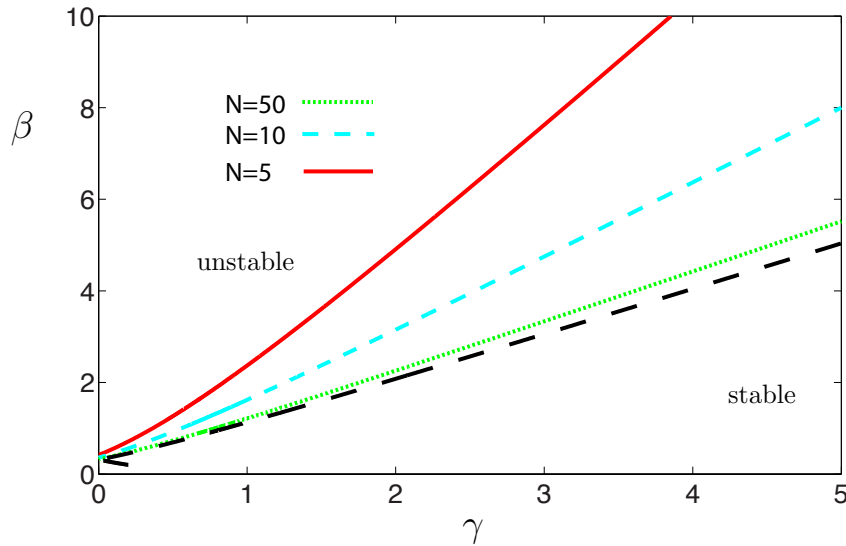


Figure 4.1: Stability bounds for $E = 3$ and different values of N where $R = 1/N$. The black dashed line indicates the stability bound for the discrete delay system.

the distributed and discrete delay systems. We show only the first curve that indicates crossing of the first pair of eigenvalues across the imaginary axis to the right half plane. As N increases the stability bound approaches that of the system with a single discrete delay. Figure 4.2 shows similar bifurcation curves for the same distribution (N constant) with varying mean E . We see that as the delay increases the stability bound approaches a delay independent stability bound. The discrete delay system is always stable for $\beta \leq \gamma$ [4].

To relate this back to the primary motivating example of the autoregulatory network, recall that N relates to the length of the gene and a to the rate of transcription. In this case, it would make sense to look at stability as the transcription rate remains fixed and the length of the gene increases. Recall that the mean is directly proportional to the length N and the relative variance is inversely proportional to the length N . Increasing N with a fixed rate a would increase the mean and decrease the relative variance of the distribution, both of which have been shown to decrease the stability region. Figure 4.3 shows bifurcation curves for a constant rate a and varying gene length N . Note that the bifurcation curves approach each other relatively quickly as N increases. Of course, an average gene is well on the order of 10^3 if not more. It is clear that trying to change the gene length alone is not an effective method of increasing the region of stability. However, there may exist other methods of arriving at a desirable delay distribution, which is to be investigated in future work.

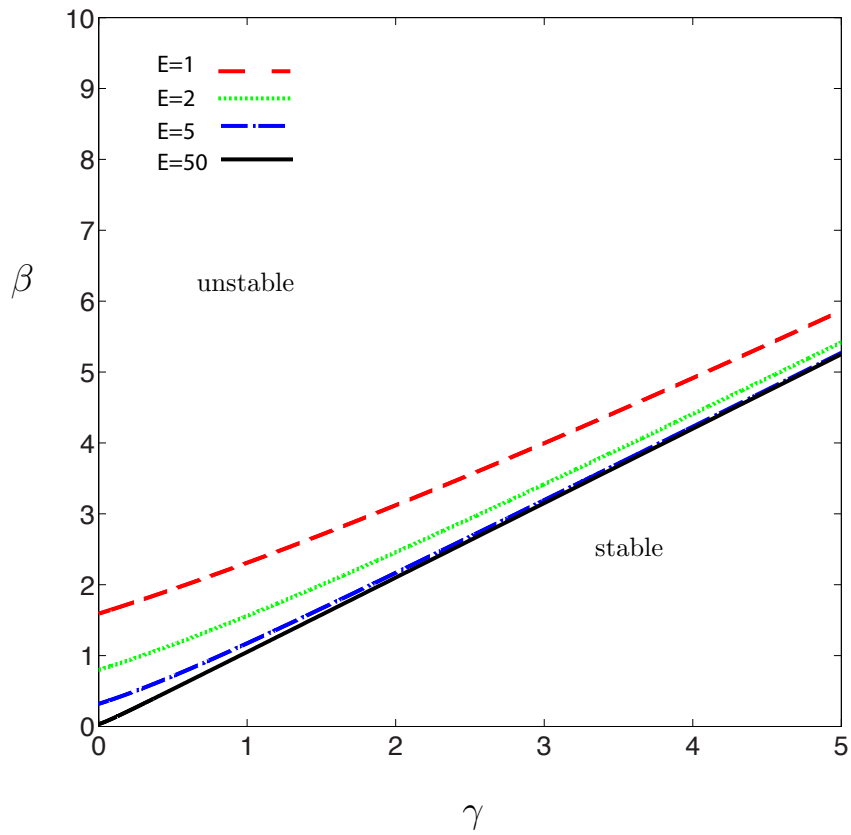


Figure 4.2: Stability bounds for $N = 100$ and different values of E .

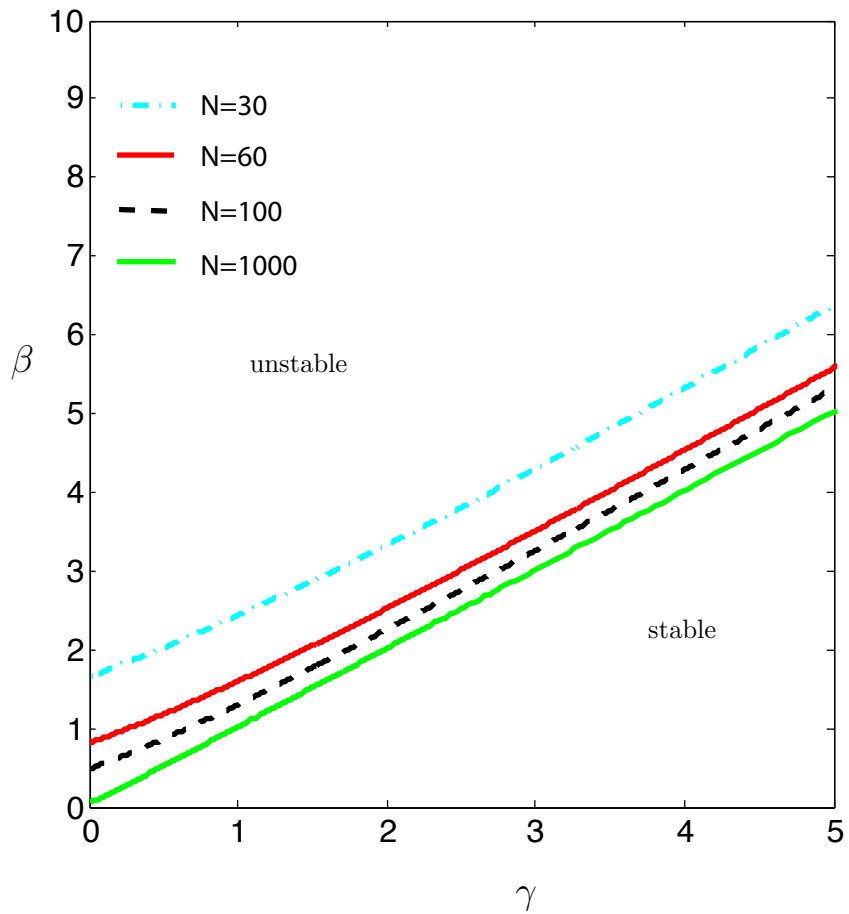


Figure 4.3: Stability bounds for $a = 30$ and different values of N .

4.2.2 Frequency Response

Consider the open loop system

$$F(s) = \beta \frac{G(s)}{s + \gamma} \quad (4.19)$$

and the frequency response of the system. To find the frequency response plot we substitute $s = i\omega$ and evaluate the magnitude and phase of the system as a function of the frequency ω . Note that any complex scalar function f can be expressed as

$$f = |f|e^{i\underline{f}} = |f| (\cos(\underline{f}) + i \sin(\underline{f})),$$

where

$$|f| = \sqrt{\text{Im}(f)^2 + \text{Re}(f)^2}$$

and

$$\underline{f} = \text{atan2}\left(\frac{\text{Im}(f)}{\text{Re}(f)}\right).$$

Correspondingly the product of two complex scalar functions can be expressed as

$$fg = |f||g|e^{\underline{f} + \underline{g}},$$

which lends to the properties

$$|fg| = |f||g| \quad \text{and} \quad \underline{fg} = \underline{f} + \underline{g}. \quad (4.20)$$

The phase for a delay is

$$\underline{e^{-i\omega E}} = -\omega E \quad (4.21)$$

and $|e^{-i\omega E}| = 1$. For the distribution $G(s)$ first consider the phase and gain

$$\begin{aligned} \underline{\left(\frac{a}{i\omega + a}\right)} &= -\text{atan}\left(\frac{\omega}{a}\right) \\ \left|\frac{a}{i\omega + a}\right| &= \frac{a}{\sqrt{\omega^2 + a^2}}. \end{aligned} \quad (4.22)$$

Applying the properties (4.20) gives

$$\begin{aligned}\angle G(i\omega) &= -N \operatorname{atan}\left(\frac{\omega}{a}\right) \\ |G(i\omega)| &= \left(\frac{a}{\sqrt{\omega^2 + a^2}}\right)^N.\end{aligned}\tag{4.23}$$

The frequency response of a delay distribution is essentially a low-pass filter with the bandwidth dependent on a and N as expected. These results will become useful in subsequent sections. Additionally, we can investigate how the frequency response compares to that of a discrete delay. It was previously shown that the distribution approaches a delta function in the limit as $N \rightarrow \infty$ with N/a held constant. We verify here, that there is convergence in the frequency response as well.

At $\omega = 0$, we have

$$\angle e^{-i0E} = \angle G(i0) = 0$$

Let us compare the change in phase of the distribution with the discrete delay, namely,

$$\frac{d}{d\omega} [-\omega E] = -E\tag{4.24}$$

and

$$\frac{d}{d\omega} \left[-N \operatorname{atan}\left(\frac{\omega}{a}\right) \right] = -E \frac{1}{1 + (\omega/a)^2} \geq -E.\tag{4.25}$$

For both the phase is negative, monotonically decreasing and for all ω , $\angle e^{-i\omega E} \leq \angle G(i\omega)$ with equality holding at $\omega = 0$. Notice if one takes the limit as $N, a \rightarrow \infty$ such that $N/a \equiv \text{constant}$, the inequality remains close to equality for large ω .

Now let us analyze the relation between the gain and the variance of the distribution. To do this we first express the gain in terms of N and E :

$$|G(i\omega)| = \left(\frac{N}{\sqrt{(E\omega)^2 + N^2}} \right)^N.\tag{4.26}$$

Also, note that

$$|G(i0)| = \left(\frac{N}{\sqrt{(E0)^2 + N^2}} \right)^N = 1.$$

As $N \rightarrow \infty$ equation (4.26) approaches 1 for all frequencies, which is the gain for a discrete delay.

4.2.3 Gain margin

The gain margin is defined here as the minimum gain in feedback permissible before stability is lost.

Consider the modification to system (4.9)

$$\begin{aligned}\dot{x} &= -\gamma x + f(k\tilde{x}) \\ \tilde{x} &= \int_0^\infty x(t-\tau)g(\tau) d\tau.\end{aligned}\tag{4.27}$$

Note that an added gain changes the equilibrium point of the system, namely, the equilibrium point is given by the solution x^* to the following system

$$\gamma x^* = f(kx^*).\tag{4.28}$$

Also, note that the equilibrium point is independent of the delay distribution. The linearized system becomes

$$\frac{dx'}{dt} = -\gamma x' - \beta(k)\tilde{x}',\tag{4.29}$$

where x' and \tilde{x}' are as defined previously. Furthermore,

$$\beta(k) = -k \left. \frac{\partial f(\tilde{y})}{\partial \tilde{y}} \right|_{\tilde{y}=kx^*} > 0.$$

The gain margin defined here can be implicitly found by determining the gain margin \hat{k} for a closed loop system whose open loop system is given by

$$H(s) = \frac{G(s)}{s + \gamma}.\tag{4.30}$$

Subsequently, the corresponding gain k is found through the relation

$$\hat{k} = \frac{1}{|H(i\omega_k)|} = \beta(k),$$

where ω_k is the gain crossover frequency for system (4.30). Figure 4.5 shows stability bounds on the (k, R) parameter space for different effective delays. Note that the stable range of k , or the gain margin, increases with an increased variance R . Additionally, the gain margin becomes infinite for a large enough relative variance, depending on the effective delay.

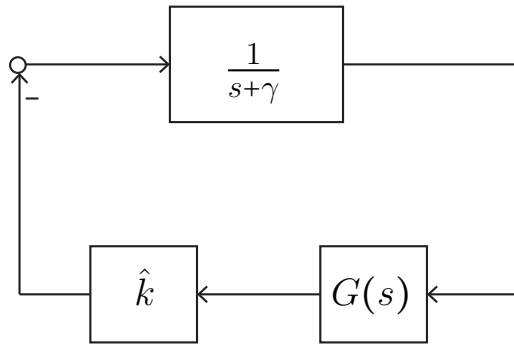


Figure 4.4: Diagram of the linearized system in the presence of gain-variations in the feedback path.

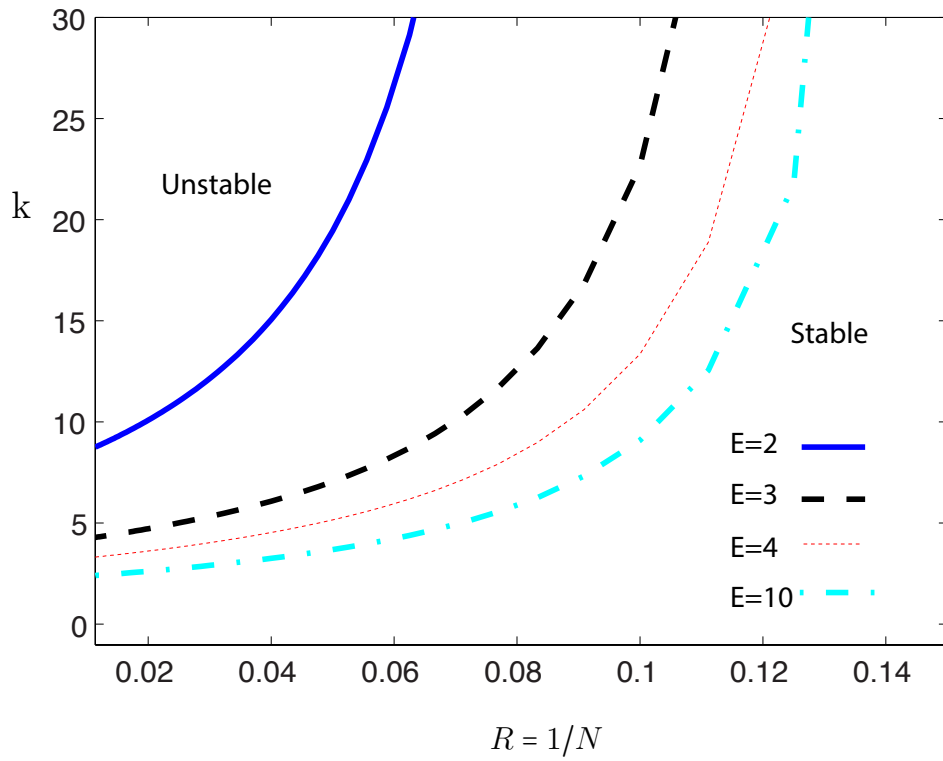


Figure 4.5: Plot showing the gain margin as a function of the relative variance $R = 1/N$ with $\gamma = 1$.

4.2.4 Limit cycles

Here we investigate limit cycles for the Goodwin-type oscillator as a function of mean and variance of the delay distributions. In order to simplify the results for some added insight, we set $\gamma = a$ in system (4.9):

$$\begin{aligned}\dot{x} &= -ax + f(\tilde{x}) \\ \tilde{x} &= \int_0^\infty x(t-\tau)g(\tau) d\tau,\end{aligned}\tag{4.31}$$

where $g(\tau)$ is still defined by the Erlang distribution. We consider a positive-definite, continuous, and time-invariant nonlinearity

$$f(x) > 0\tag{4.32}$$

for which system (4.31) has a single positive solution x_* . Note that system (4.31) is a monotone cycle feedback system. If the integral over the state is expanded back out into a finite set of ordinary differential equations, the system can be shown to have the following structure:

$$x_i = f_i(x_i, x_{i-1}) \quad \text{for } i = 1, \dots, N+1.\tag{4.33}$$

Moreover, for some $\delta_i \in \{-1, +1\}$,

$$\delta_i \frac{\partial f_i(x_i, x_{i-1})}{\partial x_{i-1}} > 0.\tag{4.34}$$

Therefore, system (4.31) is a monotone system since each state x_i forces the subsequent state x_{i+1} monotonically. Given the stated assumptions, system (4.31) can be shown to have a stable limit cycle through an extension of the Poincaré-Bendixson Theorem when the single positive solution is unstable and the state trajectory is bounded for any initial condition [58]. One can show that system (4.9) is always bounded through the Lyapunov function

$$V(x) = x^2.$$

The time derivative of $V(x)$ is given by

$$\begin{aligned}
 \dot{V}(x) &= 2x\dot{x} \\
 &= 2x\left(-\gamma x + \int_0^\infty f(x(t-\tau))g(\tau)d\tau\right) \\
 &= \underbrace{-2\gamma x^2}_{<0} + 2x \underbrace{\int_0^\infty f(x(t-\tau))g(\tau)d\tau}_{>0}.
 \end{aligned} \tag{4.35}$$

Since $x \geq 0$,

$$\begin{aligned}
 \dot{V}(x) &= \underbrace{-2\gamma x^2}_{<0} + 2x \underbrace{\int_0^\infty f(x(t-\tau))g(\tau)d\tau}_{>0} \\
 &< -2\gamma x^2 + 2x f_{\max}
 \end{aligned} \tag{4.36}$$

and $\dot{V}(x) < 0$ for $x \gg 0$. Consequently, the state remains bounded for all time and system (4.31) admits a limit cycle when the equilibrium point is unstable.

First we introduce some background information on the describing function method. For single-input single output (SISO) oscillatory systems one can apply the describing function method to derive constraints for an appropriate approximating function. This method ensures (under suitable conditions [51]) that the approximating system will have a limit cycle of the same amplitude and frequency of the original system.

The describing function method is derived from the method of harmonic balance. A brief outline of the method will be given below. See [51] for a more detailed description on harmonic balancing and the describing function method.

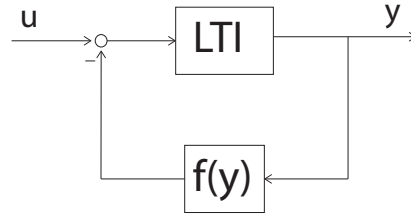


Figure 4.6: Nonlinear feedback system.

The method of harmonic balance is a general method of finding periodic solutions, given a system of the form in Figure 4.6. The input of the LTI and the output of the nonlinearity can be expanded

in a complex Fourier series:

$$y = \sum_{k=-\infty}^{\infty} c_k e^{ik\omega t},$$

$$f(y) = \sum_{k=-\infty}^{\infty} a_k e^{ik\omega t}.$$

With zero input into the system, the input into the LTI is the negative of the output of the nonlinearity. We apply the harmonic balance method by combining like terms. The harmonic balance method gives the following constraint for all values of k :

$$G(ik\omega)c_k + a_k = 0, \quad k = -\infty, \dots, -1, 0, 1, \dots, \infty.$$

This is an infinite dimensional problem, so the solution is approximated with a finite set of terms such that the error is minimized to a desired bound. We only need to look at solutions for $k \geq 0$. Assuming a SISO system and considering $k = \{0, 1\}$, the solution is reduced to solving

$$G(0)c_0(a_0, a_1) + a_0 = 0,$$

$$G(i\omega)c_1(a_0, a_1) + a_1 = 0.$$

This method is justified by the assumption that the LTI is an adequate low pass filter, so that higher harmonics in the steady state solution are damped out, leaving the first harmonic as a good approximation.

Notice the dependence of c_0 and c_1 on the coefficients a_1 and a_0 . Each coefficient in the expansion of y depends on all the terms included in the approximation of $f(y)$. Since the dependence of y on $f(y)$ is known, the explicit relationship between the coefficients can be found using the principle of orthogonality.

Defining the first order describing function as

$$N(a_1) = c_1(a_0(a_1), a_1)/a_1$$

for the simplified case in which $c_0 = 0$, the condition for potential stable limit cycles reduces to

$$G(j\omega) = \frac{-1}{N(a_1)}. \tag{4.37}$$

The describing function method does not prove the existence of a stable limit cycle but can ap-

proximate the solution if one exists [36]. There must exist a solution to (4.37), and furthermore there must be an acute angle between $G(jw)$ and the describing function at their intersection. The condition in equation (4.37) is equivalent to

$$\begin{aligned} 1 + N(a_1)\text{Re}[G(jw)] &= 0 \\ \text{Im}[G(jw)] &= 0. \end{aligned} \tag{4.38}$$

It can be verified through simulations that system (4.9) oscillates when the equilibrium point is unstable. In the oscillating regime the describing function method helps to approximate the periodic response where the approximated frequency and amplitude is found by solving the system of equations in (4.38). It is worth noting that the frequency depends only on the linear part of the system and provides a good approximation. The assumptions made to arrive at equations (4.38) do not necessarily result in a good approximation of the amplitude when looking at the Goodwin oscillator, which is asymmetric across its mean. Nonetheless, we make the argument that maintaining robustness in the frequency of the oscillations is the most crucial in the context of biological systems. Past research has suggested that certain sensory systems depend on changes in input concentrations rather than absolute values [65].

We apply this method to predict the frequency of a limit cycle arising in the closed loop system

$$\begin{aligned} \dot{x}_0 &= a x_0 + a \frac{1}{1 + (\tilde{x}_0/K_x)^2} \\ \tilde{x}_0 &= \int_0^\infty g(\tau)x_0(t-\tau)d\tau, \end{aligned} \tag{4.39}$$

where

$$g(\tau) = \frac{a^N \tau^{N-1}}{(N-1)!} e^{-a\tau}.$$

Given the form of the nonlinearity, it can be shown through Descartes' rule of signs that only one real solution exists to equation (4.28) and it is a positive solution. Now, we need only turn to the linear portion of the system to predict the frequency of the resulting limit cycle in the case of an unstable equilibrium point. The second condition in equation (4.38) is equivalent to the condition, in this case, to

$$\angle G(i\omega) = -\pi, \tag{4.40}$$

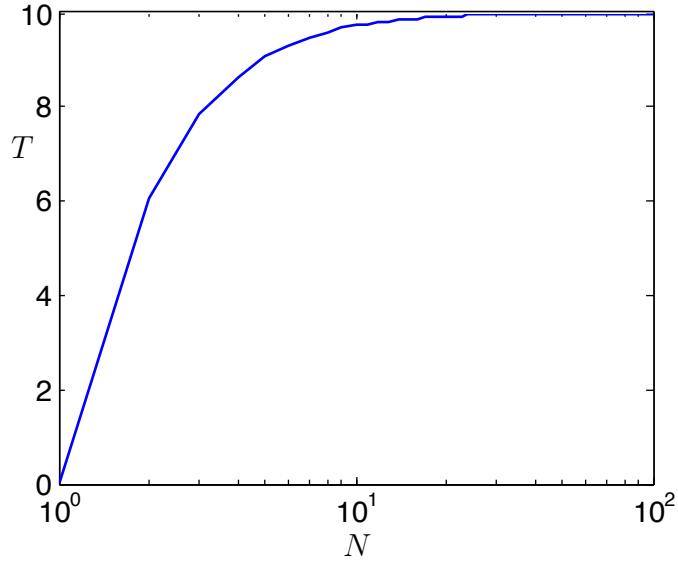


Figure 4.7: Plot showing predicted period of limit cycle as a function on N with $E = (N + 1)/a = 5$.

which gives

$$\omega_c = a \tan\left(\frac{\pi}{N + 1}\right), \quad (4.41)$$

where the period $T = 2\pi/\omega_c$. Figure 4.7 shows the predicted period of the limit cycle as a function of the relative variance. For $N \gg 1$ we have the approximation

$$\omega \approx a \frac{\pi}{N + 1}, \quad (4.42)$$

which gives

$$T \approx 2E. \quad (4.43)$$

Equality holds in the limit as the distribution function approaches a delta function. The period approaches twice the value of the mean of the distribution. Furthermore, Fig. 4.7 indicates a quick convergence of the limit cycle to a periodic signal with frequency $2E$ as N increases. For a system with a tight distribution ($N \gg 1$), the mean of the distribution becomes a good predictor for the induced limit cycle.

4.3 Temperature dependent oscillators

Studying temperature dependence in biochemical networks remains important, and yet is less understood in oscillators. Much related research has come about through the study of circadian rhythms. It is well known that circadian clocks robustly maintain a 24 hr period, typically thought to be entrained by light, as can be seen in a detailed model of the mammalian circadian clock proposed in [44] by Leloup and Goldbeter. Temperature dependence in circadian clocks has been slowly emerging as a topic of interest. Lahiri et al. [42] present a compelling argument to consider temperature dependence as a strong driving factor in the zebrafish circadian clock, but past work on time-varying Arrhenius scaled rate constants in oscillators has mainly been seen in the study of temperature compensation of circadian clocks. Current theoretical work utilizes mathematical conditions that minimize sensitivity of the period to changes in temperature to reverse engineer a temperature compensating model. For example, Hong et al. [31] provide a theory for how temperature compensation might work in circadian oscillators that depends on a balance of temperature dependent effects. Takeuchi et al. [72] use a similar concept to determine rate constants in a more detailed model taken from Gonze et al. [26], which is then modified to include temperature dependence. Ruoff et al. [63] use the same method to determine rate constants, as they consider the Goodwin model to study temperature effects.

With the methods derived in section 2.2 we can investigate models with delays under time-varying temperature conditions. We study the limit cycle of the resulting Goodwin model as we close the open loop delay system with a nonlinearity in feedback. Assuming that the rate coefficient's dependence on temperature can be described by the Arrhenius equation of the form

$$a(t) = Ae^{-E_a/(RT(t))},$$

oscillations in temperature $T(t)$ will result in oscillations in the rate coefficient $a(t)$. Furthermore, increasing temperature increases the rate coefficient a as expected. We simplify the model by assuming $a(t)$ is a sinusoidal function with a given period, amplitude, and mean value.

$$a(t) = a_0 \delta_p \sin(\omega t + \phi) + a_0. \quad (4.44)$$

From equation (2.46) in Section 2.2, the effective delay reduces to solving

$$\int_{t-\tau_{\text{eff}}}^t \frac{\delta_p}{E} \sin(\omega s + \phi) + \frac{1}{E} ds = 1, \quad (4.45)$$

where E is the expected or nominal delay. Note that a larger E leads to larger τ_{eff} and vice versa. In addition, for increasing E and frequency w , one can make the approximation,

$$\tau_{\text{eff}} \approx E$$

alternatively, as $w \rightarrow 0$,

$$\tau_{\text{eff}} \approx \frac{E}{\delta_p \sin \phi + 1}.$$

In Fig. 2.8, Section 2.2, there is an interesting phenomenon in the peak-to-peak amplitude of the effective delay as a function of the frequency for the time-varying rate coefficient in equation (4.44). The peak-to-peak amplitude appears to be zero when $w = 2\pi/E$. This is investigated further. Taking the integral in equation (4.45), the solution can be shown to be the intersection of the line

$$f_1 = 1 - \frac{1}{E}\tau + \frac{\delta_p}{wE} \cos(wt + \phi) \quad (4.46)$$

and the cosine function

$$f_2 = \frac{\delta_p}{wE} \cos(w(t - \tau) + \phi). \quad (4.47)$$

Substituting $w = 2\pi/E$ and $\tau = E$ gives

$$\begin{aligned} f_1 &= 1 - \frac{1}{E}E + \frac{\delta_p}{2\pi} \cos((2\pi/E)t + \phi) \\ &= \frac{\delta_p}{2\pi} \cos((2\pi/E)t + \phi) \end{aligned} \quad (4.48)$$

and

$$\begin{aligned} f_2 &= \frac{\delta_p}{2\pi} \cos((2\pi/E)t - 2\pi + \phi) \\ &= \frac{\delta_p}{2\pi} \cos((2\pi/E)t + \phi). \end{aligned} \quad (4.49)$$

Therefore, $f_1 = f_2$, making $\tau = E$ (i.e., the expected time delay equal to one period of the sinusoidal $a(t)$) a solution to equation (4.45) when $w = 2\pi/E$. This suggests that a limit cycle emerging from a dynamical system with a single delay may be minimally affected by time-varying temperature when the period is comparable to the delay.

Indeed, after closing the loop, it is demonstrate through simulation that the frequency of the limit cycle is robust with respect to changes in the frequency or phase of the periodically time-varying

rate coefficients. Simulations suggest the frequency of the limit cycle is dominated by the mean of the time-varying rate coefficient. The method is then applied to a temperature compensating circuit where the effects on the limit cycle of a multiple-input multiple-output system with multiple delays are investigated.

4.3.1 Goodwin oscillator

We now close the open loop system presented in Chapter 2

$$\dot{x}_i(t) = a(t) (x_{i-1} - x_i) \quad \text{for } i = 1 : N \quad (4.50)$$

with a nonlinearity in negative feedback

$$u = \frac{1}{1 + (x_N/K_x)^2}, \quad (4.51)$$

where we choose $K_x = 0.1$ to ensure oscillations. The closed loop system is then given by

$$\begin{aligned} \dot{x}_0 &= a(t) x_0 + a(t) \frac{1}{1 + (\tilde{x}_0/K_x)^2} \\ \tilde{x}_0 &= \int_0^\infty h(\tau) x_0(t - \tau) d\tau. \end{aligned} \quad (4.52)$$

As $N \rightarrow \infty$ with N/a_0 constant in the limit we have

$$\dot{x}_0 = a(t) x_0 + a(t) \frac{1}{1 + \left(\frac{x_0(t - \tau(t))}{K_x} \right)^2}, \quad (4.53)$$

where $\tau(t)$ is periodically time-varying delay given by equation 4.44.

Let us return to the Goodwin model with a constant rate coefficient. As was seen in section 4.2.4, the describing function method allows us to approximate the frequency and amplitude of the resulting limit cycle, should a limit cycle exist. Recall that using the describing function method the predicted frequency of the presumed limit cycle is

$$\omega = a_0 \tan\left(\frac{\pi}{N + 1}\right), \quad (4.54)$$

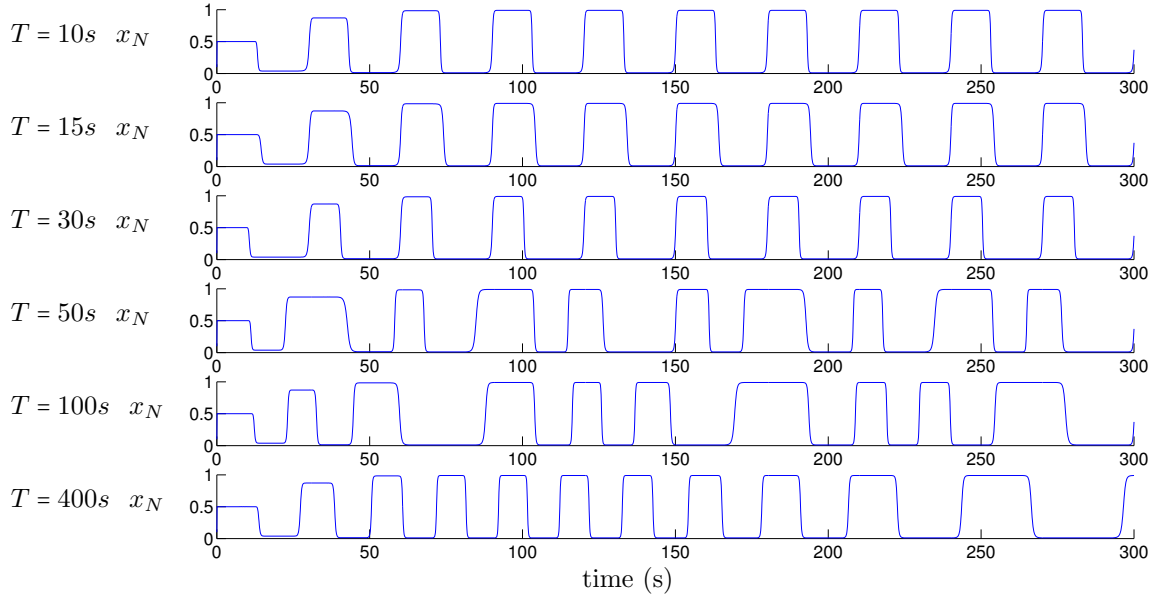


Figure 4.8: Simulations for different w with constants $\delta_p = .5$, $E = 15$, and $\phi = 0$.

with the period $T = \frac{2\pi}{\omega}$, and for $N \gg 1$ we have the approximation

$$\omega \approx a_0 \frac{\pi}{N+1}, \quad (4.55)$$

which gives

$$T \approx 2E. \quad (4.56)$$

The period approaches twice the value of the mean of the distribution.

For the time-varying $a(t)$ it is interesting to note that we still obtain a delta function in the limit; however, it is no longer necessarily centered at $E = \frac{N+1}{a_0}$ but oscillates around it with a frequency determined by the frequency of the temperature fluctuations and amplitude determined by the relative size of the perturbation and possibly frequency, as indicated in Fig. 2.8. For small perturbations, one would expect the limit cycle to have a frequency close to that of the nominal system with $a(t) = a_0$. We choose a relatively large perturbation of $\delta_p = .5$ and investigate how the limit cycle changes as the period of $a(t)$ increases. Figure 4.8 shows simulations of the closed loop system for $N = 10,000$ and $E = 15$ for varying periods of $a(t)$. It is apparent that the period of the limit cycle is robust to oscillatory fluctuations in $a(t)$. The period remains close to $2E$ for a large range of frequencies w . In Fig. 2.8 in Section 2.2 it was clear that when the mean delay had the same value as the period of oscillation of the temperature, the peak-to-peak amplitude of

the delay was reduced to zero. The delay was essentially constant and thus we would expect the behavior deduced from the application of harmonic balancing as witnessed above. In addition, the peak-to-peak amplitude in general remained small for fast temperature variations. However, as the period gets really large there is an apparent change in the frequency of the limit cycle over time. There is a higher frequency at high temperatures and a lower frequency at decreasing temperatures. This gives a limit cycle whose frequency appears to also be periodically changing with time.

This is further investigated in Fig. 4.9. The time span of the last simulation in Fig. 4.8 is extended and analyzed further. The middle plot in Fig. 4.9 shows τ_{eff} as a function of time for $T = 400\text{s}$ and the bottom plot shows the single-sided amplitude spectrum of $x_N(t)$ obtained by taking the fast Fourier transform of the signal. The vertical lines indicate the frequencies corresponding to the period of the limit cycle we would expect given a constant delay at the minimum and maximum values achieved by τ_{eff}

Next, we investigate whether entrainment occurs with a change in phase. Different phases ϕ for $a(t)$ lead to changes in the effective delay. The effective delay changes with ϕ in much the same way as it changes with time. We investigate the effects on the phase of the output x_N of the closed loop system. Just as circadian clocks experience a phase shift when we overcome jet lag, we investigate whether there is a similar effect with temperature, namely, is there entrainment? If the period changes even slightly, there is a phase shift that changes linearly as a function of time; however, there is also an initial phase shift due to the change in τ_{eff} . As the reactions approach a delta function, we can imagine that if we go from $a(t) = a_0$ to time-varying $a(t)$ at $t = 0$, we essentially change the delay in the loop, effectively adding

$$e^{-s(\tau_{\text{eff}}(0)-E)}$$

with associated phase $-w(\tau_{\text{eff}}(0)-E)$ in radians, which we expect to be the phase change. A positive term in the exponential does not make sense on its own since that would assume we have information of future states (no longer a delay), but in this case it is reasonable because when added to e^{-sE} it remains a delay, just a smaller delay. Figure 4.10 shows simulations for different phase shifts ϕ . The shift in the fall of the signal corresponds to the predicted phase shift, but because the width of oscillations change the actual change in phase is much smaller. In this case, the phase shift seems to be cut by half of what is predicted, and the frequency of oscillations remain fairly robust to phase shifts.

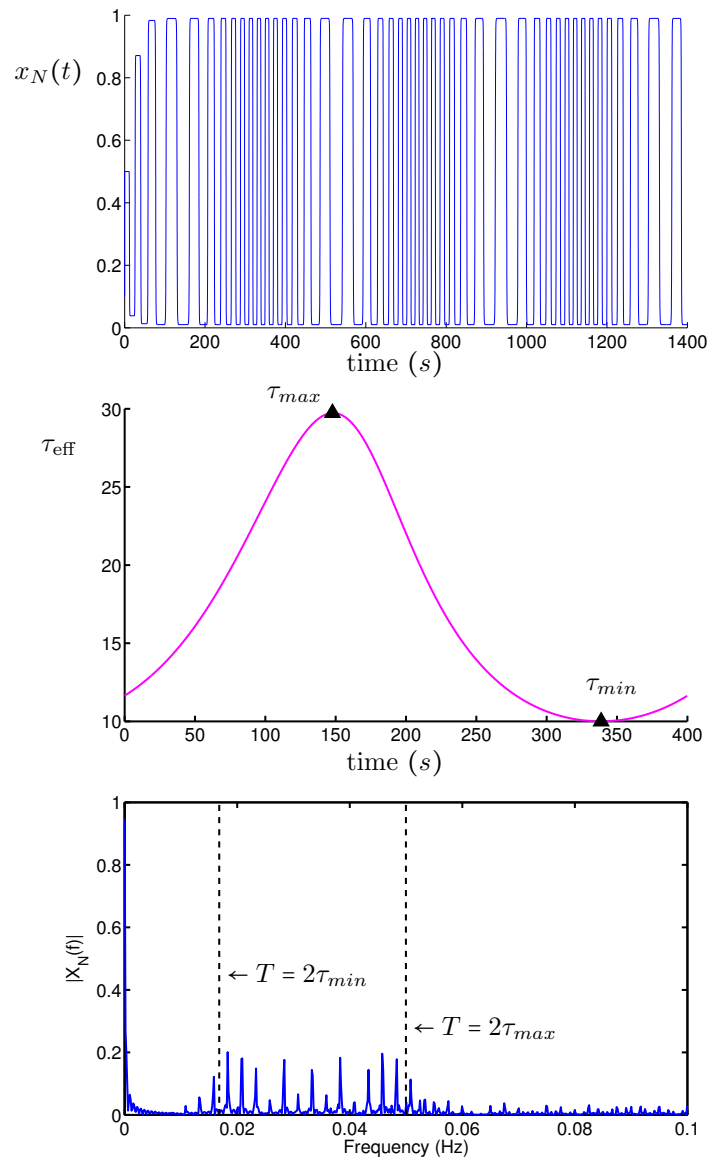


Figure 4.9: Top: Extended simulation from Fig. 4.8 with $T = 400$. Middle: τ_{eff} as a function of time. Bottom: Single-sided amplitude spectrum of $x_N(t)$.

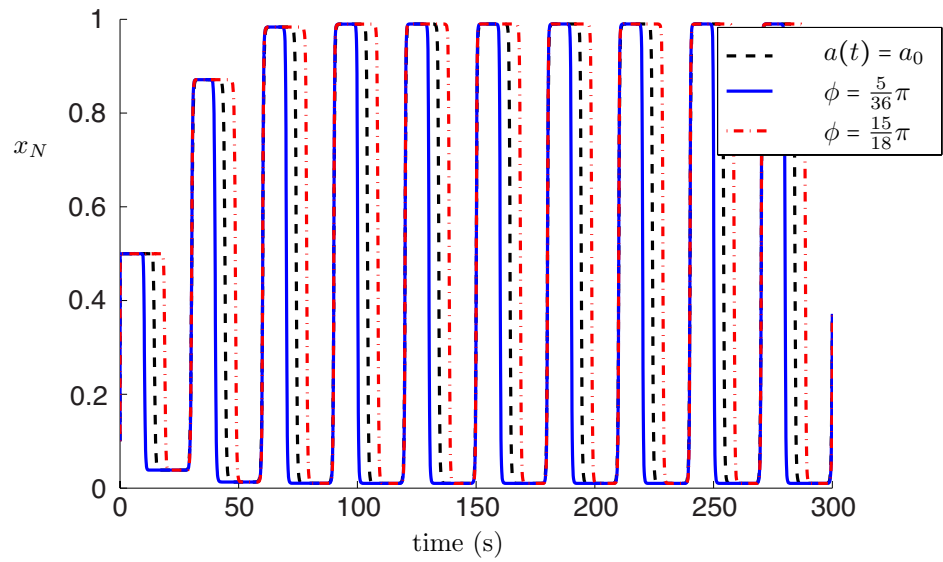


Figure 4.10: Simulations for different ϕ with constants $\delta_p = .5$, $E = 15$ and $w = \pi/E$.

4.3.2 Temperature compensating circuit

Here, the methods derived in Section 2.2 are applied to the delay-based model of the temperature compensator designed in [32]. The effect of the temperature compensating mechanism in the temperature sensitive *LacI* is investigated with respect to entrainment. As was seen in the previous section, a phase shift in time-varying temperature does not effectively entrain the limit cycle of the oscillator. In the case of the temperature compensator, the time-varying temperature not only affects the reaction rates but also changes the binding efficiency of *LacI* to the corresponding promoter sites. The model for the temperature compensator is given by

$$A(T) \cdot \frac{dr}{dt} = \frac{\alpha_r \left(f^{-1} + \frac{a(t-A(T) \cdot \tau_r)}{C_a} \right)}{\left(1 + \frac{a(t-A(T) \cdot \tau_r)}{C_a} \right) \left(1 + \frac{r(t-A(T) \cdot \tau_r)}{C_r(T)} \right)^N} - \beta r(t) - \frac{\gamma_r r(t)}{R_0 + r(t) + a(t)}, \quad (4.57)$$

$$A(T) \cdot \frac{da}{dt} = \frac{\alpha_a \left(f^{-1} + \frac{a(t-A(T) \cdot \tau_a)}{C_a} \right)}{\left(1 + \frac{a(t-A(T) \cdot \tau_a)}{C_a} \right) \left(1 + \frac{r(t-A(T) \cdot \tau_a)}{C_r(T)} \right)^N} - \beta a(t) - \frac{\gamma_a a(t)}{R_0 + r(t) + a(t)}, \quad (4.58)$$

where

$$A(T) = \exp \left\{ \theta \left[\frac{1}{T + 273} - \frac{1}{T_{\text{ref}} + 273} \right] \right\} \quad (4.59)$$

and

$$C_r(T) = (C_{r,\text{max}} - C_{r,\text{min}}) \frac{(T/T_0)^b}{1 + (T/T_0)^b} + C_{r,\text{min}}. \quad (4.60)$$

The system parameters are taken directly from the paper [32] (see Table 4.1). Note that in system (4.58), the delay is linearly scaled by the Arrhenius factor $A(T)$, however, from the analysis in Section 2.2, it is clear that this is an incorrect assumption for a time-varying rate coefficient $A(T)$. Therefore, $A(T) \cdot \tau_r$ and $A(T) \cdot \tau_a$ will be replaced by appropriate time-varying delay values using the method derived. The temperature is chosen to vary according to

$$T = 6 \sin(\omega t + \phi) + 36, \quad (4.61)$$

where $\omega = 2\pi/50$. To investigate entrainment, the period of the time-varying temperature is chosen to be close to that of the limit cycle. Subsequently $A(T)$ also varies periodically with the same frequency and is fit to a sinusoidal function

$$A(T) = \delta_p a_0 \sin(\omega t + \phi) + a_0. \quad (4.62)$$

The variables τ_r and τ_a are chosen as the effective delays E_r and E_a for each of the genes. To investigate the effects of the temperature compensation mechanism on entrainment the system is simulated under different conditions. Figure 4.11 shows simulations of system (4.58) with and without a phase shift in the temperature. Figure 4.12 shows simulations of system (4.58) without temperature compensation (i.e., $C_r(T)=\text{const.}$). Both systems demonstrate entrainment, however, the transients in the phase shift are longer in the system without temperature compensation.

Parameter	Value
τ_r	13.5 min.
τ_a	15 min.
β	.0275 min ⁻¹
γ_r	76 (mol./cell)min ⁻¹
γ_a	76 (mol./cell)min ⁻¹
R_0	1.8 mol./cell
f	2 (unitless)
C_a	5 mol./cell
α_r	265 (mol./cell)min ⁻¹
α_a	92.75 (mol./cell)min ⁻¹
θ	4500 K
T_{ref}	36°C
$C_{r,\text{max}}$	830 mol./cell
$C_{r,\text{min}}$	50 mol./cell
T_0	38°C
b	20 (unitless)
N	4

Table 4.1: System parameter values.

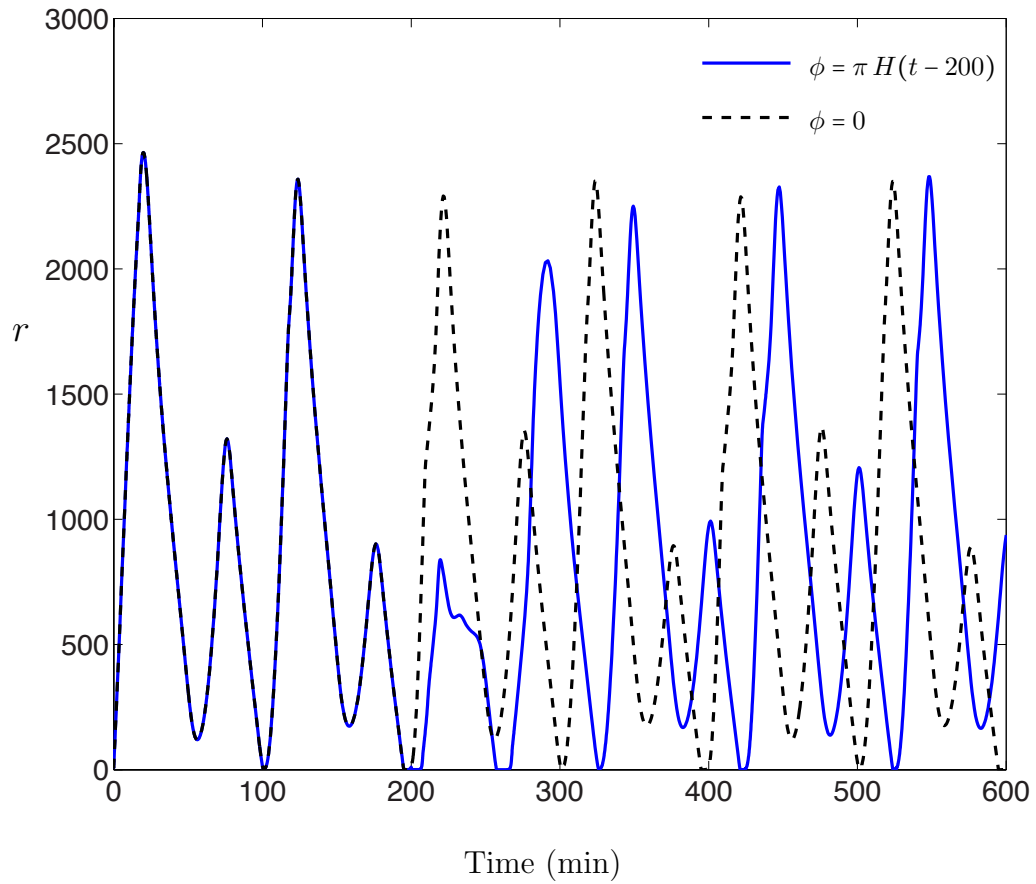


Figure 4.11: This plot shows simulations of the model in system (4.58) for the time-varying temperature indicated in equation (4.61). The blue line indicates a simulation with a phase shift applied to the temperature function at time $t = 200s$.

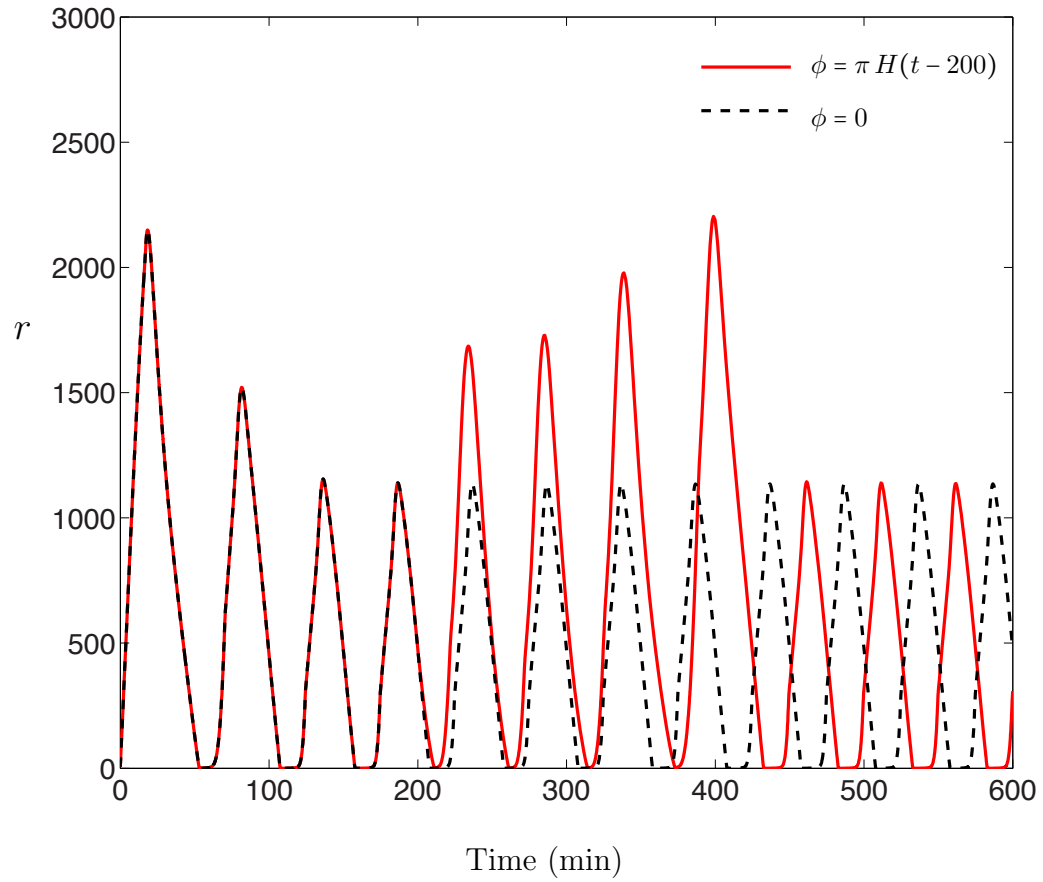


Figure 4.12: This plot shows simulations of the model in system (4.58) without temperature compensation ($C_r = C_r(T_{\text{ref}})$) for the time-varying temperature indicated in equation (4.61). The red line indicates a simulation with a phase shift applied to the temperature function at time $t = 200s$.

Chapter 5

Delay-Based Controllers

Consider the following linear system:

$$\dot{x} = \mathbf{A}x + \mathbf{B}u \quad (5.1)$$

where the feedback controller output u is a function of the delayed state

$$u = \int_0^t x(t-\tau)g(\tau)d\tau. \quad (5.2)$$

We investigate system stability and performance with respect to the distribution $g(\tau)$. In Section 5.1 we investigate the case where

$$g(\tau) = \frac{1}{2}\delta(t-\tau_1) + \frac{1}{2}\delta(t-\tau_2) \quad (5.3)$$

and draw a relation between the delay margin of the system and the variance of the distribution function

$$V = \frac{(\tau_1 - \tau_2)^2}{4}.$$

In Section 5.2, we consider a method of designing $g(\tau)$ to maximize H_∞ performance, which is defined and discussed in detail. This is done in collaboration with Seungil You using optimization techniques. The positive role of the dual-feedback path is then supported through an application of the results to an autoregulatory network.

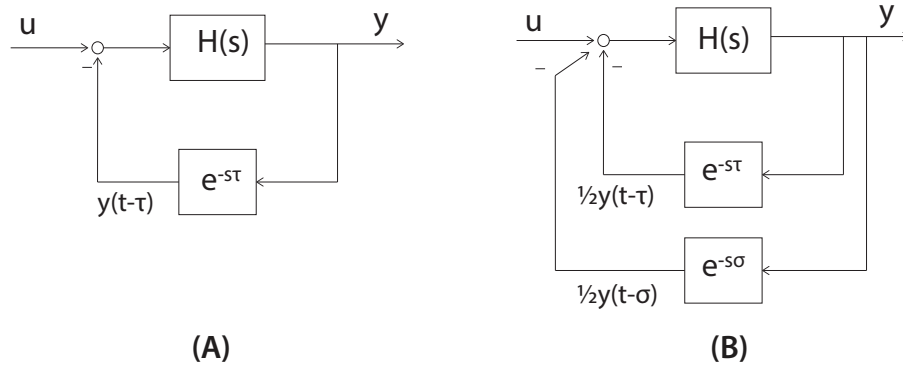


Figure 5.1: (a) Single delay feedback system. (b) Two delay feedback system.

5.1 Dual-delayed feedback system

Suppose we have a system such as that shown in Figure 5.1 (a) with a single delayed feedback. The delay $e^{-s\tau}$ is replaced with the distributed delay

$$G(s) = \frac{1}{2}e^{-s\sigma} + \frac{1}{2}e^{-s\tau},$$

which has the corresponding distribution function

$$g(t) = \frac{1}{2}\delta(t-\sigma) + \frac{1}{2}\delta(t-\tau).$$

We put equal weights on both delays. The factor of $\frac{1}{2}$ is necessary in order to keep from adding a gain to the signal in the feedback. With $\int_0^\infty g(t)dt = 1$ we get unity gain. Convolution of the output $y(t)$ with the distribution function gives $\frac{y(t-\sigma)+y(t-\tau)}{2}$, so the input is the average of the feedbacks and not the sum.

The system dynamics are deterministic, but we use the properties of the distribution functions as parameters. In Anderson [5], the author shows that stability of a delayed system can be investigated using only the properties of the time delay distribution. Accordingly, we expect that the mean and variance for a symmetric distribution will directly influence the stability of a system. From now on we will refer to the mean of the distribution as the effective delay. The effective delay of the new distribution function is

$$T = \frac{\sigma + \tau}{2}$$

and the variance, V , of the new distribution function is

$$V = \frac{(\sigma - \tau)^2}{4}.$$

We have chosen, without loss of generality, $\sigma \geq \tau$. This new system is shown in Figure 5.1 (b). Furthermore, the distribution is symmetric so that higher moments of the distribution are zero. In Bernard *et al.* [6] there has been evidence to suggest that higher moments, when not zero, may play a role in stability in addition to mean and variance.

We assume that $H(s)$ is a stable linear system. By the Nyquist criterion, any encirclement of -1 by the Nyquist plot of the loop transfer function will indicate an unstable system [61].

$$H_{cl} = \frac{H(s)}{1 + H(s)(e^{-s\sigma} + e^{-s\tau})/2} \quad (5.4)$$

and, by the Nyquist criterion, at the boundary of instability we have that the loop transfer function

$$H(j\omega)(e^{-j\omega\sigma} + e^{-j\omega\tau})/2 = -1, \quad (5.5)$$

for some ω, σ and τ . With some algebraic manipulation we will show the loop transfer function to take the form

$$G(s)e^{-sT},$$

where G is a complex function. In this form the permissible effective delays of the distributed system is determined by the plot of $G(s)$ on the complex plane.

The loop transfer function is

$$\begin{aligned} L(s) &= H(s)(e^{-s\sigma} + e^{-s\tau})/2 \\ &= H(s)(1 + e^{-s(\sigma-\tau)})e^{-s\tau}/2 \\ &= H(s)\frac{(e^{s\frac{\sigma-\tau}{2}} + e^{-s\frac{\sigma-\tau}{2}})}{2}e^{-s\frac{\sigma-\tau}{2}}e^{-s\tau} \\ &= H(s)\frac{(e^{s\frac{\sigma-\tau}{2}} + e^{-s\frac{\sigma-\tau}{2}})}{2}e^{-s\frac{\sigma+\tau}{2}}. \end{aligned} \quad (5.6)$$

If we evaluate the transfer function at $s = j\omega$ we can further simplify the equation to

$$\begin{aligned} L(s)|_{s=j\omega} &= H(j\omega) \frac{(e^{j\omega \frac{\sigma-\tau}{2}} + e^{-j\omega \frac{\sigma-\tau}{2}})}{2} e^{-j\omega \frac{\sigma+\tau}{2}} \\ &= H(j\omega) \cos\left(\omega \frac{\sigma-\tau}{2}\right) e^{-j\omega \frac{(\sigma+\tau)}{2}} \end{aligned} \quad (5.7)$$

$$= H(j\omega) \cos\left(\omega \frac{\sigma-\tau}{2}\right) e^{-j\omega T}. \quad (5.8)$$

Note that this resembles a loop transfer function for a SISO system with a single delayed feedback e^{-sT} and will be treated as such. One can now deduce gain and phase margins using the general methods involving the Nyquist plot of the open loop system. In this case one can determine the permissible effective delay for the new distributed delay system by finding the phase margin from the plot of the “open loop” system

$$\begin{aligned} G &= H(j\omega) \cos\left(\omega \frac{\sigma-\tau}{2}\right) \\ &= H(j\omega) \cos(\omega\sqrt{V}) \end{aligned} \quad (5.9)$$

on the complex plane. If the permissible time delay is larger than the effective delay T , then the system is stable, moreover, the disparity gives a measure of robustness. One can also isolate the effects of the variance V on the stability and robustness of the system. Although both $G(j\omega)$ and $e^{-j\omega T}$ are functions of σ and τ , they can be isolated in such a way that T can be varied while keeping G constant and vice versa, since V and T can be varied independently; however, the maximum variance is necessarily limited by the effective delay ($\sqrt{V} \leq T$).

We can define a utility function as

$$J_V = \frac{\theta_\beta}{\omega_\beta} - T, \quad (5.10)$$

where θ_β and ω_β are the phase margin and gain-crossover frequency of the newly defined open loop function G for the double feedback system as defined in equation (5.9). T is the expected or average value of the two delays. J_V gives the difference between the permissible delay,

$$T_{PM} = \frac{\theta_\beta}{\omega_\beta}, \quad (5.11)$$

due to the new increased phase margin and the new effective delay,

$$T = \sqrt{V} + \sigma, \quad (5.12)$$

as a result of the second feedback. For the system to be stable we require $J_V > 0$.

Solving for the gain-crossover frequency ω_β or the frequency at which the magnitude of the loop transfer function is equal to 1 gives

$$|\cos(\omega_\beta\sqrt{V})H(j\omega_\beta)| = |\cos(\omega_\beta\sqrt{V})||H(j\omega_\beta)| = 1 \quad (5.13)$$

$$|\cos(\omega_\beta\sqrt{V})| = \frac{1}{|H(j\omega_\beta)|}. \quad (5.14)$$

The first equality in equation (5.13) holds, since one can factor out the cosine term in calculating the magnitude. This gives the constraint $|H(j\omega_\beta)| \geq 1$. Solutions to equation (5.14) are given by

$$\sqrt{V} = \frac{1}{\omega_\beta} \cos^{-1} \left(\pm \frac{1}{|H(j\omega_\beta)|} \right). \quad (5.15)$$

We consider a feedback system described by

$$H_{cl}(s) = \frac{H(s)}{1 + H(s)e^{-s\tau_1}}, \quad (5.16)$$

where $H(s)$ is the open loop system

$$H(s) = \frac{0.2}{(s+1)(s+0.1)}. \quad (5.17)$$

Applying equation (5.15) we can find the region of stability as an implicit function of the delay added via a second feedback channel. We use T_{PM}^+ and T_{PM}^- to refer to the solutions corresponding to the plus and minus term in equation (5.15), respectively. Figure 5.2 shows the solution curves to equations (5.11) and (5.12) as functions of the variance for the system. The minimum delay σ was calculated from the phase margin of the original system, therefore, the unmodified system is unstable. Positive values of J_V correspond to the region where the T_{PM} curve lies above the T curve. The plot shows that a minimum variance of 4.4^2 is required to stabilize the system. This corresponds to a second delay value of $\tau = 20.19$ s. Maximizing the utility function is not necessarily the best choice when designing the added feedback. This occurs at approximately $\sqrt{V} = 17.7$ s and it is obvious that the system is not robust to uncertainty or variance in the delay. It can easily perturb into the unstable region. Figure 5.3 shows the Nyquist plots and corresponding simulations for step inputs into the single feedback system with delay $T_{min} = 12$ s and the double feedback system with two different values for the second delay. We see that the system can indeed be stabilized by adding a longer delay to the feedback path.

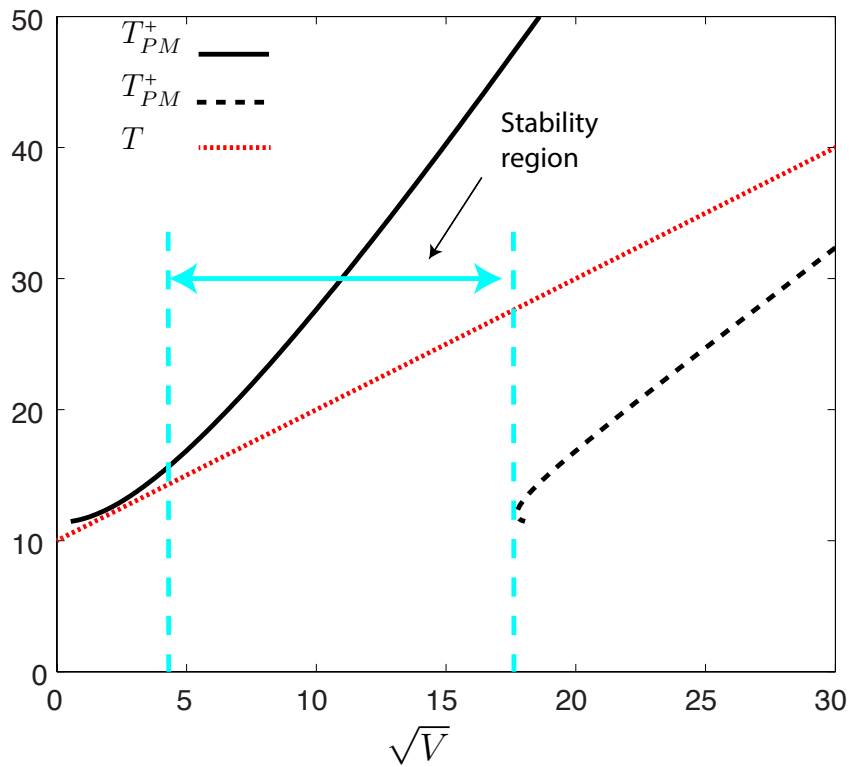


Figure 5.2: Time delay margin for the loop transfer function and average delay as a function of variance with $\sigma = 11.39s$.

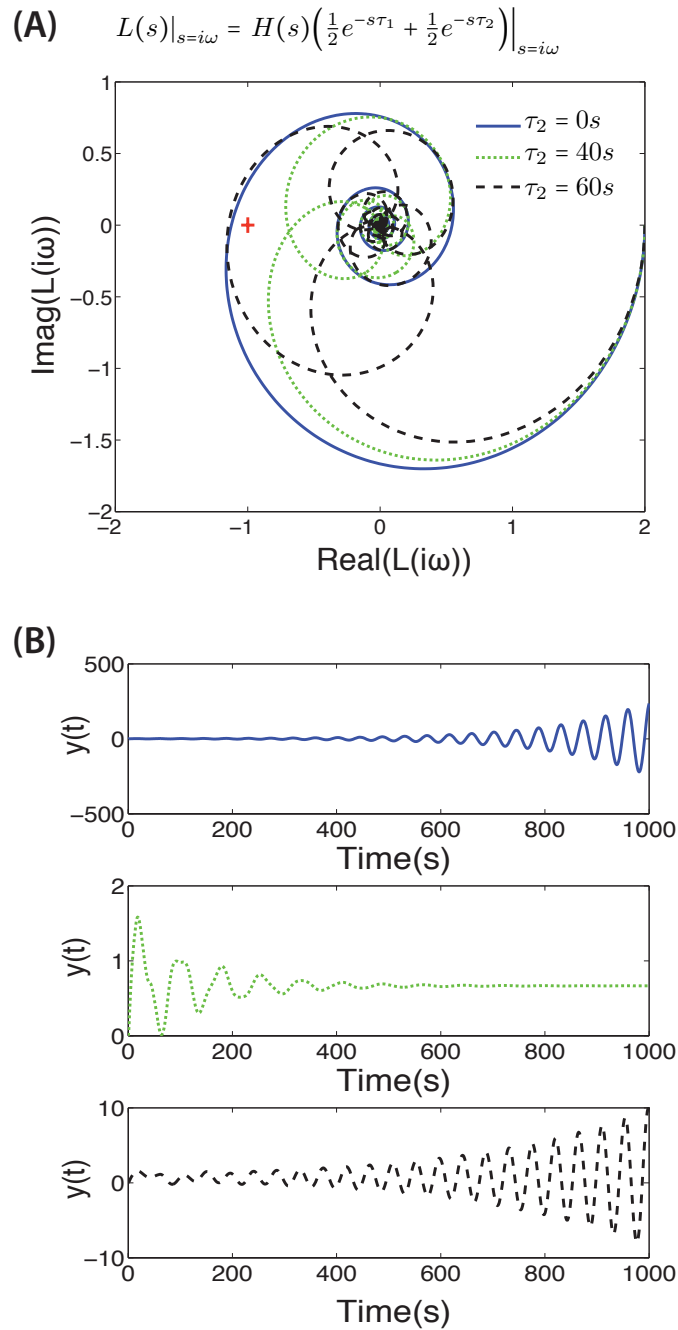


Figure 5.3: Plots showing the effects of dual-delayed feedback through Nyquist plots and simulations for $\tau_1 = 14s$ and various values of τ_2 . (A) Comparing Nyquist plots of the loop transfer function for a single delayed feedback system and dual-delayed feedback systems. Encirclements of -1 indicate instability. (B) Simulation of dual-delayed feedback system.

5.2 Delay-based controller design

This section contains collaborative work with colleague Seungil You. Consider the auto regulatory network

$$\dot{x} = f(x(t - \tau)) - \gamma x + \eta, \quad (5.18)$$

where x is the observed protein concentration, γ is the protein degradation rate, f is a repressive Hill function, and η is an unknown disturbance. We propose designing a delay based controller through design of the delay distribution function $g(\tau)$ in

$$\dot{x} = \int_{\tau}^N f(x(t - \sigma))g(\sigma)d\sigma - \gamma x + \eta \quad (5.19)$$

that minimizes the sensitivity to the disturbance η . Directly designing a continuous distribution $g(\tau)$ and in continuous time is a difficult task. We propose to do this through linearization and discretization in time. First we constrain the distribution to the form

$$g(\sigma) = \sum_{k=\tau}^N w_k \delta(\sigma - kT), \quad (5.20)$$

then the linearized system becomes

$$\dot{x} - \gamma x(t) + \beta \sum_{k=\tau}^N w_k \delta(t - kT) + \eta, \quad (5.21)$$

and the time discretization gives

$$x(k + 1) = d_2 x(k) + d_1 \beta \sum_{i=\tau}^N w_i x(k - i) + \eta. \quad (5.22)$$

The controller design problem deduces to a design on the weights in (5.22). The optimization is over H_{∞} of the transfer function from the disturbance η to the output x .

5.2.1 Problem Formulation

Consider the following single-input single-output discrete-time system with a delayed state feedback:

$$\begin{aligned} \mathbf{x}_{k+1} &= \mathbf{A} \mathbf{x}_k + \mathbf{B} u_{k-\tau} + \mathbf{D} \eta_k \\ y_k &= \mathbf{C} \mathbf{x}_k \\ u_k &= y_k, \end{aligned} \tag{5.23}$$

where $\mathbf{x}_k \in \mathbb{R}^n$, $u_k \in \mathbb{R}$, $\tau \in \mathbb{Z}^+$, and $\eta_k \in \mathbb{R}$ represents an input disturbance. Note, we restrict our attention to the case $\lim_{k \rightarrow \infty} (\mathbf{A} - \mathbf{B}\mathbf{C})^k < \infty$. Previous work has shown the stabilizing effects of added delays to unstable systems, but here we are interested in characterizing performance. We propose a delay-based controller such that

$$u_k = \sum_{i=\tau}^N w_i y_{k-i}, \tag{5.24}$$

where $N \geq \tau$ is a positive integer.

We look to the frequency response of the system to the input disturbance n_k to design the optimal weights $\{w_i\}$. The transfer function from n_k to the feedback state y_k is given by

$$H_{\eta \rightarrow x}(z) = \left(zI - A - BC \sum_{i=\tau}^N w_i z^{-i} \right)^{-1} D. \tag{5.25}$$

Futhermore, assuming unwanted disturbances reside in the higher frequency regime, we apply a weighting function [13], namely, a pre-determined filter F to ensure signals at higher frequencies are more greatly penalized. This is achieved with a first order high-pass filter

$$F(z) = \frac{(1 + \alpha)z}{z - \alpha}, \tag{5.26}$$

where $0 \leq \alpha < 1$. Accordingly, the optimal weights can be found by solving the optimization problem

$$\begin{aligned} &\underset{w_\tau, \dots, w_N}{\text{minimize}} && \|FH_{\eta \rightarrow x}\|_\infty \\ &\text{subject to} && \{w_\tau, \dots, w_N\} \in \mathcal{W}, \end{aligned} \tag{5.27}$$

where \mathcal{W} is a convex set of $\{w_\tau, \dots, w_N\}$, and the objective function

$$\|FH_{\eta \rightarrow x}\|_\infty = \sup_{\|\eta\|_2 \leq 1} \frac{\|\mathbf{x}\|_2}{\|\eta\|_2} \quad (5.28)$$

is the H_∞ norm of the transfer function. In the example to follow we will enforce the additional constraint $\sum_{i=\tau}^N w_i = 1$ due to physical constraints. This also makes sense if one considers the distribution to come from a probability density function. In the general setup we only require convex constraints. For $\sum_{i=\tau}^N w_i > 1$ the feedback can be thought to have an added overall gain in addition to the distribution of the delayed feedback. Although the H_∞ norm is the \mathcal{L}_2 gain of the system, it can be shown that it is equivalent to consider the power norm [12], where we can include non-vanishing disturbances and, in fact, the supremum is achieved by a periodic disturbance with constant amplitude.

Using the generalized plant model, we can convert the optimization (5.27) to a static output feedback H_∞ problem with additional affine constraints on the gain in order to apply more traditional methods. The static output feedback H_∞ design is well studied in the literature (see [18,71]). Let us first define the vectors

$$\tilde{\mathbf{x}}_k = \begin{bmatrix} \mathbf{x}_k \\ v_k \end{bmatrix}, \quad \hat{\mathbf{x}}_k = \begin{bmatrix} \tilde{\mathbf{x}}_k \\ \tilde{\mathbf{x}}_{k-1} \\ \vdots \\ \tilde{\mathbf{x}}_{k-N} \end{bmatrix}, \quad (5.29)$$

where $\tilde{\mathbf{x}}_k \in \mathbb{R}^{n+1}$ and $\hat{\mathbf{x}}_k \in \mathbb{R}^{(N+1)(n+1)}$. Accordingly, the state dynamics can be re-written as

$$\begin{aligned} \hat{\mathbf{x}}_{k+1} &= \hat{\mathbf{A}} \hat{\mathbf{x}}_k + \hat{\mathbf{B}}_1 \eta_k + \hat{\mathbf{B}}_2 u_k \\ z_k &= \hat{\mathbf{C}}_1 \hat{\mathbf{x}}_k + \hat{\mathbf{D}}_{11} \eta_k + \hat{\mathbf{D}}_{12} u_k \\ \mathbf{y}_k &= \hat{\mathbf{C}}_2 \hat{\mathbf{x}}_k \\ u_k &= \mathbf{w}^T \mathbf{y}_k, \end{aligned} \quad (5.30)$$

where

$$\begin{aligned}
\hat{\mathbf{A}} &= \begin{bmatrix} \mathbf{A}_0 & \mathbf{0} & \cdots & \mathbf{0} \\ \mathbf{I} & \mathbf{0} & & \\ \mathbf{0} & \mathbf{I} & \mathbf{0} & \\ \vdots & \ddots & \ddots & \ddots & \vdots \\ \mathbf{0} & \cdots & \mathbf{0} & \mathbf{I} & \mathbf{0} \end{bmatrix}, \\
\mathbf{A}_0 &= \begin{bmatrix} \mathbf{A} & \mathbf{0} \\ (1-\alpha)\mathbf{C}\mathbf{A} & \alpha \end{bmatrix} \\
\hat{\mathbf{B}}_1 &= \begin{bmatrix} \mathbf{D}^T & \mathbf{0}_{1 \times N(n+1)+1} \end{bmatrix}^T, \\
\hat{\mathbf{B}}_2 &= \begin{bmatrix} \mathbf{B}^T & (1-\alpha)(\mathbf{C}\mathbf{B})^T & \mathbf{0}_{1 \times N(n+1)} \end{bmatrix}^T, \\
\hat{\mathbf{C}}_1 &= \mathbf{0}, \quad \hat{\mathbf{D}}_{11} = \mathbf{0}, \quad \hat{\mathbf{D}}_{12} = \mathbf{0}, \\
\hat{\mathbf{C}}_2 &= (\mathbf{I}_d \otimes [\mathbf{C} \ \mathbf{0}])\tilde{\mathbf{C}} \\
\tilde{\mathbf{C}} &= \begin{bmatrix} \mathbf{0}_{d \times \tau} & \mathbf{I}_{d \times d} \end{bmatrix}, \\
\mathbf{w} &= \begin{bmatrix} w_\tau & w_{\tau+1} & \cdots & w_N \end{bmatrix}^T, \tag{5.31}
\end{aligned}$$

and $d = N - \tau + 1$.

Utilizing the state space representation, the discrete-time KYP lemma [14] converts the H_∞ norm minimization problem (5.27) into the following optimization problem with linear matrix inequalities (LMI):

$$\begin{aligned}
&\underset{\mathbf{w}, \mathbf{X}, \mathbf{Y}, \gamma}{\text{minimize}} \quad \gamma \\
&\text{subject to} \quad \mathbf{w} \in \mathcal{W}, \\
&\quad \mathbf{X}\mathbf{Y} = \mathbf{I}, \mathbf{X} > \mathbf{0}, \\
&\quad \mathbf{P} < \mathbf{0}, \mathbf{P} = \mathbf{P}^T, \tag{5.32}
\end{aligned}$$

where

$$\mathbf{P} = \begin{bmatrix} -\mathbf{Y} & \mathbf{A}_0 + \mathbf{B}_2\mathbf{w}\mathbf{C}_2 & \mathbf{B}_1 & \mathbf{0} \\ * & -\mathbf{X} & \mathbf{0} & (\mathbf{C}_1 + \mathbf{D}_{12}\mathbf{w}\mathbf{C}_2)^T \\ * & * & -\gamma & \mathbf{D}_{11}^T \\ * & * & * & -\gamma \end{bmatrix}.$$

For a review of LMI and convex optimization, see [9]. This problem is known to be non-convex because of the non-affine equality $\mathbf{XY} = \mathbf{I}$, and an NP-hard problem can be formulated in this form [8]. Therefore a global optimum of (5.32) cannot be obtained by a computationally tractable method. However, in practice there exist good solvers which give reasonable solutions in many cases. Sometimes one can convert the non-convex problem (5.32) to a convex one through a change of variables [64]; however, (5.32) does not satisfy the necessary assumptions in [64]. Therefore, a cone complementarity linearization algorithm [15] is used to handle the bilinear matrix equality. This is based on collaborative work. Please refer to [24] for more details on the optimization technique used to find the controller.

5.2.2 A Cone Complementarity Linearization Algorithm

Since the optimization (5.32) is not convex, we present an approximate semidefinite program which gives us a suboptimal solution of the problem (5.32). Let us start with following observation.

Proposition 5.2.1 *The optimal solution of following problem, $(\mathbf{X}^*, \mathbf{Y}^*)$, satisfies $\mathbf{X}^* \mathbf{Y}^* = \mathbf{I}$.*

$$\begin{aligned} & \underset{\mathbf{X}, \mathbf{Y}}{\text{minimize}} && \text{Tr}(\mathbf{XY}) \\ & \text{subject to} && \begin{bmatrix} \mathbf{X} & \mathbf{I} \\ \mathbf{I} & \mathbf{Y} \end{bmatrix} \succeq \mathbf{0} \\ & && \mathbf{X} > \mathbf{0}, \mathbf{Y} > \mathbf{0}. \end{aligned}$$

Proof 2 *By taking Schur complement to the first LMI, we have, $\mathbf{Y} - \mathbf{X}^{-1} \succeq \mathbf{0}$. This is equivalent to $\mathbf{X}^{1/2} \mathbf{Y} \mathbf{X}^{1/2} \succeq \mathbf{I}$. Since $\text{Tr}(\mathbf{X}^{1/2} \mathbf{Y} \mathbf{X}^{1/2}) = \text{Tr}(\mathbf{XY})$, the minimum is achieved when $\mathbf{X}^{1/2} \mathbf{Y} \mathbf{X}^{1/2} = \mathbf{I}$. This implies $\mathbf{XY} = \mathbf{I}$.*

Now for a given γ , consider the following optimization problem:

$$\begin{aligned} & \underset{\mathbf{w}, \mathbf{X}, \mathbf{Y}}{\text{minimize}} && \text{Tr}(\mathbf{XY}) \\ & \text{subject to} && \mathbf{w} \in \mathcal{W}, \\ & && \begin{bmatrix} \mathbf{X} & \mathbf{I} \\ \mathbf{I} & \mathbf{Y} \end{bmatrix} \succeq \mathbf{0} \\ & && \mathbf{X}, \mathbf{Y} \succeq \mathbf{0}, \mathbf{P} < \mathbf{0}, \mathbf{P} = \mathbf{P}^T \end{aligned}$$

where

$$\mathbf{P} = \begin{bmatrix} -\mathbf{Y} & \mathbf{A}_0 + \mathbf{B}_2 \mathbf{w} \mathbf{C}_2 & \mathbf{B}_1 & \mathbf{0} \\ * & -\mathbf{X} & \mathbf{0} & (\mathbf{C}_1 + \mathbf{D}_{12} \mathbf{w} \mathbf{C}_2)^T \\ * & * & -\gamma & \mathbf{D}_{11}^T \\ * & * & * & -\gamma \end{bmatrix}.$$

If there exists a triplet $(\mathbf{w}, \mathbf{X}, \mathbf{Y})$ that satisfies all the constraints and $\mathbf{X}\mathbf{Y} = \mathbf{I}$, then the above optimization problem recovers this triplet. Therefore, we can successfully construct a \mathbf{w} such that the H_∞ norm of the transfer function is less than γ . However, since the objective function is not convex, we use a linearization technique to solve this problem, namely:

$$\begin{aligned} & \underset{\mathbf{w}, \mathbf{X}, \mathbf{Y}}{\text{minimize}} && \text{Tr}(\mathbf{X}_k \mathbf{Y} + \mathbf{X} \mathbf{Y}_k) \\ & \text{subject to} && \mathbf{w} \in \mathcal{W} \\ & && \begin{bmatrix} \mathbf{X} & \mathbf{I} \\ \mathbf{I} & \mathbf{Y} \end{bmatrix} \geq 0 \\ & && \mathbf{X}, \mathbf{Y} \geq \mathbf{0}, \mathbf{P} < \mathbf{0}. \end{aligned} \tag{5.33}$$

Cone complementary solver:

1. Set $k = 0$, and $\mathbf{X}_0 = \mathbf{Y}_0 = \mathbf{I}$.
2. Solve the optimization problem (5.33) to generate $\mathbf{X}_{k+1}, \mathbf{Y}_{k+1}$.
3. Set $k = k + 1$, and do step 2 until \mathbf{X}_k converges.

Note that if iterative procedure above finds $(\mathbf{w}, \mathbf{X}, \mathbf{Y})$ where $\mathbf{X}\mathbf{Y} = \mathbf{I}$, then this weight \mathbf{w} guarantees the stability of the closed loop system and the H_∞ norm is less than γ . However, since the above procedure uses a linearized version of the true objective function, the procedure may fail to recover the solution $(\mathbf{w}, \mathbf{X}, \mathbf{X}^{-1})$ in some cases. In this sense, this procedure is only an approximate solver for the original problem. In practice, this approach works well.

Finally, since we can approximately solve the problem given γ , we now apply a bisection search to obtain the minimum γ .

Bisection search:

1. Set $l = 0$, and $\gamma = 1$.
2. Solve the optimization problem (5.33) for γ .

3. If (5.33) recovers $\mathbf{XY} = \mathbf{I}$, then set $u = \gamma$, otherwise $l = \gamma$.
4. Set $\gamma = \frac{1}{2}(l + u)$. Go to step 2 until γ converges.

Again, since (5.33) is an approximate solver, the above bisection search can converge to a point which is not a true minimum.

5.3 Application to a genetic auto-regulatory network

5.3.1 Model

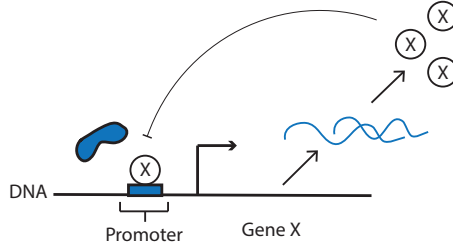


Figure 5.4: Self regulating protein production.

In this section we apply the numerical method to the design of a scalar auto-regulatory genetic system, an example is shown in Fig. 5.4, where protein x inhibits further production of itself by not allowing the RNA polymerase to bind, therefore inhibiting initiation of transcription. Consider the modified scalar example from Section 2.1:

$$\begin{aligned}
 dy = & \left(\int_0^\infty a x_0(t - \tau) g(\tau) d\tau - \gamma y \right) dt \\
 & + \frac{1}{\sqrt{\Omega}} \sqrt{\left(\int_0^\infty a x_0(t - \tau) g(\tau) d\tau + \gamma y \right)} dW.
 \end{aligned} \tag{5.34}$$

A feedback path is implemented by making the input x_0 a function of the measured protein y ,

$$\begin{aligned}
 dy = & \left(\int_0^\infty a f(y(t - \tau)) h(\tau) d\tau - \gamma y \right) dt \\
 & + \frac{1}{\sqrt{\Omega}} \sqrt{\left(\int_0^\infty a f(y(t - \tau)) h(\tau) d\tau + \gamma y \right)} dW,
 \end{aligned} \tag{5.35}$$

where

$$f(y) = \frac{d}{1 + Ky^2}$$

is a Hill function representing the rate of transcription initiation. The variable d represents the total number of genes and K is the ratio of the association rate to the dissociation rate of the transcription factor proteins with the genes. The variables are set to $\gamma = 0.01$, $d = 10$, $a = 0.1$, and $K = 0.1$. From the example, it can be seen that a source of noise on protein production can come from the stochastic nature of the system and is state dependent. In addition, there can be other sources of noise, such as temperature fluctuations, cell division, and crosstalk, which are not modeled. The nature of the noise is oversimplified and lumped into a non-state dependent term η assumed to be bounded for sake of simplicity:

$$dy = \left(\int_0^\infty a f(y(t-\tau)) h(\tau) d\tau - \gamma y \right) dt + \eta. \quad (5.36)$$

The noise rejection properties of the deterministic system will be investigated.

The distribution $g(\tau)$ is no longer assumed to be an Erlang distribution. Now it is taken to be a design variable such that $\int_0^\infty g(\tau) d\tau = 1$, and $g(t) \geq 0$ for all t . More generally we would like to design the optimal distribution $g(t)$. In the discretization of the system, $g(t)$ takes on the form

$$g(\sigma) = \sum_{k=\tau}^N w_k \delta(\sigma - kT), \quad (5.37)$$

where T is the sampling period, and δ is the Dirac delta function. Note that we inherently place the additional constraints on the weights $w_i \geq 0$ and $\sum_{i=\tau}^N w_i = 1$. Therefore our convex set $\mathcal{W} = \{\mathbf{w} : w_i \geq 0, \sum_{i=\tau}^N w_i = 1\}$.

In this example we ignore the possibility of negative weights, which requires a different nonlinearity and will be addressed in future work. The constraint on the sum ensures that we do not require a change in the overall effective feedback gain, which is important in order to avoid a need to change production rates. One can imagine implementing such a controller simply by changing the ratio of plasmids with respective delays or applying competitive binding so that the weights correspond to the probability of each particular delayed state binding to the promotor site.

System (5.36) is linearized around the equilibrium point $x_e = \frac{1}{2} \left(\sqrt{(1/K)^2 + 4ad/(K\gamma)} - 1/K \right)$ of the non-perturbed system, which gives

$$\dot{x} = -\delta x(t) + \kappa \sum_{k=\tau}^N w_k x(t - kT) + \eta, \quad (5.38)$$

where $\kappa = -a \frac{dK}{(x_e K+1)^2}$. Applying the zero order hold method with a sampling time of T , an equivalent discrete time system is given by

$$x(k+1) = d_2 x(k) + d_1 \kappa \sum_{i=\tau}^N w_i x(k-i) + \eta, \quad (5.39)$$

where $d_2 = e^{-T\gamma}$ and $d_1 = \frac{1}{\gamma}(1 - e^{-T\gamma})$. We optimize over the weights and implement into the full nonlinear system.

5.3.2 Design Results

For the discretization, we use $T = 60$ s (1 minute) as a sampling period, and assume the minimum time delay $\tau = 10$, which corresponds to 10 minutes. For maximum delays, we test $N = 10, 15, 20, 25$, and 30 as an example, and set the filter parameter $\alpha = 0.99$. The resulting delay distribution vectors are shown in the first panel of Fig. 5.5. Notice that the first and the last delay channels are most important, and other channels have similar weights to each other. The second panel of Figure 5.5 shows the Bode magnitude plot of the transfer function

$$H_{\eta \rightarrow x}(z) = \frac{1}{z - d_2 - d_1 \kappa \sum_{i=\tau}^N w_i z^{-i}} \quad (5.40)$$

corresponding to system (5.39) for the various weight vectors. To draw a bode plot in s -domain from the data in the z -domain, we substitute $z = e^{j\omega T}$ to obtain a complex valued function $H(e^{j\omega T})$ and plot $|H(e^{j\omega T})|$ as a Bode magnitude plot by varying $\omega \in [0, \frac{\pi}{T}]$. For details, see [57].

A larger maximum delay N results in more degrees of freedom in the design stage, hence, we should expect better performance in the result. As we can see, when $N = 30$ the transfer function $H(z)$ shows better attenuation. Notice that we optimized the filtered version of the H_∞ norm, $\|FH\|_\infty$, and not the unweighted one, so a direct numerical comparison of Bode magnitude plots should be considered carefully.

We apply the results obtained to the original nonlinear system (5.36). The final model representing the modified network is described by

$$\dot{y}(t) = a \frac{d}{K \left[\sum_{k=\tau}^N w_k x(t - kT) \right] + 1} - \gamma y(t) + \eta. \quad (5.41)$$

The nonlinear system with multiple delayed feedback is simulated in Fig. 5.6. The noise is modeled as a sum of periodic functions at various equally spaced frequencies beginning at 10^{-3} Hz. The

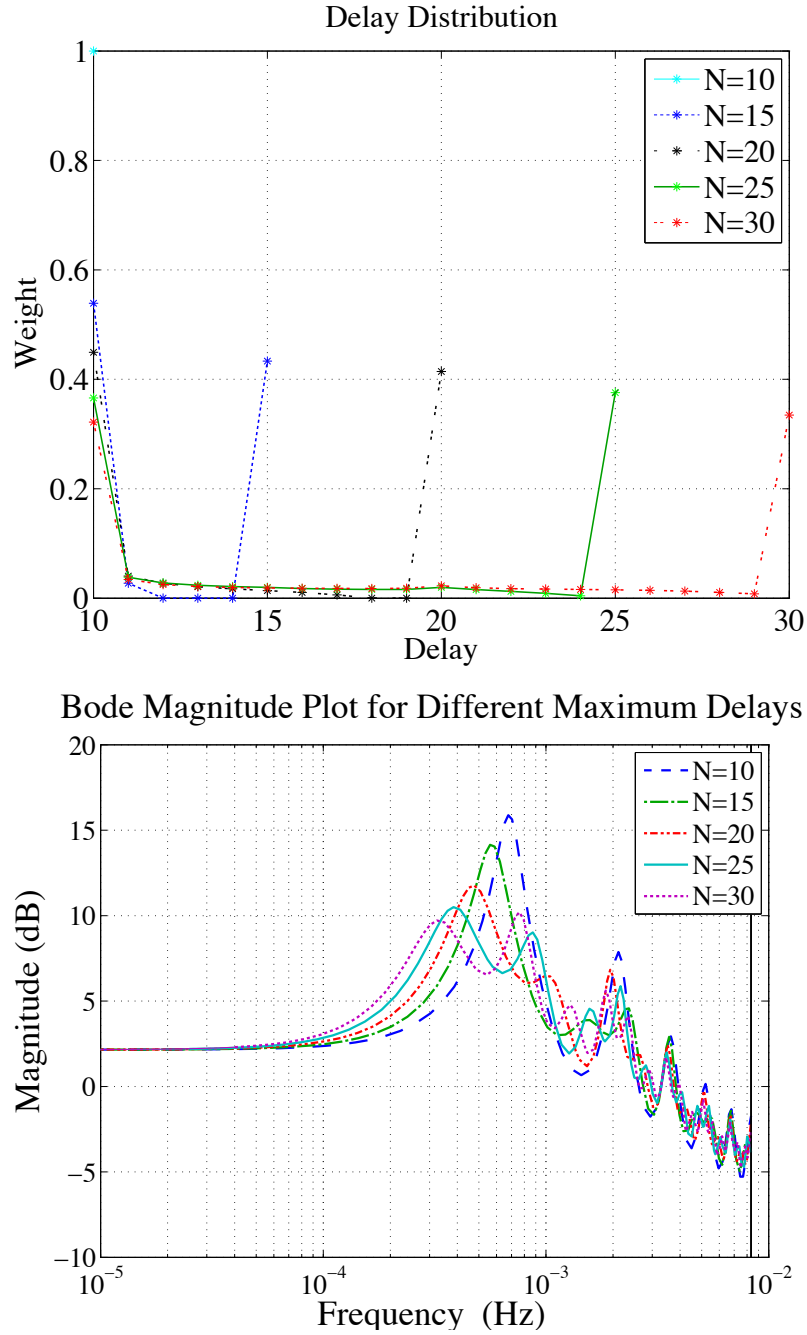


Figure 5.5: Top: Resulting delay distribution for multiple maximum delays N . Bottom: Frequency response plot of transfer function (5.40) for multiple maximum delays N .

initial condition is chosen away from the equilibrium point to demonstrate the effect on transients as well. Notice that in Fig. 5.6, our designed multiple delayed feedback channels help to decrease the fluctuations in protein production.

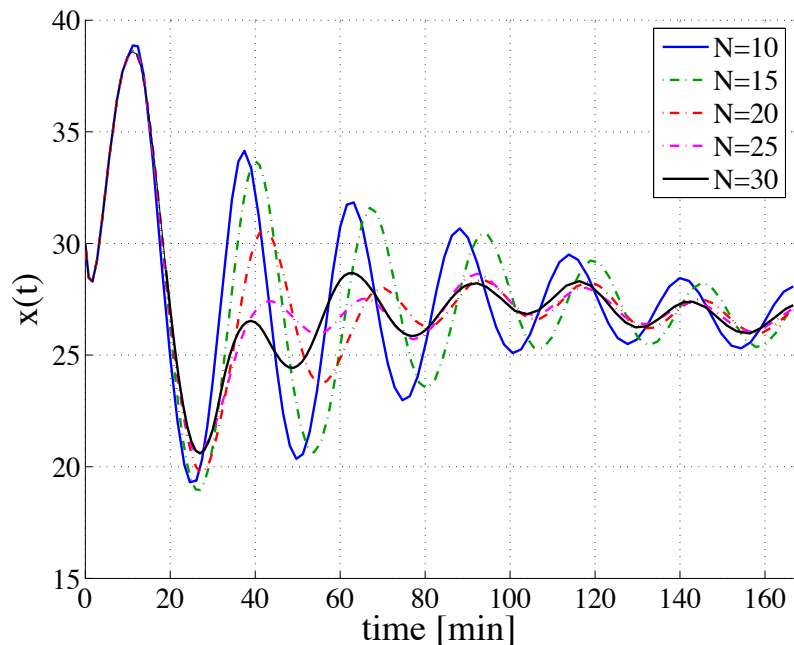


Figure 5.6: Simulations of nonlinear system with distributed delays.

5.3.3 Implementation

The final discrete-time systems resembles an autoregressive system but cannot be implemented in the same way. In the motivating example, the controller is to be implemented in live cells versus hardware. There is no known method to store past state values. Instead the delay-based controller is implemented through added dynamical components. As was seen before, when modeling dynamics for average protein expression (protein expression in the thermodynamics limit), the stochastic nature of transcriptional delays leads to a distributed delay differential equation. To some extent, we are addressing a synthesis problem for these genetic regulatory systems utilizing the mean dynamics, where we design an optimal distribution function for the stochastic delays. We can consider adding pathways that will give us desirable delay distributions. In a cellular network, it would be near impossible to implement the exact controller found in the previous section. Fine tuning the weights for each of the delayed states would be challenging. However, we consider the results as guides to robust network motifs in genetic regulatory networks as we look for control architectures that will exploit the stochasticity in the system. A distribution similar to the resulting controller can be achieved with two different transcriptional pathways of different lengths and with relatively tight distributions. We now know we can achieve tight distributions with large gene sequences. The weights on each of the pathways could be tuned by manipulating the binding affinities of the

transcription factor proteins resulting from each pathway.

5.3.4 Discussion

We have designed a system robust to system input disturbances, however, we have no guarantees on robustness of the system with respect to changes in parameters. We now investigate the stability regions of the system. Furthermore, we investigate the unexpected design results. It is curious to see that the majority of the weight is distributed among the first and last delay even as the second delay continues to increase. We investigate this with a purely dual-delayed feedback system.

Stability regions for the different sets of delays and their respective weights are considered. The stability region for the general system (5.24) is determined by the characteristic equation

$$z - a - b \sum_{i=\tau}^N w_i z^{-i} = 0 \quad (5.42)$$

given by the denominator of the transfer function (5.40). For discrete-time systems, a system is unstable when $|z| \geq 1$, therefore, the characteristic equation is evaluated at $|z| = 1$ to map out the curves on the (a, b) parameter space when an eigenvalue crosses the unit circle. These curves can be obtained by evaluating the characteristic equation at $z = 1$, $z = -1$, and $z = e^{i\theta}$ [28,41]. It is worth noting that $z = 1$ (black curve) gives a delay independent stability condition $b = 1 - a$.

Fig. 5.7 shows the stability region for the original system with a single delay. If the system parameters (a, b) are in the shaded region, then the system is stable. From our nominal parameter values, we obtain $(a, b) = (0.5488, -0.3293)$, which is indicated by a circle marker in Fig. 5.7.

Fig. 5.8 shows the stability regions for the various distributed delayed systems. The overlaying green shaded region and grey curves correspond to the stability region for the original system shown in Fig. 5.7. One can see that the area of the stability region increases as the maximum delay N increases. There is also a notable difference in the robustness to uncertainty in parameter values.

Now, we consider the system (5.39) with a purely dual-delayed feedback. The transfer function is given by

$$H_{n_1 \rightarrow x}(z) = \frac{1}{z - d_2 - d_1 \kappa (w_1 z^{-\tau_1} + w_2 z^{-\tau_2})}, \quad (5.43)$$

where $\tau_2 \geq \tau_1$. The mean and the standard deviation of the distribution of the delays is given by

$$E = \frac{\tau_2 + \tau_1}{2}, \quad S = \frac{\tau_2 - \tau_1}{2}, \quad (5.44)$$

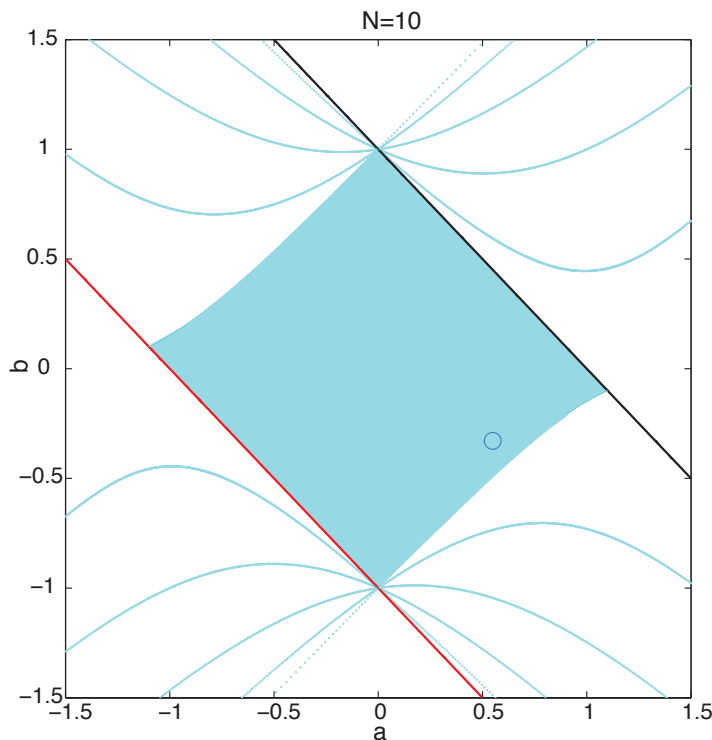


Figure 5.7: Stability plot for the system with a single delay $\tau = 10$. The black circle indicates the parameter values corresponding to the simulations.

respectively. Figure 5.9 shows how the H_∞ norm changes as the second delay is increased. For system parameters $(a, b) = (0.5488, -0.3293)$ the system does not lose stability. This can be verified by applying the Nyquist criterion, similar to the method presented in Section 5.1.

We see evidence to support that distributing the weights to the ends can improve the system. For a large enough primary delay, as the second delay increases, the system improves until a critical value is reached, after which the system performance begins to degrade again. This was observed in Section 5.1 as well. However, for a small enough delay, any added delay will make the system worse. Therefore, this method is only applicable to systems with relatively large delays, which is a reasonable assumption in some genetic regulatory networks, as shown in more recent models fitted to experimental data [47,11,32].

However, we saw in the previous section that the system continued to improve as N increased. A possible reason for this may be that the non-zero weights on the delays in between the end values decrease the gain on the two largest weighted delays, resulting in a larger region of stability with respect to the second delay. This combines the benefit of a dual-delayed feedback and a reduction

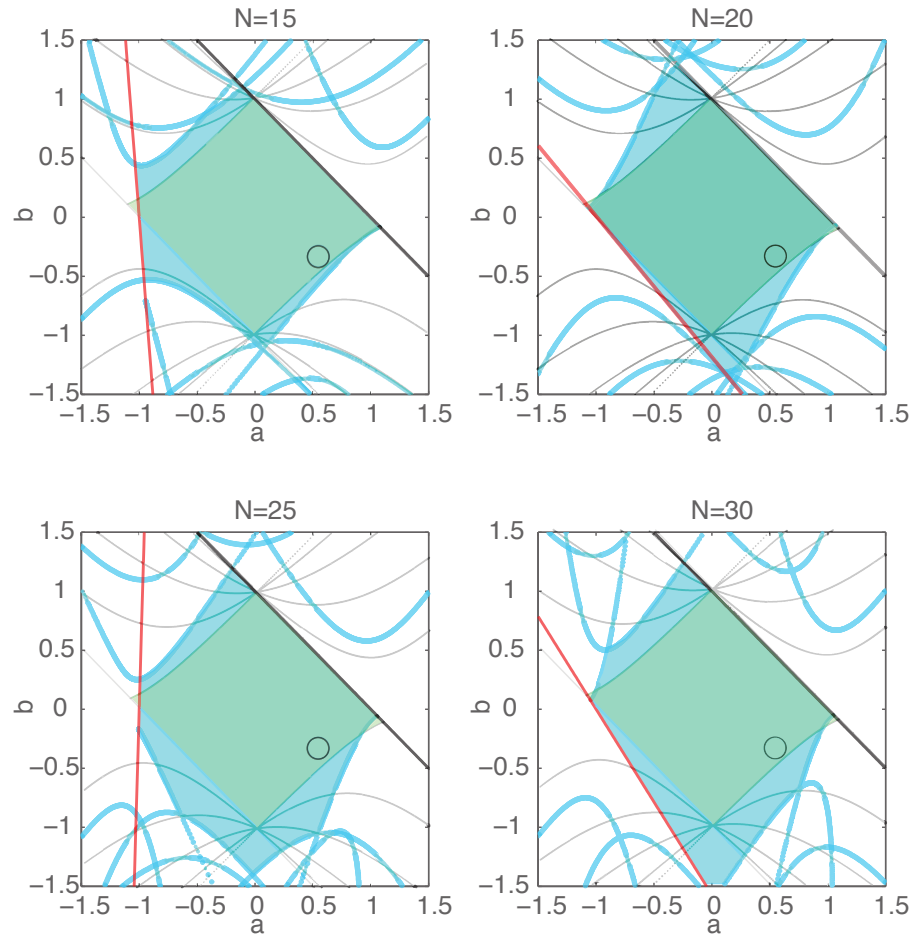


Figure 5.8: Stability plots for different delay ranges and distributions (blue). The shaded green region and grey lines correspond to the stability plot in Fig. 5.7. The black circle indicates the parameter values corresponding to the simulations.

in the effective gain. We initially assumed that the primary delay was a single discrete, but we see how a distributed delay (a possibly more accurate description due to variation in the delays) can potentially benefit the system.

Notice that even though adding additional delays decreases the H_∞ norm from the input to the output, the waterbed effect can result in larger magnitudes at the higher frequencies. It appears as though the distribution which gives the smallest H_∞ norm may not always be the best choice. One could imagine designing the weighting filter such that improvement is obtained where needed, based on knowledge of the uncertainty.

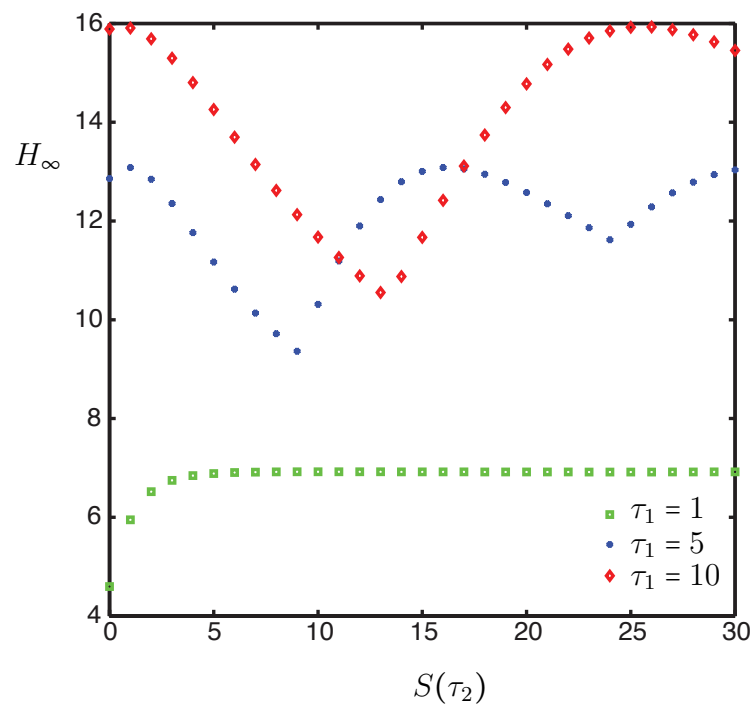


Figure 5.9: Plot of H_∞ norm as a function of the standard deviation S for different values of τ_1 .

Chapter 6

Conclusions and Future Work

6.1 Conclusions

The noisy nature of genetic regulatory networks has been viewed as a real obstacle in designing networks with predictable behavior, but results suggest that the stochastic nature of the delay may help to increase stability regions. In addition, delays can play a positive role in the performance of systems. Interestingly enough, introns add significant delays in eukaryotes and reduce the relative variance of the delay distribution in transcription. In humans for example, it is odd to think that introns (noncoding DNA) account for 94% of the transcriptional delay, increasing the delay more than 15 fold. If one considers a simple feedback system, the larger delay with a tighter distribution may be more likely to destabilize, however, introns allow for more complex regulatory mechanisms. One of the long-term goals of this work is understanding how delays influence dynamics in genetic regulatory networks and the evolved control mechanisms that handle them.

It was shown that transcriptional and translational delays can be well approximated by an Erlang distribution. This approximation is a common assumption but only now has been substantiated more rigorously. The distribution for a time-varying rate coefficient was also derived, which we showed to be useful in applications to temperature sensitive oscillators.

This modeling framework then served as a powerful tool to investigate the effect of delays on the dynamics of regulatory networks, albeit in simplified networks, but with interesting results nonetheless. Feedback systems were investigated with varying distribution parameters and varying temperature. With the modeling framework used for the delays, the distribution parameters can be directly related to properties of the system, namely, reaction rates and gene lengths. This told us that while an increased gene length decreases the relative variance of the distribution, it also reduces the stability region. We found the same general trends in the stochastic and deterministic modeling

framework. In addition, the bifurcation curve for the stochastic system approached that of the deterministic system quickly as the relative variance decreased. Considering average gene lengths are at minimum on the order of 10^3 , we find that the deterministic system (the average dynamics in the thermodynamic limit) provides a good approximation of the stability region.

The relation between the delay distribution and the period of limit cycles induced in autoregulatory networks was explored. As would be expected, larger delays lead to larger periods of oscillations. However, as the relative variance decreased, the period quickly approached twice the mean delay of the distribution. Under the conditions of time-varying temperatures, it was shown that a robust limit cycle can be achieved if the delay is near the period of oscillation of the temperature.

A common recurring motif in biological systems is the dual-feedback system. One can consider this a different level of distributed delayed feedback. From the results obtained with a single feedback path, one may guess that a second feedback path may also aid in stabilizing a system since it increases the variance of the distribution. It is demonstrated that this is indeed possible but may not always hold true. There is a definite tradeoff between the stabilizing effects of an increasing variance and the destabilizing effects of increased delay. In some collaborative work, a delay-based controller design method is proposed. In a motivating example, the dual-delayed feedback path is shown to re-emerge as an effective network structure for increased stability and even noise rejection, suggesting, along with previous work, that the second feedback path may be an intentional easily-implementable controller design.

6.2 Future Work

In Chapter 3, stability conditions were found for stochastic feedback systems with identically independently distributed delays. Future work includes generalizing the results. Namely considering stochastic delays that may not necessarily be identically independently distributed. This assumption was key to the results in Chapter 3. Finding conditions that imply convergence with probability one (w.p.1) is not a trivial task; however, there are many well known convergence theorems for Martingales [78]. These results can allow one to determine stability of systems with more general dynamics on the stochastic evolution of the delay τ with conditional probabilities.

In future work we also propose using results on general phase-type distributions [17]. Results indicate that any positive distribution can be arbitrarily approximated by phase-type distributions. Erlang is a special case of a phase-type distribution. An advantage to the phase-type distribution is that it can be represented by a first passage time of a Markov process. Furthermore, a distribution

resulting from the convolution of different Erlang distributions is also a phase-type distribution. The resulting distribution is not trivial, but in the framework of a phase-type distribution one can easily calculate the first and second moment. We have seen that the second moment plays a crucial role in stability. Using this approach, one can determine the properties of the distribution capturing not only transcription but also translation and protein folding.

In Chapter 5 delay-based controllers were considered. Delayed pathways were added to a feedback system to improve stability and performance. In future work we would like to consider the possibility of applying a time-varying delay based controller. For example, instead of adding multiple delays, a single delay can be designed to adaptively change with time. This concept is similar to adaptive control where a time-varying feedback gain is designed.

In a much broader scope, future work entails developing control theoretic tools for analysis and design of synthetic networks. This will incorporate experimental assays and new systems theory tailored to genetic regulatory networks. This includes developing a systematic way of deriving reduced state delay-based models for easier analysis.

Designing robustness in man-made systems has been key to advancements in technology such as aircraft or satellites in orbit. To make similar advancements in genetic regulatory networks, one can apply the same control theoretic tools to analyze and systematically design networks. However, isolating and identifying control mechanisms in regulatory networks in existing biological systems is a difficult task due to the complexity of the networks and highly nonlinear couplings. Interactions such as “cross-talk” or undesirable biochemical processes are not well understood, and so further problematize research. To effectively manage these issues, the objective is to investigate control mechanisms and recurring motifs in existing regulatory networks in search of evolved phenotypic control mechanisms to gauge the effectiveness of controller motifs via modeling and synthetic engineering. Using a control theoretic approach, one can investigate the robustness properties of motifs such as was done with the promising dual-delayed feedback. To deal with the fundamental differences between biological systems and man-made systems, one can anticipate the need to develop new control theory-based tools as part of a long-term objective.

The significance of deduced analytical results depends upon the model’s ability to accurately capture important dynamics; therefore, a predictive model is essential in systematically designing a regulatory network. The chemical master equation is the most widely accepted description of intracellular dynamics and often simulated through Gillespie algorithms because they are difficult to deal with analytically [79]. Generalized mass action models, models consisting of ordinary differ-

ential equations derived from rate equations, are more tractable analytically. However, in order to gain a more rigorously qualitative understanding, generalized mass action models are often reduced through Michaelis-Menten [53] and Hill-type function approximations [25]. Accurately predicting behavior with reduced models is challenging and often deters biologists from using models for design. Additionally, more involved models have limitations due to a lack of full understanding of cellular processes and the inability to measure all system parameters [46]. Even assuming full knowledge of a system, the complexity of the model would not lend to design easily because of the difficulty in identifying the components most influential to stability and performance. In modeling, there is a need to find a balance between accuracy (complexity) and capturing essential qualitative behavior, which involves identifying important system properties.

Future work aims to identify a suitable modeling framework for controller design. We propose that this will be a distributed-delay based model, thus, we will design assays that measure delay distributions in system response. We will explore stochastic as well as deterministic models. The main reason we adopt this model is its generality and applicability without having to characterize all chemical processes involved in protein production. This ensures a working predictable model suitable for pursuing design efforts, while accurately quantifying robustness properties and effectiveness of delay-based controller designs in regulatory networks.

The variability we are most interested in capturing is delay distributions of system response to an inducer because we would like to have control over the initiation of transcription. We can treat a subsystem as a black box, in which we can measure the output response to a known input, a characterization of systems typical in engineering. One may not be able to measure times required for the intermediate steps in protein production such as binding time of transcription factor protein to the promoter site, transcription, and protein folding time; however, one can get a distribution on the time needed for these lumped processes to take place or the time required for all intermediate process to complete. We can then achieve a low dimensional accurate model by implicitly capturing intermediate processes through distributed, delayed differential equations. Figure 6.1 illustrates how we will utilize single-cell tracking methods to capture variability in the delays for “turn on” times, the time from initiation of transcription to the time we see fluorescence or protein production time. In addition, we can look at the response time of more complex circuits, such as a full feedback network.

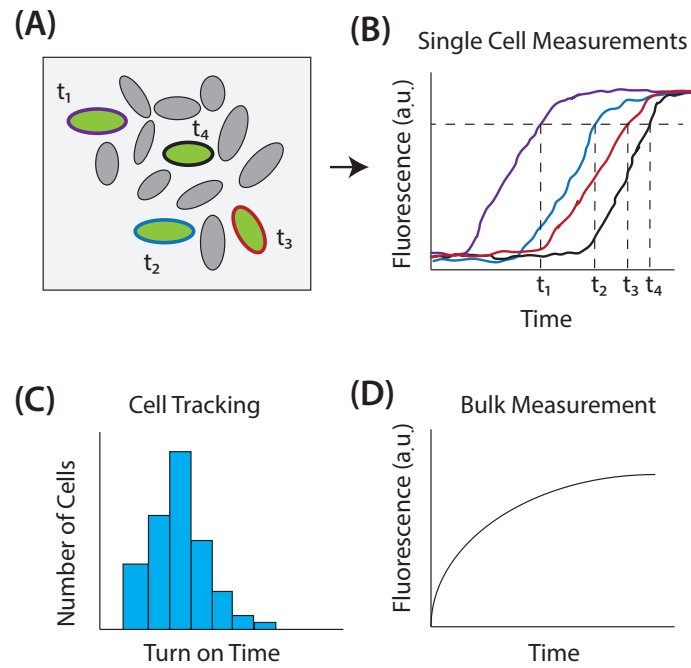


Figure 6.1: Characterizing delay distributions using single-cell measurements. (A) Cartoon image of cells under a microscope in which “turn on” times of fluorescence are indicated by labels t_1 , t_2 , t_3 , and t_4 . (B) Single-cell fluorescence plots. The cells are considered “on” after exceeding an indicated threshold. (C) Cartoon histogram of cell “turn on” times allocated into bins and used to fit a distribution function. (D) Cartoon response time of a population of cells. The response time of a population of cells may likely depend on the measured single-cell distribution.

Bibliography

- [1] C. Abdallah, P. Dorato, and J. Benites-Read. Delayed positive feedback can stabilize oscillatory systems. In *American Control Conference, ACC*, 1983.
- [2] B. Alberts. *Molecular Biology of the Cell*. Taylor & Francis, 2007.
- [3] R. P. Alexander, G. Fang, J. Rozowsky, M. Snyder, and M. B. Gerstein. Annotating non-coding regions of the genome. *Nat Rev Genet*, 11:559–571, 2010.
- [4] R. Anderson. Geometric and probabilistic stability criteria for delay systems. *Math Biosci*, 105:81–96, 1991.
- [5] R. Anderson. The relative variance criterion for stability of delay systems. *J Dynam Differential Equations*, 5(1):105–128, 1993.
- [6] S. Bernard, J. Bélair, and M. C. Mackey. Sufficient conditions for stability of linear differential equations with distributed delay. *Discret Contin Dyn Sys*, 1(2):233–256, 2001.
- [7] S. Bhartiya, N. Chaudhary, K. Venkatesh, and F. J. D. III. Multiple feedback loop design in the tryptophan regulatory network of Escherichia coli suggests a paradigm for robust regulation of processes in series. *J R Soc Interface*, (3):383–391, 2006.
- [8] V. Blondel and J. N. Tsitsiklis. Np-hardness of some linear control design problems. *SIAM Journal on Control and Optimization*, 35(6):2118–2127, 1997.
- [9] S. P. Boyd and L. Vandenberghe. *Convex Optimization*. Cambridge university press, 2004.
- [10] H. Bremer and D. Yuan. RNA chain growth-rate in Escherichia coli. *J Mol Biol*, 38(2):163–80, 1968.
- [11] T. Danino, O. M. Palomino, . Tsimring, and J. Hasty. A synchronized quorum of genetic clocks. *Nature*, 463:326–330, 2010.

- [12] J. Doyle, K. Zhou, K. Glover, and B. Bodenheimer. Mixed H_2 and H^∞ performance objectives II: Optimal control. *IEEE Trans Autom Control*, 39(8):1575–1587, 1994.
- [13] J. C. Doyle, B. A. Francis, and A. Tannenbaum. *Feedback Control Theory*, volume 1. Macmillan Publishing Company New York, 1992.
- [14] G. E. Dullerud and F. Paganini. *A Course in Robust Control Theory*, volume 6. Springer New York, 2000.
- [15] L. E. Ghaoui, F. Oustry, and M. AitRami. A cone complementarity linearization algorithm for static output-feedback and related problems. *IEEE Trans Autom Control*, 42(8):1171–1176, 1997.
- [16] M. B. Elowitz, A. J. Levine, E. D. Siggia, and P. S. Swain. Stochastic gene expression in a single cell. *Science*, 297:1183–1186, 2002.
- [17] R. M. Feldman and C. V. Flores. *Applied Probability and Stochastic Processes*. Springer, 2010.
- [18] J. Gadewadikar, F. L. Lewis, and M. Abu-Khalaf. Necessary and sufficient conditions for h-infinity static output-feedback control. *Journal of Guidance, Control, and Dynamics*, 29(4):915–920, 2006.
- [19] H. Gao and T. Chen. New results on stability of discrete-time systems with time-varying state delay. *IEEE Trans Autom Control*, 52(2):328–334, 2007.
- [20] M. Ghasemi, S. Zhao, T. Insperger, and T. Kalmár-Nagy. Act-and-wait control of discrete systems with random delays. *American Control Conference, ACC*, pages 5440–5443, 2012.
- [21] D. T. Gillespie. Exact stochastic simulation of coupled chemical reactions. *J Phys Chem*, 81:2340–2361, 1977.
- [22] D. T. Gillespie. The chemical langevin equation. *J Chem Phys*, 113(1):297–306, 2000.
- [23] M. M. Gomez and R. M. Murray. Stabilization of feedback systems via distribution of delays. In *10th IFAC Workshop on Time Delay Systems*, IFAC, pages 203–208, 2012.
- [24] M. M. Gomez, S. You, and R. M. Murray. Time-delayed feedback channel design: discrete-time H_∞ approach. 2014.
- [25] D. Gonze and W. Abou-Jaoudé. The goodwin model: Behind the hill function. *PLoS ONE*, 8(8), 2013.

- [26] D. Gonze, J. Halloy, and A. Goldbeter. Robustness of circadian rhythms with respect to molecular noise. *Proc Natl Acad Sci USA*, 99(2):673–678, 2002.
- [27] G. R. Grimmet and D. R. Stirzaker. *Probability and Random Processes*. Oxford University Press, 2001.
- [28] J. Guckenheimer and P. Holmes. *Nonlinear Oscillations, Dynamical Systems, and Bifurcations of Vector Fields*, volume 42 of *Applied Mathematical Sciences*. Springer, 1983.
- [29] C. Gupta, J. M. Lopez, R. Azencott, and M. R. Bennett. Modeling delay in genetic networks: From delay birth-death processes to delay stochastic differential equations. *J Chem Phys*, 140, 2014.
- [30] J. K. Hale and S. M. V. Lunel. *Introduction to Functional Differential Equations*. Springer-Verlag, 1993.
- [31] C. I. Hong, E. D. Conrad, and J. J. Tyson. A proposal for robust temperature compensation of circadian rhythms. *Proc Natl Acad Sci USA*, 104(4):1195–1200, 2007.
- [32] F. Hussain, C. Gupta, A. J. Hirning, W. R. Ott, K. S. Matthews, K. Josic, and M. R. Bennett. Engineered temperature compensation in a synthetic genetic clock. *Proc Natl Acad Sci USA*, 111:972–977, 2014.
- [33] T. Insperger and S. Gábor. *Semi-Discretization for Time-Delay Systems: Stability and Engineering Applications*, volume 178. Applied Mathematical Sciences, 2011.
- [34] K. Josić, J. M. López, W. Ott, L. Shiau, and M. R. Bennett. Stochastic delay accelerates signaling in gene networks. *PLoS Comput Biol*, 7(11), 2011.
- [35] T. B. Kepler and T. C. Elston. Stochasticity in transcriptional regulation: origins, consequences, and mathematical representations. *Biophys J*, 81:3116–3136, 2001.
- [36] H. K. Khalil. *Nonlinear Systems*. Prentice Hall, 2002.
- [37] V. L. Kharitonov, S. I. Niculescu, J. Moreno, and W. Michiels. Static output feedback stabilization: Necessary conditions for multiple delay controllers. *IEEE Trans Autom Control*, 50(1):82–86, 2005.
- [38] S. Klumpp. A superresolution census of RNA polymerase. *Biophys J*, 105(12):2613–2614, 2013.

- [39] V. B. Kolmanovskiy and V. R. Nosov. *Stability of Functional Differential Equations*. San Diego, CA: Academic, 1986.
- [40] H. Kushner. *Introduction to Stochastic Control*. Holt, Rinehart and Winston, Inc., 1971.
- [41] Y. A. Kuznetsov. *Elements of Applied Bifurcation Theory*, volume 112 of *Applied Mathematical Sciences*. Springer, 3rd edition, 2004.
- [42] K. L., D. V., S. B. Gondi, C. Santoriello, T. Dickmeis, and N. S. Foulkes. Temperature regulates transcription in the zebrafish circadian clock. *PLoS Biol*, 3(11):2005–2016, 2005.
- [43] J. Lavaei, S. Sojoudi, and R. M. Murray. Simple delay-based implementation of continuous-time controllers. In *American Control Conference, ACC*, pages 5781–5788, Baltimore, MD, 2010.
- [44] J. C. Leloup and A. Goldbeter. Towards a detailed computation model for the mammalian circadian clock. *Proc. Natl. Acad. Sci. U.S.A.*, 100(12):7051–7056, 2003.
- [45] S. Liang, M. Bipatnath, Y. Xu, S. Chen, P. Dennis, M. Ehrenberg, and H. Bremer. Activities of constitutive promoters in Escherichia coli. *J Mol Biol*, 292(1):19–37, 1999.
- [46] G. Lillacci and M. Khammash. Parameter estimation and model selection in computational biology. *PLoS Comput Biol*, 6(3):e1000696, 2010.
- [47] D. M. Longo, J. Selimkhanov, J. D. Kearns, J. Hasty, A. Hoffman, and L. S. Tsimring. Dual delayed feedback provides sensitivity and robustness to the NF- κ B signaling module. *PLoS Comput Biol*, 9(6), 2013.
- [48] S. M. V. Lunel and B. Krauskopf. The mathematics of delay equations with an application to the Lang-Kobayashi equations. *AIP Conf Proc*, 548(66), 2000.
- [49] M. Lynch and J. S. Conery. The origin of genome complexity. *Science*, 302(5649):1401–1405, 2003.
- [50] N. MacDonald. Time lag in a model of a biochemical reaction sequence with product inhibition. *J Theor Biol*, 67(3):549–556, 1977.
- [51] A. I. Mees. *Dynamics of Feedback Systems*. John Wiley and Sons, 1981.
- [52] A. I. Mees and P. Rapp. Periodic metabolic systems: Oscillations in multiple-loop negative feedback biochemical control networks. *J Math Biol*, 5:99–114, 1978.

- [53] L. Michaelis and M. L. Menten. Die kinetik der invertinwirkung. *Biochem Z*, 49:333–369, 1913.
- [54] W. Michiels, S. I. Niculescu, and L. Moreau. Using delays and time-varying gains to improve the static output feedback stabilizability of linear systems: a comparison. *IMA J Math Control Info*, 21(4):393–418, 2004.
- [55] A. N. Naganathan and V. M. Noz. Scaling of folding times with protein size. *J Am Chem Soc*, 2(127):480–481, 2005.
- [56] S. I. Niculescu, K. Gu, and C. T. Abdallah. Some remarks on the delay stabilizing effect in siso systems. In *Proceedings of the American Control Conference, ACC*, 2003.
- [57] A. V. Oppenheim, A. S. Willsky, and S. H. Nawab. *Signals & Systems (2nd ed.)*. Prentice-Hall, Inc., Upper Saddle River, NJ, USA, 1996.
- [58] J. M. Paret and H. L. Smith. The Poincaré-Bendixson theorem for monotone cyclic feedback systems. *J Dyn Differ Equ*, 2(4), 1990.
- [59] P. G. Park. A delay-dependent stability criterion for systems with uncertain time-invariant delays. *IEEE Trans Autom Control*, 44(4):876–877, 1999.
- [60] P. E. M. Purnick and R. Weiss. The second wave of synthetic biology: from modules to systems. *Nature*, 10:410–422, 2009.
- [61] K. J. Åström and R. M. Murray. *Feedback Systems: An Introduction for Scientist and Engineers*. Princeton University Press, 2008.
- [62] I. B. Rogozin, K. S. Makarova, D. A. Natale, A. N. Spiridonov, R. L. Tatusov, Y. I. Wolf, J. Yin, and E. V. Koonin. Congruent evolution of different classes of non-coding in prokaryotic genomes. *Nucl Acids Res*, 30(19):4264–4271, 2002.
- [63] P. Ruoff and L. Rensing. The temperature-compensated goodwin model simulates many circadian clock properties. *J Theor Biol*, 179:275–285, 1996.
- [64] C. W. Scherer. An efficient solution to multi-objective control problems with LMI objectives. *Systems & Control Letters*, 40(1):43–57, 2000.
- [65] O. Shoval, L. Goentoro, Y. Hart, A. Mayo, E. Sontag, and U. Alon. Fold-change detection and scalar symmetry of sensory input fields. *PNAS*, 107(36):15995–16000, 2010.

- [66] J. Singh and R. A. Padgett. Rates of in situ transcription and splicing in large human genes. *Nat Struct Mol Biol*, 16(11):1128–1133, 2009.
- [67] P. Smolen, D. A. Baxter, and J. H. Byrne. A reduced model clarifies the role of feedback loops and time delays in the *Drosophila* circadian oscillator. *Biophys J*, 83:2349–2359, 2002.
- [68] T. Su and C. Huang. Robust stability of delay dependence for linear uncertain systems. *IEEE Trans Autom Control*, 37(10):1656–1659, 1992.
- [69] P. S. Swain, M. B. Elowitz, and E. D. Siggia. Intrinsic and extrinsic contributions to stochasticity in gene expression. *Proc Natl Acad Sci USA*, 99:12795–12800, 2002.
- [70] I. A. Swinburne and P. A. Silver. Intron delays and transcriptional timing during development. *Developmental Cell*, 14(3):325, 2008.
- [71] V. L. Syrmos, C. T. Abdallah, P. Dorato, and K. Grigoriadis. Static output feedback survey. *Automatica*, 33(2):125–137, 1997.
- [72] T. Takeuchi, T. Hinohara, G. Hurosawa, and K. Uchida. A temperature-compensated model for circadian rhythms that can be entrained by temperature cycles. *J Theor Biol*, 246(1):195–204, 2007.
- [73] A. Thiel, H. Schwegler, and C. W. Eurich. Complex dynamics is abolished in delayed recurrent systems with distributed feedback times. *Wiley Periodicals*, 8(4):102–108, 2003.
- [74] O. S. Venturelli, H. El-Samad, and R. M. Murray. Synergistic dual positive feedback loops established by molecular sequestration generate robust bimodal response. *Proc Natl Acad Sci USA*, 109(48):E3324–E3333, 2012.
- [75] U. Vogel and K. F. Jensen. The RNA chain elongation rate in *Escherichia coli* depends on the growth rate. *J Bacteriol*, 176(10):2807–2813, 1994.
- [76] D. Volfson, J. Marciniak, W. J. Blake, N. Ostroff, L. S. Tsimring, and J. Hasty. Origins of extrinsic variability in eukaryotic gene expression. *Nature*, 439:861–864, 2006.
- [77] Wikibooks. Control systems/time variant system solutions — wikibooks, the free textbook project, 2014. [Online; accessed 9-August-2014].
- [78] D. Williams. *Probability with Martingales*. Cambridge University Press, 1991.

- [79] O. Wolkenhauer, M. Ullah, W. Kolch, and K. Cho. Modeling and simulation of intracellular dynamics: Choosing an appropriate framework. *IEEE Trans Nanobiosci*, 3(3):200–207, 2004.
- [80] D. Yue, Y. Zhang, E. Tian, and C. Peng. Delay-distribution-dependent exponential stability criteria for discrete-time recurrent neural networks with stochastic delay. *IEEE Transactions on Neural Networks*, 19(7):1299–1306, 2008.